LEVEL

CRREL

13

Block motion from detonations of buried near-surface explosive arrays

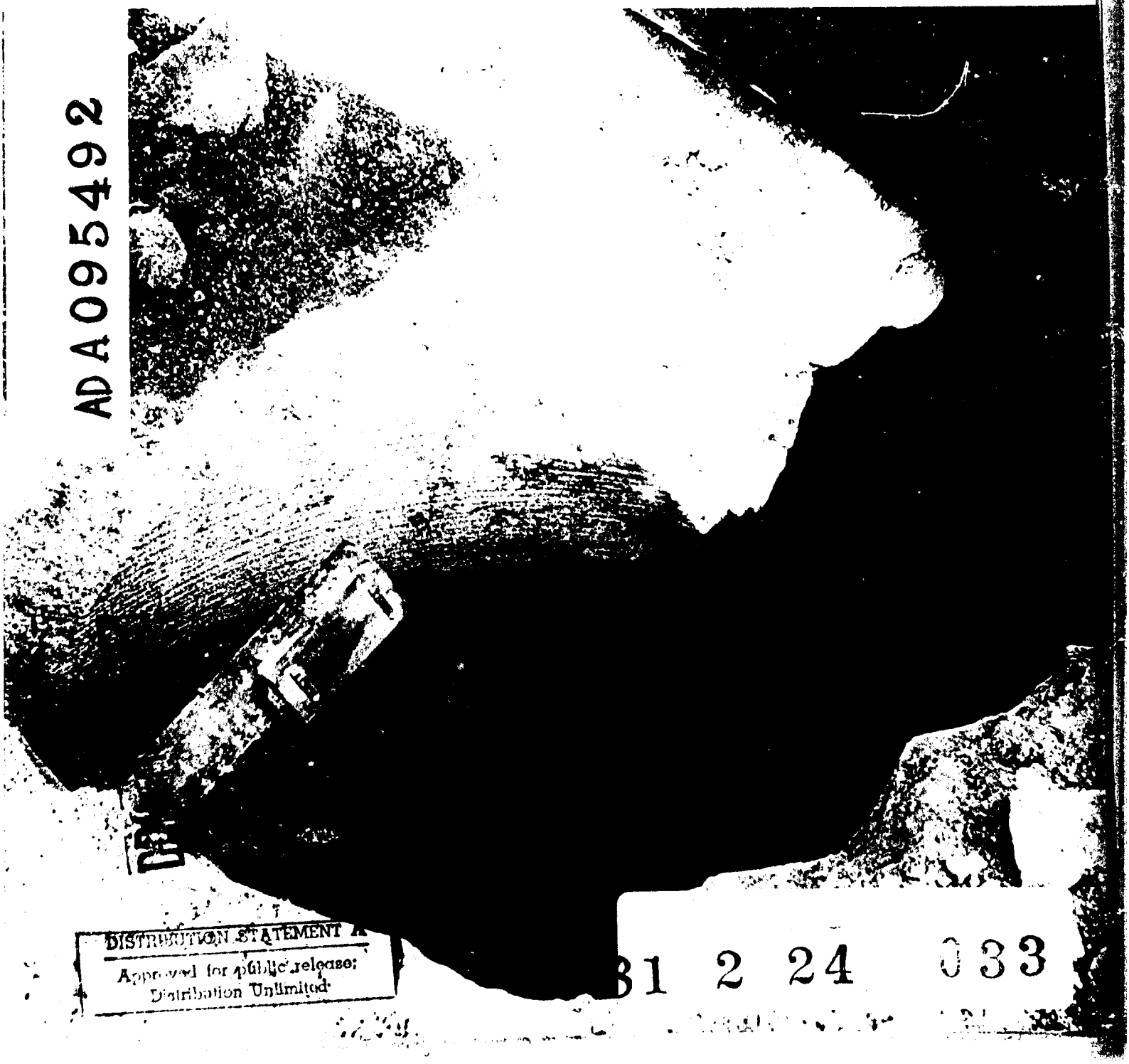

Cover: *Collapse of structure in rock due to relative displacements from high-explosive loading (HANDEC II DIHEST), Cedar City, Utah.*

CRREL Report 80-26

Block motion from detonations of buried near-surface explosive arrays

Scott Blouin

December 1980

Prepared for
U.S. AIR FORCE
By
UNITED STATES ARMY
CORPS OF ENGINEERS
COLD REGIONS RESEARCH AND ENGINEERING LABORATORY
HANOVER, NEW HAMPSHIRE, U.S.A.

Unclassified
SECURITY CLASSIFICATION OF THIS PAGE (When Data Entered)

REPORT DOCUMENTATION PAGE

READ INSTRUCTIONS BEFORE COMPLETING FORM

1. REPORT NUMBER: CRREL Report 80-26
2. GOVT ACCESSION NO.: AD-A095492
3. RECIPIENT'S CATALOG NUMBER:

4. TITLE (and Subtitle): BLOCK MOTION FROM DETONATIONS OF BURIED NEAR-SURFACE EXPLOSIVE ARRAYS
5. TYPE OF REPORT & PERIOD COVERED:
6. PERFORMING ORG. REPORT NUMBER:

7. AUTHOR(s): Scott Blouin
8. CONTRACT OR GRANT NUMBER(s): CRREL 80-26

9. PERFORMING ORGANIZATION NAME AND ADDRESS
U.S. Army Cold Regions Research and Engineering Laboratory
Hanover, New Hampshire 03755

10. PROGRAM ELEMENT, PROJECT, TASK AREA & WORK UNIT NUMBERS
Kirtland Air Force Base Project
Order 78-165, Work Unit DBT 1-4

11. CONTROLLING OFFICE NAME AND ADDRESS
U.S. Air Force Weapons Laboratory
Kirtland Air Force Base, New Mexico 87117

12. REPORT DATE: December 1980
13. NUMBER OF PAGES: 71

14. MONITORING AGENCY NAME & ADDRESS (if different from Controlling Office)

15. SECURITY CLASS. (of this report): Unclassified
15a. DECLASSIFICATION/DOWNGRADING SCHEDULE

12/72

16. DISTRIBUTION STATEMENT (of this Report)

Approved for public release; distribution unlimited.

17. DISTRIBUTION STATEMENT (of the abstract entered in Block 20, if different from Report)

18. SUPPLEMENTARY NOTES

19. KEY WORDS (Continue on reverse side if necessary and identify by block number)

Block motion
Explosion effects
Explosives
Hardened structures
Rock dynamics

20. ABSTRACT (Continue on reverse side if necessary and identify by block number)

A vital concern to the survivability of hardened underground structures in rock is the relative displacement induced along geologic discontinuities by nearby explosions. Such displacement, commonly termed block motion, can occur along faults, joints, bedding planes and other structural weaknesses in rock. This report documents all occurrences of block motion observed during the development of DIHEST, a series of shallow-buried high explosive experiments designed to simulate the direct induced ground motions from a nuclear surface burst. Instances of block motion are described, along with pertinent details of the explosive arrays, geology and ground motion fields. The influence of these and other factors on the direction and magnitude of block motion is discussed.

DD FORM 1 JAN 73 1473 EDITION OF 1 NOV 65 IS OBSOLETE

Unclassified
SECURITY CLASSIFICATION OF THIS PAGE (When Data Entered)

037100

PREFACE

This report was prepared by Scott Blouin, formerly a Research Civil Engineer with the Applied Research Branch, Experimental Engineering Division, U.S. Army Cold Regions Research and Engineering Laboratory. Funding for this research was provided by the U.S. Air Force under Kirtland Air Force Base Project Order 78-165, Work Unit DBT1-4, *Permanent Displacement Study*.

M. Plamondon, L. Kambly, and J. Bratton of the U.S. Air Force Weapons Laboratory technically reviewed the manuscript of this report.

CONTENTS

	Page
Abstract	ii
Preface	iii
Conversion factors	vi
Introduction	1
STARMET	3
Test description	3
Test results	5
PLANEWAVE II	21
Test description	21
Test results	25
DATEX II	28
Test description	28
Test results	30
HANDEC II	36
Test description	36
Test results	39
ROCKTEST II	49
Test description	49
Test results	49
Summary and discussion	61
Literature cited	62

ILLUSTRATIONS

Figure	
1. HEST geometry	2
2. DIHEST geometry	2
3. Section view of STARMET explosive array	4
4. Joint map of STARMET test bed	4
5. Plan view of project STARMET	5
6. Pre-test aerial photograph of STARMET test bed	6
7. Post-test aerial photograph of STARMET test bed	7
8. Plan view of STARMET crater	8
9. View of the thrust block, looking south	9
10. West edge of the thrust block, looking south	9
11. STARMET permanent horizontal displacements	10
12. STARMET permanent vertical displacements	11
13. Plan view of assumed joint intersection with the test bed surface	11
14. Differential displacement measured along the thrust block boundary joint	16
15. View of the bottom of the 4-ft structure	13
16. A portion of the north wall of the 6-ft structure	13
17. Open joints on the surface of the thrust block	14
18. View of south side of the upper 5 ft of the 6-ft structure	14
19. STARMET thrust block, schematic cross section	15
20. A view north of structure S_1	16
21. A view of a rebound fracture approximately 5 ft from crater edge	16
22. A view of open joints north of structure S_1	16

Figure		Page
23.	A view of the north side of structure S_2	17
24.	Horizontal longitudinal and vertical velocities at instrumentation hole 15	18
25.	Velocity time histories, instrumentation holes 5 and 7	18
26.	Velocity and displacement, hole 22	19
27.	Displacement hodographs for opposites sides of STARMET array	20
28.	Plan view, explosive holes, PLANEWAVE II	21
29.	Schmidt hardness measured using a type N hammer on the walls of a 42-in. structural hole	21
30.	Contact between shale and sandstone units	22
31.	Gouge zone in red shale unit	23
32.	Horizontal partings in the red shale unit	23
33.	Siltstone lens in sandstone unit	23
34	Sandstone and quartz conglomerate contact	23
35	Typical fracture in the quartz pebble conglomerate	24
36.	Very large vertical fracture in the quartz pebble conglomerate	24
37	Section view, PLANEWAVE II instrumentation	25
38	Differential displacements along bedding planes — PLANEWAVE II	25
39.	Peak velocity vs range — PLANEWAVE II	26
40	Typical velocity vs time — PLANEWAVE II	26
41.	Seismic and peak horizontal stress propagation velocities for ROCK-TEST II, HANDEC II and DATEX II	27
42	Laboratory compression wave velocity for HANDEC II site specimens vs hydrostatic pressure	28
43.	Plan view of DATEX II	29
44.	North-south section of DATEX II berm and apparent crater	30
45.	East-west section of DATEX II berm and apparent crater	30
46	Upper portion of DATEX II structure 1	31
47.	Upper portion of DATEX II structure 2	31
48.	Top section of DATEX II structure 3	32
49.	Bottom section of DATEX II structure 3	32
50.	Hypothesized failure mechanism for DATEX II structu	33
51.	Top view of DATEX II structure 4	33
52.	Permanent displacement of DATEX II structures	34
53.	DATEX II displacement trajectories	34
54.	Typical computed DIHEST mean particle trajectories	35
55	DATEX II near-surface peak horizontal velocities	35
56.	DATEX II peak vertical velocities	35
57	DATEX II velocity time histories for hole 4	36
58.	Plan view of HANDEC II	37
59	North-south section of HANDEC II berm and apparent crater	37
60.	East-west section of HANDEC II berm and apparent crater	38
61.	HANDEC II pre-shot airphoto	38
62.	HANDEC II post-shot airphoto	38
63	Joint map of HANDEC II test bed	39
64.	HANDEC II permanent horizontal displacements	40
65.	HANDEC II permanent vertical displacements	40
66.	HANDEC II relative displacement, looking south	41
67.	HANDEC II relative displacement in the southwest corner of test bed	41
68.	HANDEC II relative displacement, schematic view	42
69	Cross-sectional comparison of the rock surfaces above and below the transverse slip surface in HANDEC II lined silo S_{11}	42

Figure Page
70. Projection of the transverse slip surface in lined silo S_{11} to HANDEC II DIHEST array 42
71. Plan view of HANDEC I and II test bed 42
72. View of HANDEC I lined structure S_1 44
73. View of HANDEC I unlined structure S_2 44
74. Two views of HANDEC I lined structure S_1 with the steel lining removed 45
75. Extrapolation of the near-vertical joint at the HANDEC I structures to the HANDEC II DIHEST array 46
76. Extrapolation of the transverse slip surface at the HANDEC I DIHEST array 46
77. HANDEC II displacement trajectories 46
78. HANDEC II horizontal displacement trajectories, depth—4 ft 47
79. HANDEC II horizontal displacement trajectories, depth—18 ft 47
80. HANDEC II near-surface peak horizontal velocity 47
81. HANDEC II near-surface peak vertical velocity 47
82. HANDEC II smoothed and corrected air pressure time-history 48
83. Typical HANDEC II time-history from hole 5 48
84. Plan and section views of ROCKTEST II DIHEST 50
85. Plan view, ROCKTEST II 51
86. Joint map of ROCKTEST II test bed 52
87. High angle joints in the ROCKTEST II test bed 53
88. Low angle joints in the ROCKTEST II test bed 54
89. Plan view of surface relative displacements in the ROCKTEST II test bed 55
90. Aerial view of the ROCKTEST II thrust block 55
91. View north along the ROCKTEST II low angle boundary joint 56
92. East-west cross section through structures 03A, 06, 07 and hole F04 56
93. View west of vertical joints at the north edge of the ROCKTEST II thrust block 57
94. Joints in structure 07 in which major relative motion occurred 57
95. Extrapolation of transverse slip joints from structure 07 to ROCKTEST II array 58
96. ROCKTEST II near-surface peak horizontal and vertical velocities 58
97. ROCKTEST II motion in and beyond the thrust block 59

TABLES

Table
1. Simulation experiments in rock 3
2. Block motion summary—DIHEST experience 60

CONVERSION FACTORS: U.S. CUSTOMARY TO METRIC (SI) UNITS OF MEASUREMENT

These conversion factors include all the significant digits given in the conversion tables in the ASTM *Metric Practice Guide* (E 380), which has been approved for use by the Department of Defense. Converted values should be rounded to have the same precision as the original (see E 380).

Multiply	*By*	*To obtain*
inch	25.4*	millimeter
foot	0.3048*	meter
foot/second	0.3048*	meter/second
pound	0.4535924	kilogram
pound-force/inch^2	6.894757	kilopascal
ton	907.1847	kilogram

*Exact

BLOCK MOTION FROM DETONATIONS OF BURIED NEAR-SURFACE EXPLOSIVE ARRAYS

Scott Blouin

INTRODUCTION

There is currently a great deal of interest in basing both strategic systems and command, control and communications facilities deep beneath the earth's surface to enable them to better withstand the effects of a nuclear attack. It appears that the most crucial concern to the survivability of deep based systems is the so-called "block motion" problem. Block motion, the tendency of a rock mass to shear along planes of weakness when subjected to explosive loadings, has been observed along pre-existing joints, bedding planes and faults in various rock types. These relative displacements have been observed near the earth's surface and at depth from both high explosive and nuclear loadings. Block motion has frequently intersected hardened structures with catastrophic results, generally shearing the structures in the plane of the motion in the rock.

A significant body of block motion data was accumulated during the late 1960's and early 70's by the Air Force Weapons Laboratory (AFWL), during development and fielding of Direct Induced High Explosive Simulation Technique (DIHEST) tests. Unfortunately most of these data have been reported only piecemeal and some have not been reported at all. This report is an attempt to provide as full an account of the block motions associated with the DIHEST experiments as is possible to gather from the scattered reports, unpublished material and personal interviews.

DIHEST was developed to simulate the cratering induced ground motions from a nuclear surface burst using buried arrays of high explosives. The impetus for DIHEST came from the Hard Rock Silo Program, an effort to develop an extremely hard missile silo in rock. AFWL was charged with the development of techniques using high explosives to simulate the airblast, airblast-induced ground motions and cratering-induced ground motions of the Hard Rock Silo nuclear design threat. Two simulation techniques were employed: the HEST (High Explosive Simulation Technique) to simulate the airblast and airblast-induced ground motions, and the DIHEST to simulate the cratering induced motions. As shown in Figure 1, the HEST consists of a cavity of uniform height bounded on the sides by a soil berm, above by a soil overburden of uniform thickness, and below by the test bed on the earth's surface (Cooper 1970, Bratton 1967, Bratton and Mitchell 1971). Horizontal racks of high explosive detonating cord are placed in the cavity and detonated at one end of the test bed. This detonation produces an explosive wave that propagates across the test bed, loading the earth with an over-pressure pulse that decays with time because of the compression and lifting of the overburden. Six HEST experiments, three of which were combined with DIHEST, were fielded on rock. Simulated peak overpressures up to 6000 lbf/in^2 and specific impulses to more than 100 lbf/in^2-s were achieved.

The DIHEST uses explosives buried in geometric array to produce the desired particle velocity-time histories at prescribed ranges from the array. Because of the time constraints placed on the development of the DIHEST, the experimental study was largely restricted to rectangular, planar, and vertical explosive arrays, as shown schematically in Figure 2. The planar wave front propagated across the DIHEST test bed was intended to approximate an increment

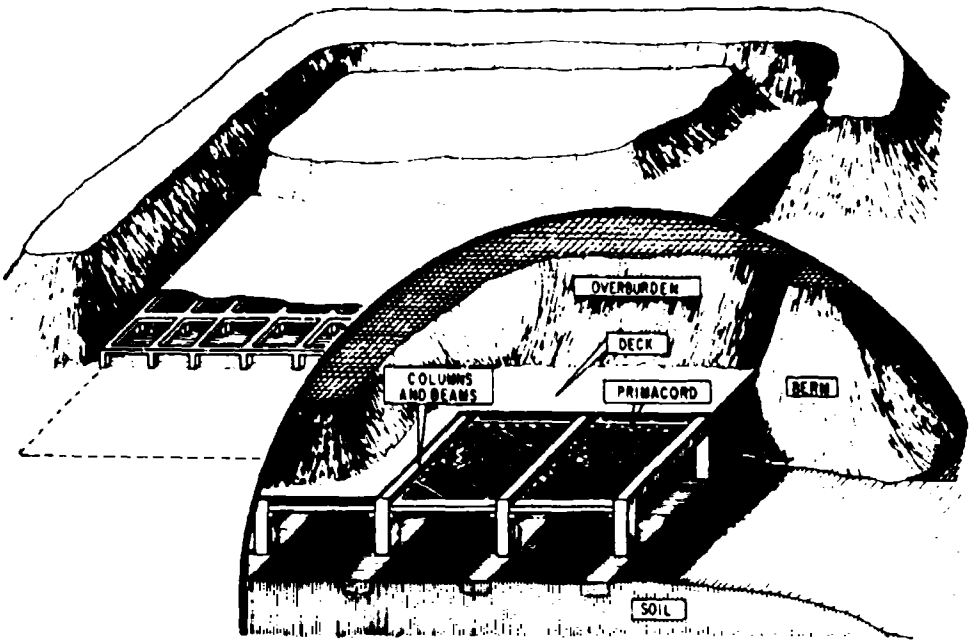

Figure 1. HEST geometry (from Blouin and Kaiser 1972).

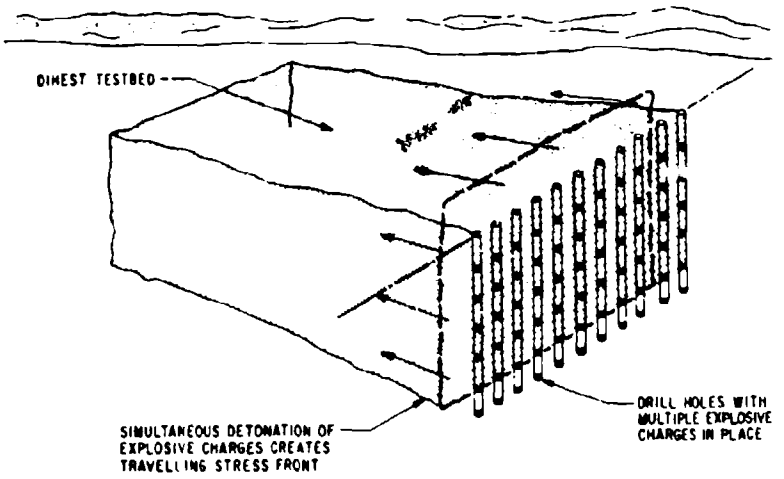

Figure 2. DIHEST geometry (from Blouin and Kaiser 1972).

of the spherical direct-induced wave front from a surface burst, which would have been approximately planar at the range of interest. Nine DIHEST experiments were fielded in rock, including the three combined HEST-DIHEST shots. DIHEST explosive array yields ranged from 800 to 234,000 lb of high explosive. Testing was carried out in three rock types: layered sedimentary rock, a rather soft weatnered tonalite, and hard granite. Block motions were observed in all three rock types. A summary of the nine DIHEST and combined HEST-DIHEST experiments in rock is given in approximate chronological order in Table 1. Of these, five produced significant block motions. These five are denoted by an asterisk.

Most DIHEST block motions were influenced by the free surface. They always occurred along pre-existing planes of weakness in the rock mass, in these cases joints or bedding planes. They ap-

Table 1. Simulation experiments in rock.

Experiment	Type	Date	Location	HEST bed dimensions (ft)	HEST design overpressure (lbf/in²)	DIHEST array	
						Dimensions (ft) (length × depth)	Weight (lb)
PLANEWAVE I	DIHEST	Oct 1967	Estancia Valley, N.M. (Interbedded sedimentary)	N/A	N/A	20 × 20	800
PLANEWAVE II*	DIHEST	Mar 1968	Estancia Valley, N.M. (Interbedded sedimentary)	N/A	N/A	45 × 20	4,200
DATEX I	DIHEST	Apr 1969	Cedar City, Utah (Tonalite)	N/A	N/A	100 × 38	4,400
DATEX II*	DIHEST	July 1969	Cedar City, Utah (Tonalite)	N/A	N/A	200 × 36	82,000
HANDEC I	HEST-DIHEST	May 1969	Cedar City, Utah (Tonalite)	40 × 60	6000	100 × 38	4,400
HANDEC II*	HEST-DIHEST	Aug 1969	Cedar City, Utah (Tonalite)	60 × 90	3000	200 × 40	92,000
ROCKTEST II*	HEST-DIHEST	Mar 1970	Cedar City, Utah (Tonalite)	250 × 400	Classified	500 × 40	234,000
PRESTARMET II	DIHEST	Jan 1969	Pedernal Hills, N.M. (Granite)	N/A	N/A	50 × 38	2,400
STARMET*	DIHEST	Nov 1970	Pedernal Hills, N.M. (Granite)	N/A	N/A	100 × 38	4,360

*Indicates significant block motions developed

pear to always be of the "driven" variety; that is, they resulted directly from the action of the dynamic stresses on the rock rather than from tectonic stress relief triggered by the dynamic input [see Bache and Lambert (1976) for a discussion of triggered block motion]. Generally, they followed paths of least resistance offered by the joint patterns or bedding planes, though there were several instances where this was not the case. They extended horizontally as much as three crater radii from the explosive arrays. Their vertical extent (depth) was never determined.

While it is difficult to extrapolate this near-surface experience to structures located below a surface burst, these test data certainly would have direct bearing on the design of the many surface and near-surface facilities associated with a deep-buried system, including antennae, utility and access shafts, and launch systems. The extent to which they can aid in understanding the deep block motion threat must be determined in the future.

In the following sections each of the five DIHEST experiments which produced permanent relative displacement is briefly described, including the explosive array, test bed instrumentation, geology, and rock properties. A complete description of the ensuing relative displacements is given, supplemented by an overview of the ground motions either measured or postulated to have occurred in the area of the displacements. Finally a summary of the displacements is presented, along with a discussion of the results and conclusion drawn from them.

STARMET

Test description

The STARMET explosive array (Fig. 3) contained a total of 4360 lb of ammonium nitrate-fuel oil explosive in standard 40-lb cratering charge canisters. The average explosive density per unit area of array was 1.27 lb/ft².

The test site was located in the Pedernal Hills of central New Mexico, 17 miles west of the town of Encino, adjacent to and south of U.S. Highway 60. The rock was a slightly metamorphosed unweathered granite of Precambrian origin that was very strong and very stiff. A thin sandy soil covered approximately half the surface area in the vicinity of the testbed. Elsewhere, the rock was exposed at the surface. It was highly jointed, with joint spacing averaging less than 6 in. The joints were very tight and exhibited no apparent weathering. Results from in-

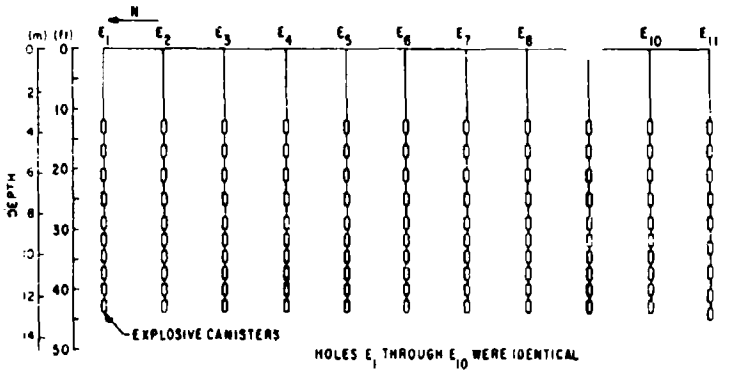

Figure 3. Section view of STARMET explosive array (from Blouin and Kaiser 1972).

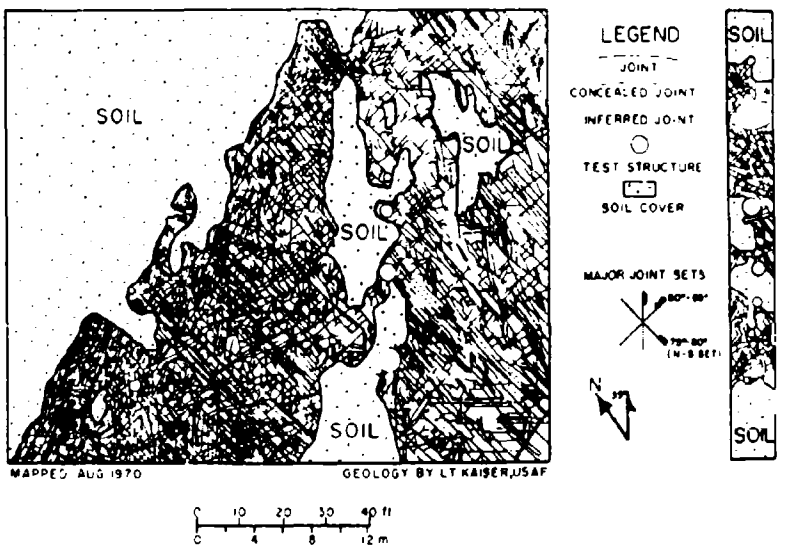

Figure 4. Joint map of STARMET test bed (from Blouin and Kaiser 1972).

tact core sample tests were reported by Stephenson and Engel (1971). Unconfined compressive strengths averaged over 30,000 lbf/in.^{2} and the secant modulus at 50% of ultimate strength averaged between 9 and 10 x 10^6 lbf./in.^{2}

A detailed joint map of exposed segments of the testbed surface was prepared by John Kaiser (Blouin and Kaiser 1972) and is reproduced in Figure 4. The map shows only the major joints; actual jointing was even more dense than indicated here. The map shows the west side of the testbed from the explosive array for a distance of 120 ft, the range of the farthest instrumentation holes, as well as a 10-ft band on the east side of the explosive array surrounding the test structures. Only outcrop was mapped; soil-covered areas are so indicated. Three major joint sets are delineated on the map, a north-south set dipping steeply to the east, a nearly orthogonal set dipping steeply to the north, and a set striking toward the northeast parallel to the explosive array and dipping steeply toward the southeast. It will be shown in the later discussion that the orientation of these joint sets largely controlled the nature and direction of the permanent displacements which occurred in the testbed beyond the DIHEST crater.

As shown in the plan view of the testbed in Figure 5, a series of unlined structures were drilled in the testbed on either side of the explosive array. These were designed to determine the influence of the ratio of joint spacing to

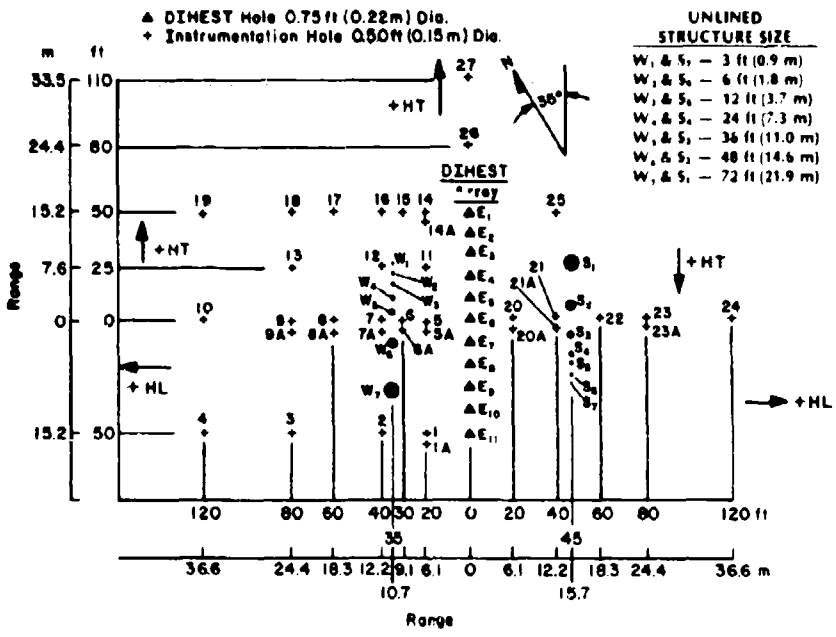

Figure 5. Plan view of project STARMET (from Blouin and Kaiser 1972).

diameter on structural performance. Structures on the east side were centered 45 ft from the array, structures on the west side 35 ft from the array. The structures were from 3 in. to 6 ft in diameter and 20 ft deep. All structures on the east side were bored using smooth wall drilling techniques except for S_1 which was perimeter drilled and excavated. Due to the close joint spacing, portions of the side walls of S_1 caved in during excavation, resulting in an irregularly shaped structure. The joints in the walls of the five largest smooth-wall structures were mapped (Blouin and Kaiser 1972). The close-spaced tight jointing at the surface was evident throughout the length of the structures. All the structures except S_1 were filled with plaster sand during the test to keep blocks of rock from falling out of the sidewalls.

Both active and passive monitoring of testbed motions were employed on STARMET. Transient motions were measured with an extensive array of velocity gages and accelerometers grouted in the instrumentation holes shown in Figure 5. Gages were grouted at depths of 4, 15, 30 and 45 ft to monitor motions near the surface and near the top, middle, and bottom of the explosive array. Gages were located on both sides of the explosive array out to a range of 120 ft, with a more complete instrumentation set to the west of the array. In addition to the motion measurements, 34 experimental strain-gaged aluminum canisters were grouted throughout the bed. These were designed to give quantitative comparisons of strain from point to point. They were not meant to measure absolute strain in the rock.

A survey of selected intersection points on a grid painted on the testbed surface was made pre- and post-test to determine the extent and magnitude of any permanent displacements. Approximately 160 intersection points were surveyed prior to the test. The grid, shown in the pre-test photograph (Fig. 6), consisted of 5-ft squares and covers the area mapped on the joint map plus a 10-ft-wide semicircular arc swung on a 45-ft radius about the northernmost explosive hole. The explosive holes and structures are also visible in the photo. Seventy-five surveyed points were located and resurveyed post-test.

Test results

The outstanding post-detonation features resulting from STARMET are identified on the airphoto in Figure 7. The ejecta distribution was extremely uneven, being concentrated almost entirely to the west of the explosive array. A large mass of rock lying to the north and west of the

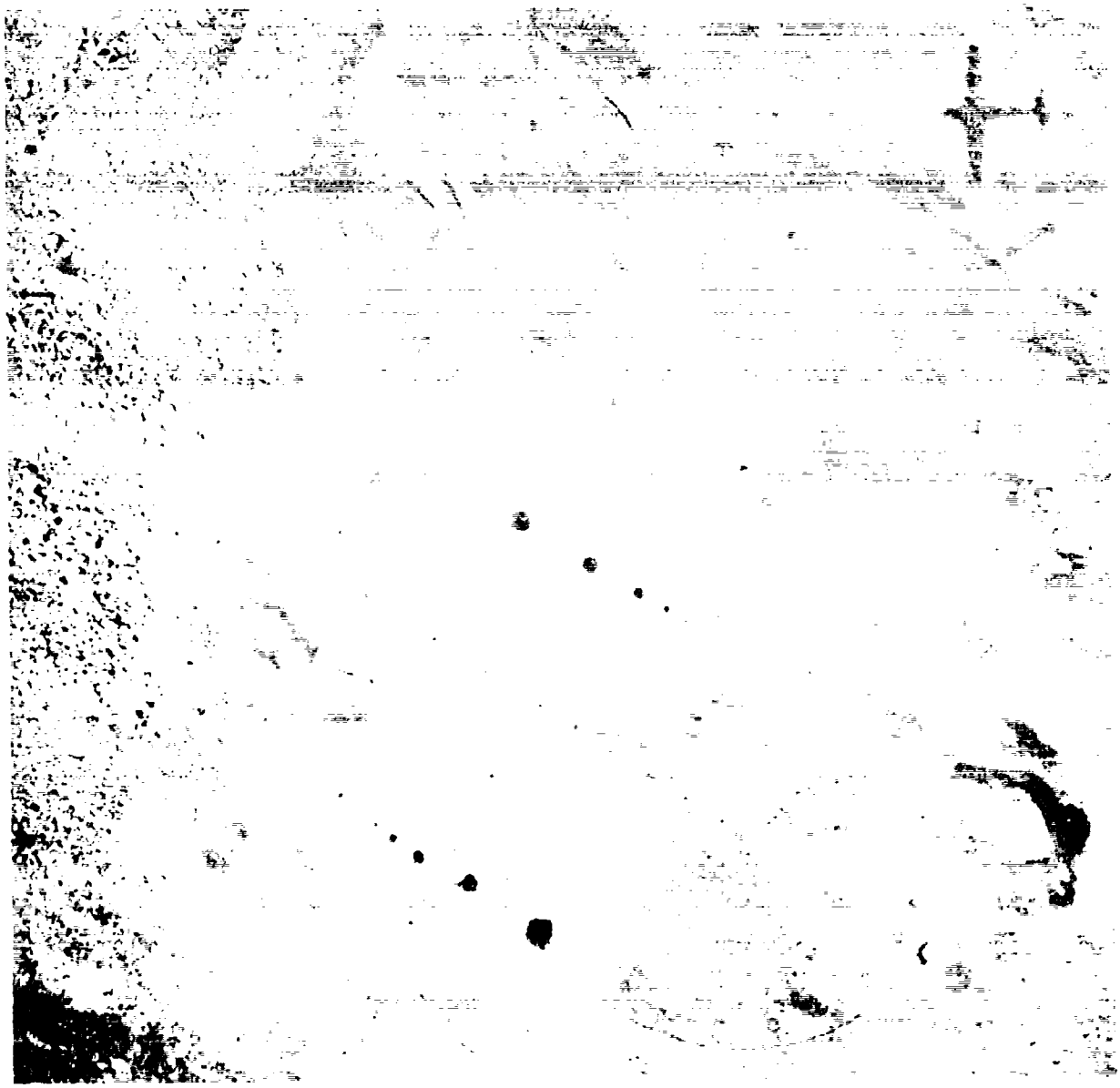

Figure 6. Pre-test aerial photograph of STARMLT test bed (from Blouin and Kaiser 1972)

array, well beyond the crater boundary, was thrust upward and outward away from the array. A series of vertical joints stood open to the northeast of the crater.

As shown in the photo, the crater tended to be symmetrical about the explosive array. The plan view crater map in Figure 8 shows that the crater lip generally paralleled the explosive array on either side and curved around the array on its ends. The outer edge of the crater cone ran roughly parallel to the lip, extending 10 to 25 ft beyond it. However, on the northeast side of the crater, adjacent to the most prominent open vertical joints, there was no lip formed. The edge of the true crater, located after the post-test cleaning of the testbed, lay approximately under the crater lip, averaging about 18 ft from the explosive array on either side.

The ejecta distribution seemed to be heavily influenced by the joint patterns. As noted, nearly

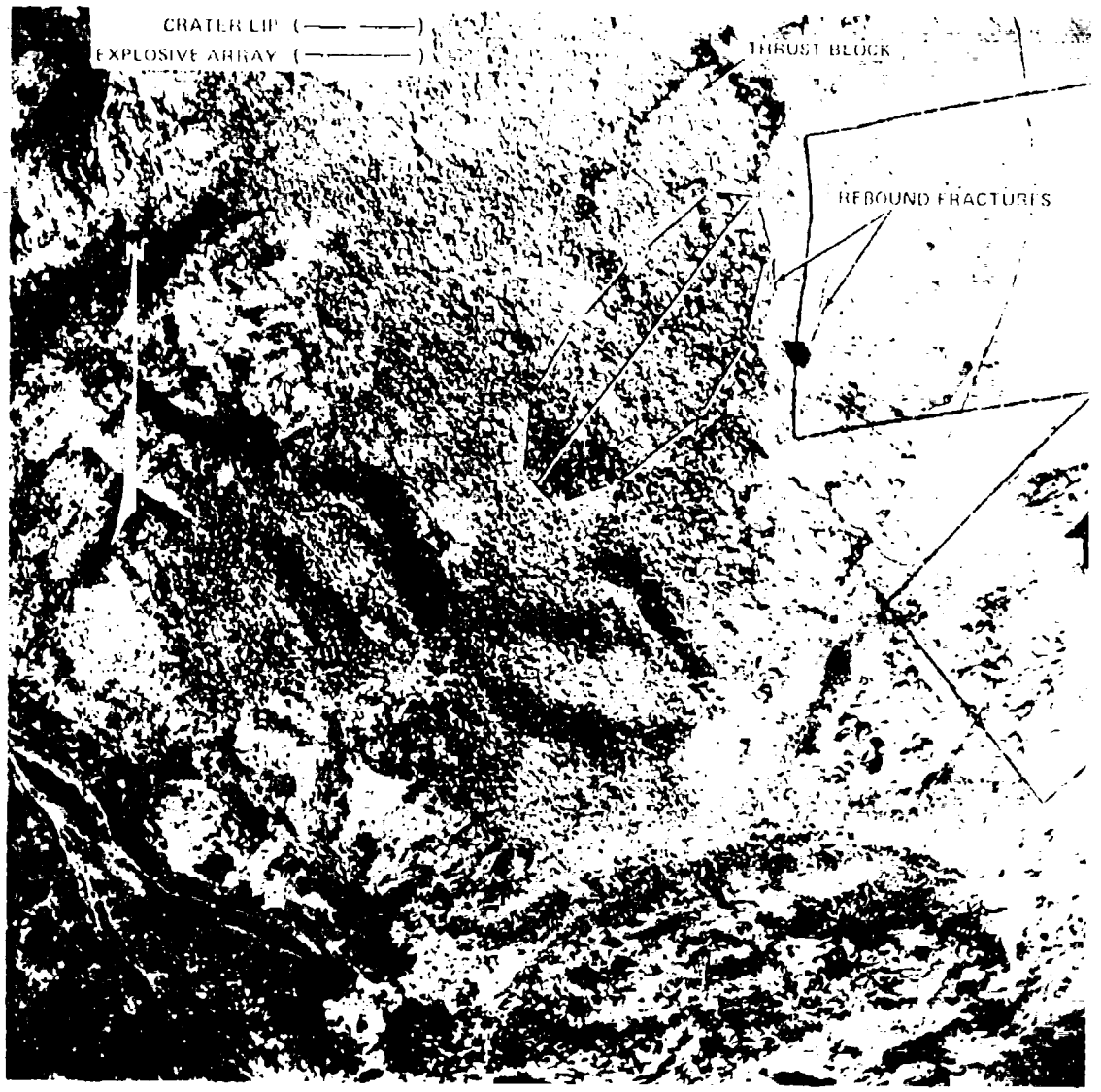

Figure 7. Post-test aerial photograph of STARMIT test bed (from Blouin and Kaiser 1972)

all ejecta landed to the west side of the array, with blanket ejecta extending beyond a range of 120 ft. The heaviest concentration lay in the northwest quadrant and appeared to have nearly paralleled the north striking joint set shown in Figure 4. The combination of that set and the joint set, which was parallel to the explosive array, would have tended to provide a path of least resistance for throwout toward the west. It is not clear why ejecta were distributed almost solely in this direction, however, because the east-west striking set should again have provided a path of least resistance toward the opposite side of the array. Aside from a slight concentration of ejecta extending perhaps 25 ft from the crater lip in the southeast quandrant, very little fell toward the east. Perhaps lack of a second "complementary" joint set precluded throwout in this direction.

Johnson (1962) reported similar instances of joint control of ejecta distribution for a series of high explosive (HE) cratering shots in basalt. He concluded that

> the orientations of vertical and nearly vertical

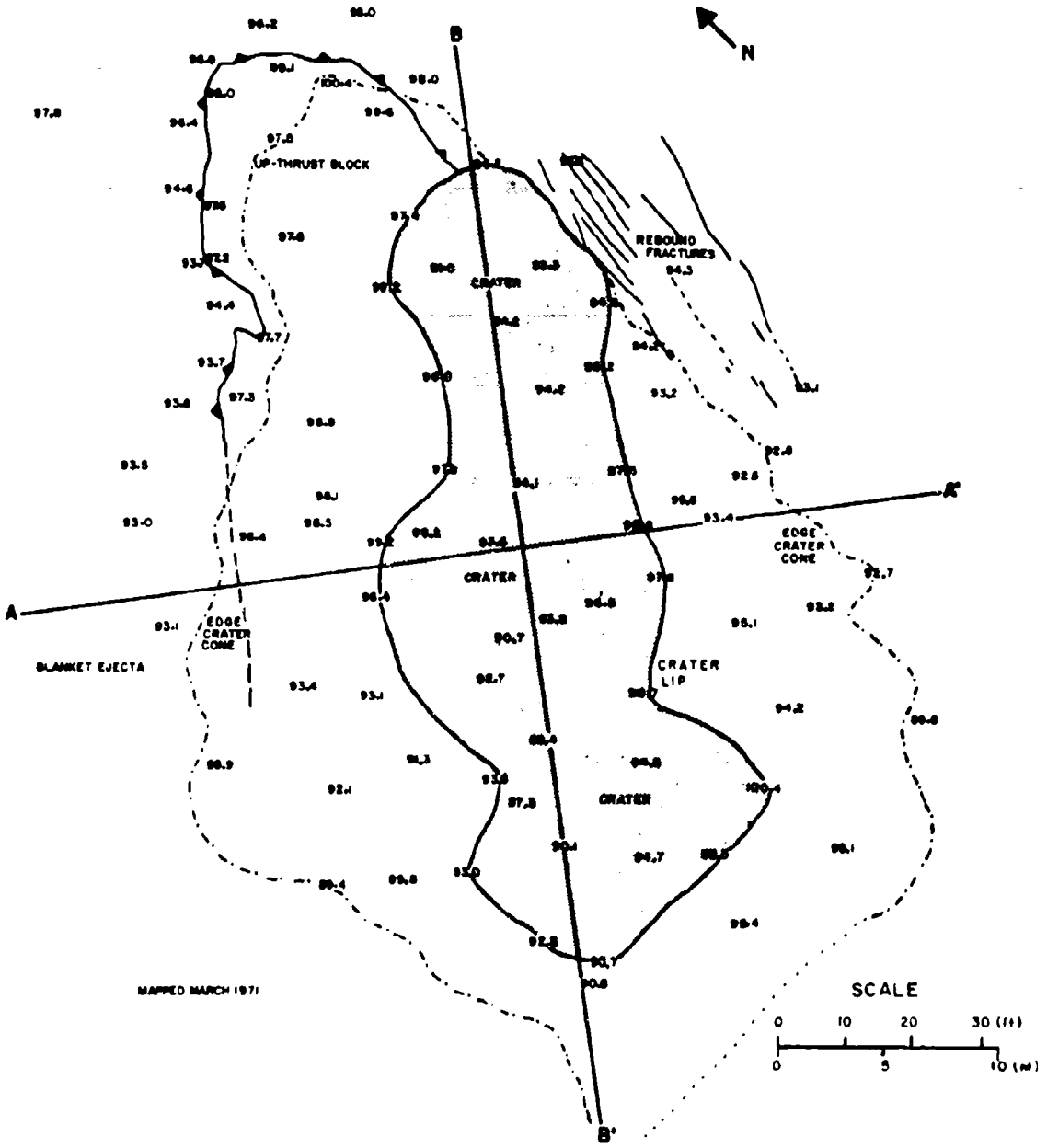

Figure 8. Plan view of STARMET crater (from Blouin and Kaiser 1972).

pre-explosion surface joints and their spatial relations to charge centers appear to have the greatest effect of any natural factor on the ejecta patterns about the craters on Buckboard Mesa.

Joints act as channels for the release of forces exerted by the expansion of the gas bubble as well as reflectors of these forces. This results in removal of more material in directions parallel to those joints that act as release channels. More material is also removed in directions normal to, and across, the crater from those joints that reflect the explosive forces of the gas bubble. Joints at the position of the explosive center appear to act mainly as release channels for the explosive forces, whereas those joints nearer the margin of the crater tend to act largely as reflectors of these forces.

This same channeling effect by vertical joint sets has been demonstrated in model experiments in testbeds of stacked sugar cubes (Melzer 1970a) and ceramic tiles (Teriecky et al.

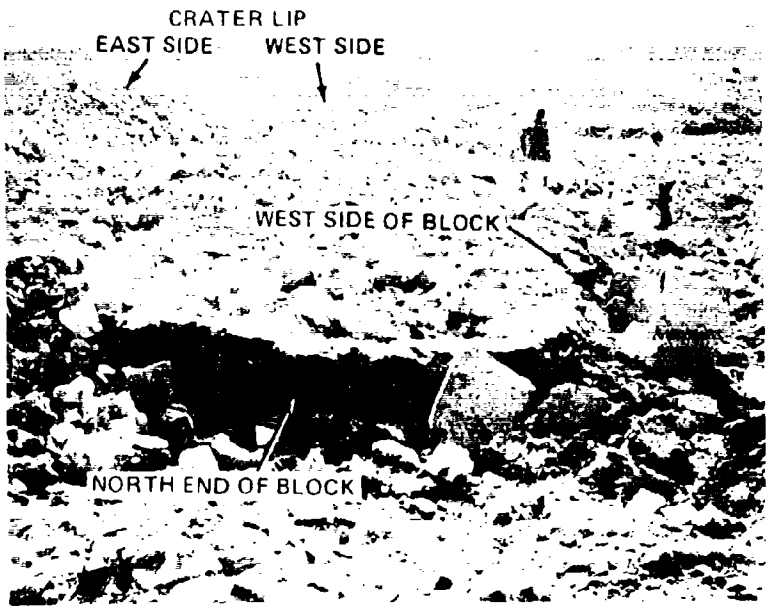

Figure 9. View of the thrust block, looking south (from Blouin and Kaiser 1972).

Figure 10. West edge of the thrust block, looking south (from Blouin and Kaiser 1972).

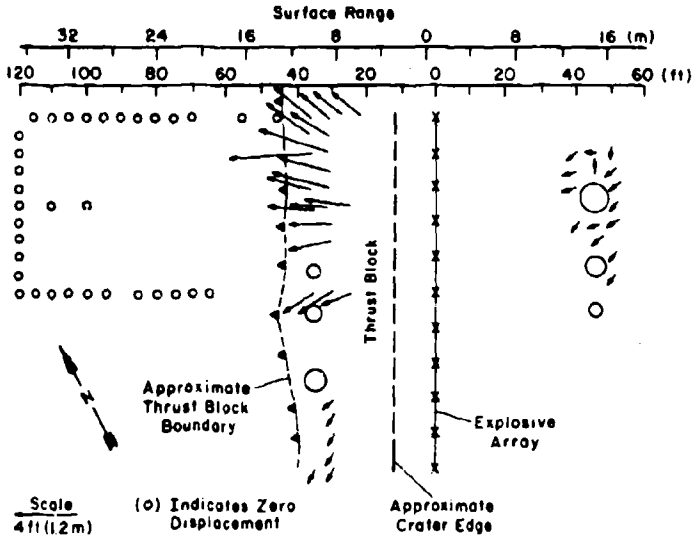

Figure 11. STARMET permanent horizontal displacements (from Blouin and Kaiser 1972).

1971). In both sets of experiments there was a strong tendency for ejecta to be thrown out along the vertical channels formed by the vertical "joint sets" which intersected the craters.

The close joint spacing tended to limit the size of the STARMET ejecta blocks. Field observation revealed that the most of the ejecta blocks were smaller than 1 to 2 ft on a side. Most block faces were formed by joint planes, with generally one or no fresh breaks per block. Typical ejecta blocks can be seen in Figures 9 and 10.

Permanent displacements seemed to be joint controlled in much the same fashion as the ejecta distribution. Figure 11 is a vector plot showing the horizontal permanent displacements for all survey points recovered post-shot. Figure 12 is a similar plot of permanent vertical displacements. Displacement of the surface of the thrust block was by far the most pronounced motion in the testbed. Displacement of the block in the northwest quandrant averaged about 2½ ft horizontally and 5 ft vertically. Toward the south end of the block, displacements tapered off to less than 1 ft to 2 ft vertically. The horizontal displacement vectors on the block's surface also indicate the motion within the block was divergent, i.e. the block tended to expand laterally in a direction parallel to the array at the same time it moved outward away from the array. The divergent displacements tended to follow the trajectories of peak particle velocities generated by the planar explosive array.

A ground-level view of the thrust block looking south in a direction parallel to the explosive array is shown in Figure 9. The block was bounded on its exposed north and west sides entirely by pre-existing joints. The northern end, shown in the photograph, had a blocky appearance as it was formed by the intersections of many joint planes. The western side, however, appeared to be formed by a single [illegible] or possibly several closely spaced parallel [illegible] section of this joint is shown in Figure 10. In most places, the protruding section of the joint was obliterated because blocks of rock either broke off the edge or were knocked off by pieces of ejecta.

A schematic plan view of the original joint intersection with the testbed is shown in Figure 13. The joint intersects the surface approximately 7 ft west of the 3-, 4- and 6-ft structures' centerlines and strikes parallel to the explosive array. Figure 14 was constructed by combining measurements made on the testbed surface with the projected intersection at the surface of the joint intersections with the 3-, 4- and 6-ft structures. The displacements along the joint, measured in each of the three structures, are shown in schematic cross section. Total slip of 5.4 ft was measured in the 3-ft structure, dropping to 2.3 ft in the 6-ft structure. Displacements measured along the boundary joint in the structures agreed closely with corresponding measurements made on the thrust block surface.

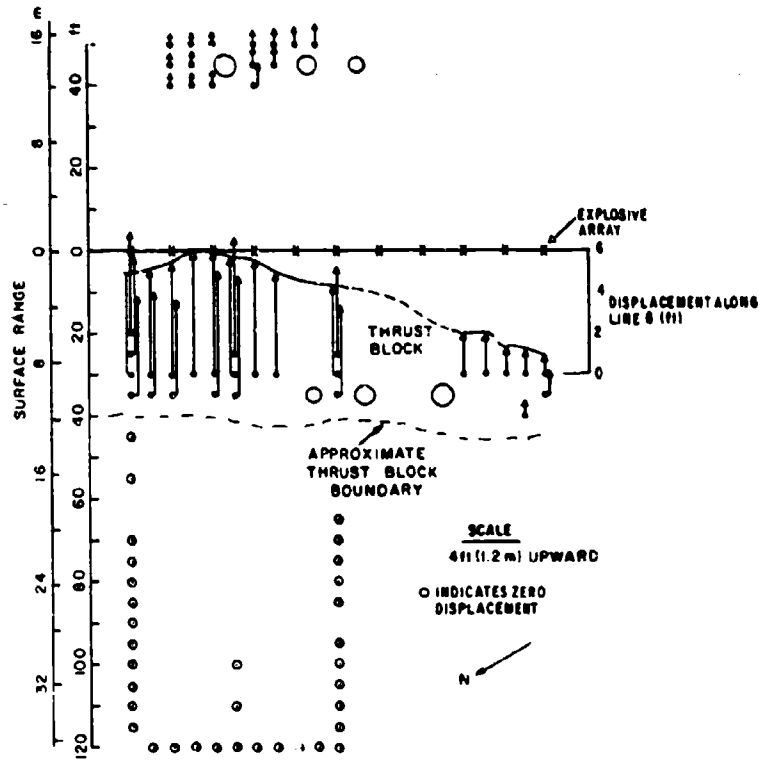

Figure 12. STARMET permanent vertical displacements (from Blouin and Kaiser 1972).

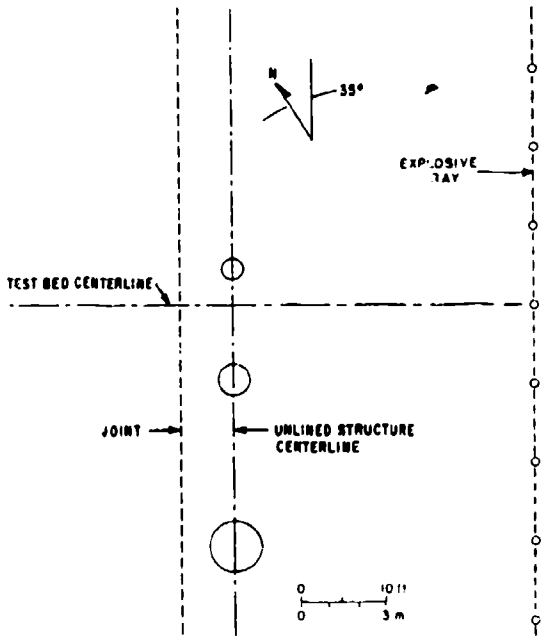

Figure 13. Plan view of assumed joint intersection with the test bed surface (from Blouin and Kaiser 1972).

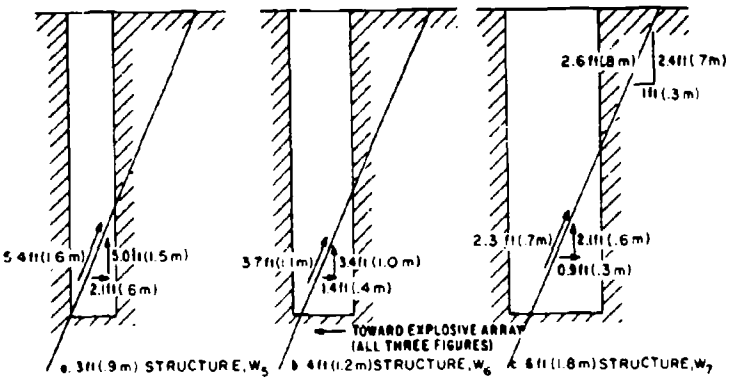

Figure 14. Differential displacement measured along the thrust block boundary joint intersecting structures W_5, W_6, and W_7 (from Blouin and Kaiser 1972).

indicating that motion along the boundary joint accounted for all but the secondary motions at the testbed surface.

Two views of the joint in the 4- and 6-ft structures are shown in Figures 15 and 16 respectively. Figure 15 shows the bottom of the 4-ft structure. The photographer's foot rests on the boundary joint, which dips toward the explosive array. The joint intersected the bottom of the hole ...he portion of the floor within the thrust block has moved upward relative to the original floor location. Figure 16 shows a portion of the 6-ft structure looking toward the north parallel to the explosive array. The boundary joint, dipping toward the array, runs diagonally across the photograph from top left to bottom right. As indicated by motion of the 15-ft contour, the thrust block has moved upward and outward 2.3 ft relative to the rest of the structure. As the vector plots of Figures 11 and 12 indicate, there were no discernible permanent displacements at any of the survey points located beyond the thrust block within the estimated ± ½ in. accuracy of the survey. Thus, the portions of each structure located beyond the boundary joint are assumed to have experienced no permanent displacements.

Numerous open joints on the surface of the thrust block and within the structures are evidence of secondary motion within the block. A view of a section of the thrust block surface is shown in Figure 17 following removal of the ejecta. Numerous open joints, all of which were tightly closed prior to the test, are shown in the vicinity of instrumentation hole 5. The prominent joints in the photo are open about 2 in. These loose and open joints extend downward into the thrust block, as shown in the photo of the top 5 ft of the 6-ft structure in Figure 18. All of these open joints were tightly closed and barely discernible prior to the test.

These numerous open joints within the thrust block signify a general expansion of the block as it moved upward and outward along the boundary joint. Such an expansion is in keeping with the divergent motion imparted by the geometry of the explosive array and the measured permanent displacements shown in Figure 11.

It is disturbing to note that the boundary joint, which controlled all permanent displacements on the west side of the testbed and which was so evident post-test both within the structures and for a length of at least 120 ft along the testbed surface, does not appear on the pretest joint map in Figure 4. Unfortunately, a thin veneer of soil covered much of the boundary joint, but approximately 40 ft of its length was exposed pretest. The only manifestation of its intersection with the testbed surface (shown in Fig. 13) is a short section of closely spaced parallel joints approximately 4 ft northwest of the 6-ft structure striking parallel to the common centerline of the structures.

Since the detail of the joint map is probably as fine as it practical, the obvious implication is that the prediction of the exact location of relative displacements in rock where joints, faults, bedding planes, etc., are relatively numerous may be impractical if not impossible. The actual spacing of discontinuities remains constant so that the complexity of the mapping and prediction problems increase with increasing explosive yield.

A hypothesized cross section of the explosive

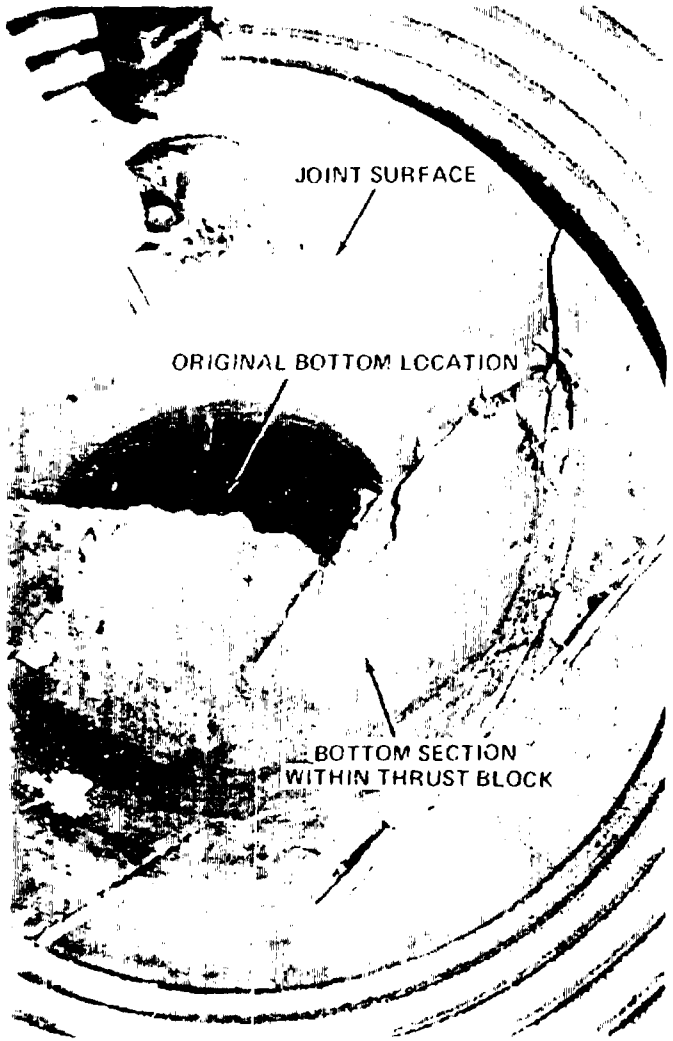

Figure 15. View of the bottom of the 4-ft structure (W_6) (from Blouin and Kaiser 1972).

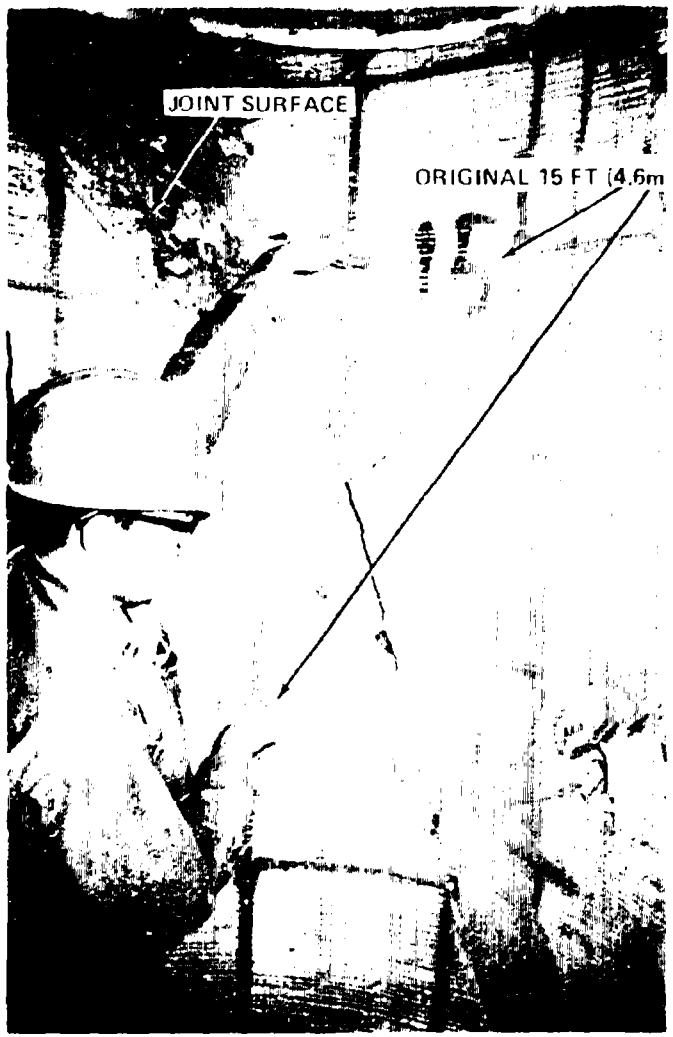

Figure 16. A portion of the north wall of the 6-ft structure (W_7) (from Blouin and Kaiser 1972).

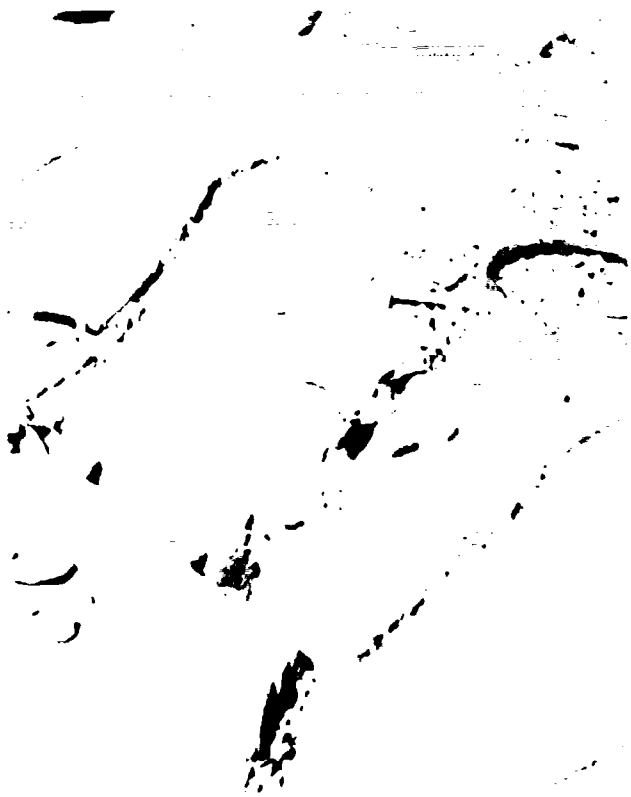

Figure 17. Open joints on the surface of the thrust block (from Blouin and Kaiser 1972).

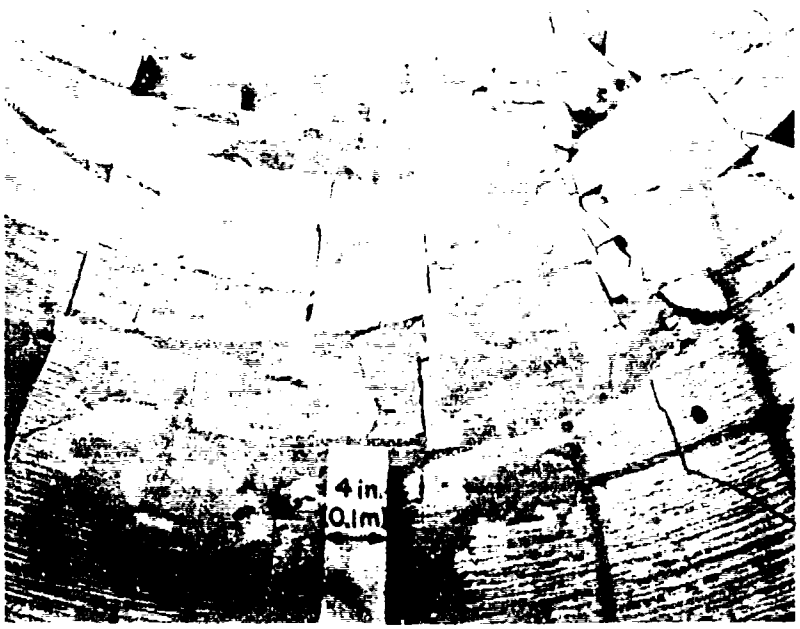

Figure 18. View of south side of the upper 5 ft of the 6-ft structure (from Blouin and Kaiser 1972).

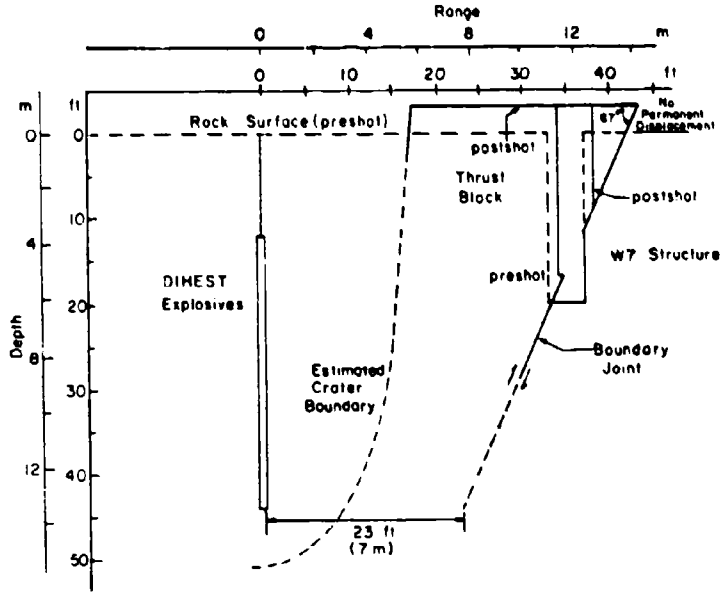

Figure 19. STARMET thrust block, schematic section (from Blouin and Kaiser 1972).

array and thrust block, taken perpendicular to the array and intersecting the 4-ft structure, is shown in Figure 19. If it is assumed that the boundary joint is planar, as suggested by its intersection with the structures, an extension at a constant dip of 67° misses the bottom of the array by 23 ft. Since the true crater extends only 18 ft beyond the array at the testbed surface, it is likely that the joint misses the crater by a substantial margin as well.

Only 15 survey points on the east side of the explosive array were relocated post-test. These were all in the northeast quadrant at ranges between 40 and 50 ft in the vicinity of structures S_1 and S_2. As shown by the displacement vectors in Figures 11 and 12, motion was upward and horizontally *toward* the explosive array. Horizontal permanent displacements averaged about 0.5 ft toward the array, generally in a direction perpendicular to the strike of the major north-south joint set. Vertical displacements ranged from about 0.7 ft north of structure S_1 to about 1 ft near structure S_2. No permanent displacements occurred at this range on the west side of the array, being beyond the intersection of the boundary joint.

The horizontal displacements toward the explosive array were attributed to late time rebound of the testbed toward the crater (Blouin and Kaiser 1972). The open joints of the north-south set shown in Figure 7 and Figure 8 evidently resulted from the rebound. Obviously, the combination of joint orientations and properties and the ground motion field was somehow not right for the type of block relief which occurred on the opposite side of the array. It appears that the major east-west joint set could have provided such relief, since it dipped toward the explosive array on the east side. However, no major block slips occurred and the rock mass rebounded toward the array following its initial compressive loading. Because the crater had already formed by the time of the rebound, the motion could not be resisted by compression of rock within the crater. Thus, the rock mass tended to go into tension which caused en-echelon opening of joints in the north-south set oriented approximately perpendicular to the maximum tensile potential.

Figure 20 is a view looking north past structure S_1, showing a prominent open joint intersecting that structure. Figure 21 shows the widest open joint, located north of S_1 approximately 5 ft from the crater. A view of some of the smaller en-echelon openings north of S_1 is shown in Figure 22. Width of openings in these figures varied from a fraction of an inch to 8 to 10 in. Depth of the open joints is not known, though it is estimated that in some cases it exceeded 30 ft. Figure 23 shows an open joint at a depth of 20 ft

Figure 20. A view north of structure S_1 (from Blouin and Kaiser 1972).

Figure 21. A view of a rebound fracture approximately 5 ft from crater edge (from Blouin and Kaiser 1972).

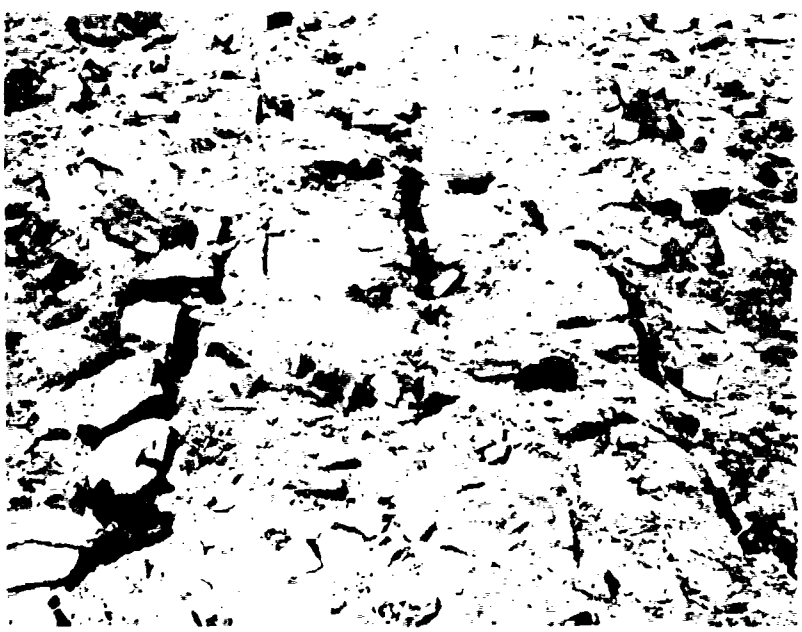

Figure 22. A view of open joints north of structure S_1 (from Blouin and Kaiser 1972).

Figure 23. A view of the north side of structure S_2 (from Blouin and Kaiser 1972).

which intersected the north side of structure S_2. Pebbles were dropped down this joint from the floor of S_2 to depths estimated in excess of 20 ft.

The upward vertical displacements on the east side, shown on the vector plot of Figure 12, evidently resulted from a general bulking of the testbed on that side. Since there were no well defined boundaries to this bulking on the test bed surface, it must gradually lessen with increasing range from the array. Close inspection of the walls of structures S_1 and S_2 in Figures 20 and 23 reveals that in addition to the open rebound joints, other joints, including horizontal ones, have been shaken loose in much the same manner as those within the joint block on the opposite side of the array. It is somewhat difficult, however, to envision that the bulking resulting from these open joints would be sufficient to cause vertical displacements on the order of ½ to 1 ft.

The motion monitoring instrumentation located throughout the STARMET testbed provided quantitative time-based comparisons between the motions within the thrust block, those outside the block and those on the opposite site of the array. From these comparisons it is possible to estimate a time-history describing the development of the relative displacement along the boundary joint. Typical particle velocity time-histories from within the thrust block are

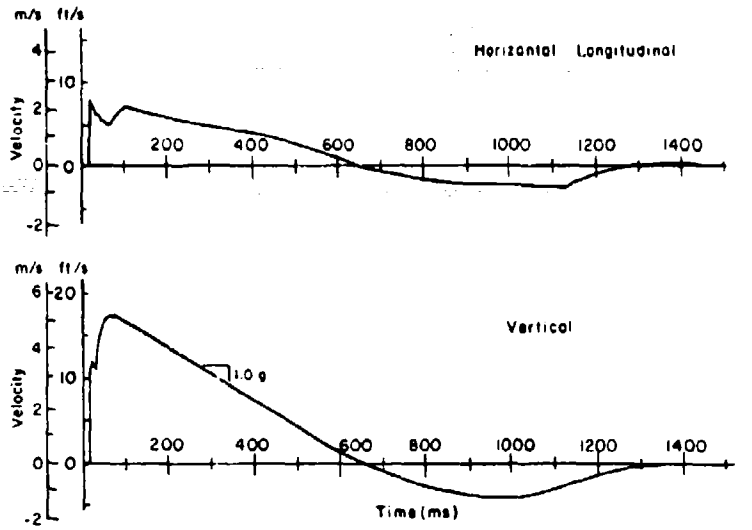

Figure 24. Horizontal longitudinal and vertical velocities at instrumentation hole 15, range—30 ft, depth—4 ft (from Blouin and Kaiser 1972).

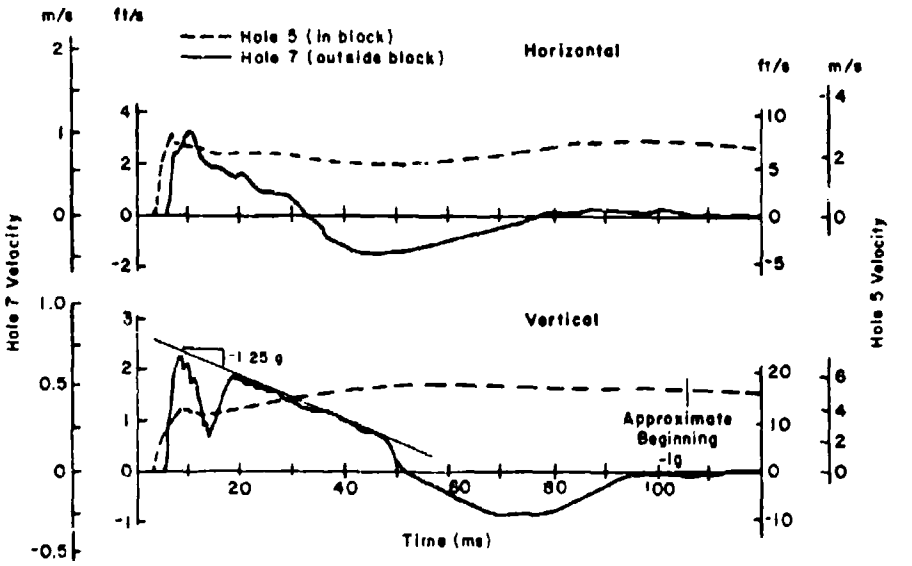

Figure 25. Velocity time histories, instrumentation holes 5 and 7, range—20 and 40 ft, respectively, depth—4 ft (from Blouin and Kaiser 1972).

shown in Figure 24. These were taken at a depth of 4 ft in instrumentation hole 15, located in the northern end of the block where displacement was at a maximum. Both the horizontal time history (positive velocities indicate motion away from the explosive array) and the vertical time history (positive velocities indicate motion upward) show a rapid rise to an initial peak followed by a short decay and then another slower rise to a second peak at 80 to 100 milliseconds (ms). The second peak is followed by a long decay to zero at 650 ms into a rebound ending back to zero at 1300 ms. The phase durations of both the positive and negative portions are approximately 650 ms. As shown in Figure 24, the long decay on the vertical time history is essentially linear at a slope of about 1 g. This would indicate that the block was in a state of

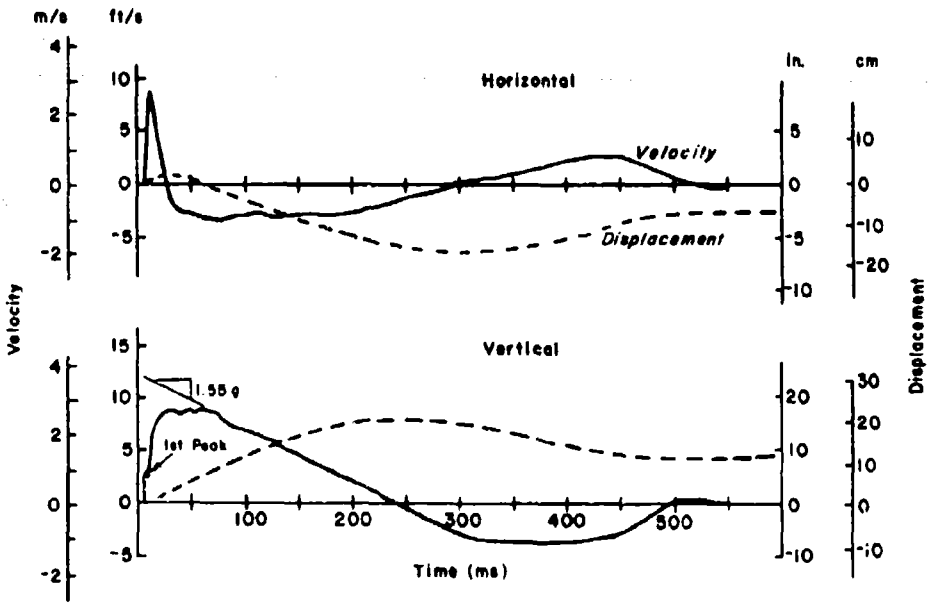

Figure 26. Velocity and displacement, hole 22, range—60 ft, depth—15 ft (from Blouin and Kaiser 1972).

free fall during this portion of the time history.

Motion within the block is contrasted with that outside the block in Figure 25, which compares the waveforms from hole 5 with those from hole 7, beyond the boundary joint, at the 4-ft depth. The rise times to initial peak are nearly equal at each location. However, beyond the boundary joint both the vertical and horizontal velocities rapidly decay, while those within the block show only a slight decay and then increase. These essential differences in the waveforms appear within 10 to 12 ms of the onset of motion and indicate that relative displacement along the boundary joint has commenced at this time. The rapid decay beyond the joint continues through both the positive and negative phases, resulting in waveforms more than an order of magnitude shorter than those from within the block. The linear portion of the vertical velocity decay in hole 7 has a slope of 1¼ g, an indication of restorative forces slightly in excess of those due to gravity.

Typical vertical and horizontal velocity time histories from a range of 60 ft on the east side of the array (hole 22) are shown in Figure 26. The rise times to first peaks are equivalent to those both within and outside the thrust block on the opposite side. The positive phase duration of the horizontal velocity is slightly shorter than that shown in Figure 25 beyond the thrust block, but the negative phase is about 6½ times as long as that beyond the block. The positive phase durations on the vertical time history are approximately equal, each lasting ¼ of a second, about the same duration as the negative phase duration on the horizontal time history. The linear portion of the vertical trace has a slope of 1½ g's, indicating some restorative force acting on the testbed in addition to gravity. The time during which this force acts is within the negative phase of the horizontal motion. If it is assumed that this restorative force is responsible for the long negative phase in the horizontal trace, then the net resultant would be a vector pushing the rock down and toward the crater.

The mechanics of this restorative force can be hypothesized from Figure 27, which shows displacement hodographs for gage stations located on opposite sides of the explosive array. These were constructed by combining the horizontal, longitudinal and vertical displacement time-histories from the 4-ft depth in hole 5 and from the 15-ft depth in hole 22. They show the displacement trajectories followed by these two points in a plane perpendicular to the explosive array viewed from the south. The point in hole 5, within the thrust block, clearly parallels the boundary joint. The thrust block slid up the joint a maximum of 78 in. at this point, then slid back down a distance of 23 in. Elapsed time was approximately 1300 ms. Indicated permanent displacements were 19½ in. horizontal and 51 in. ver-

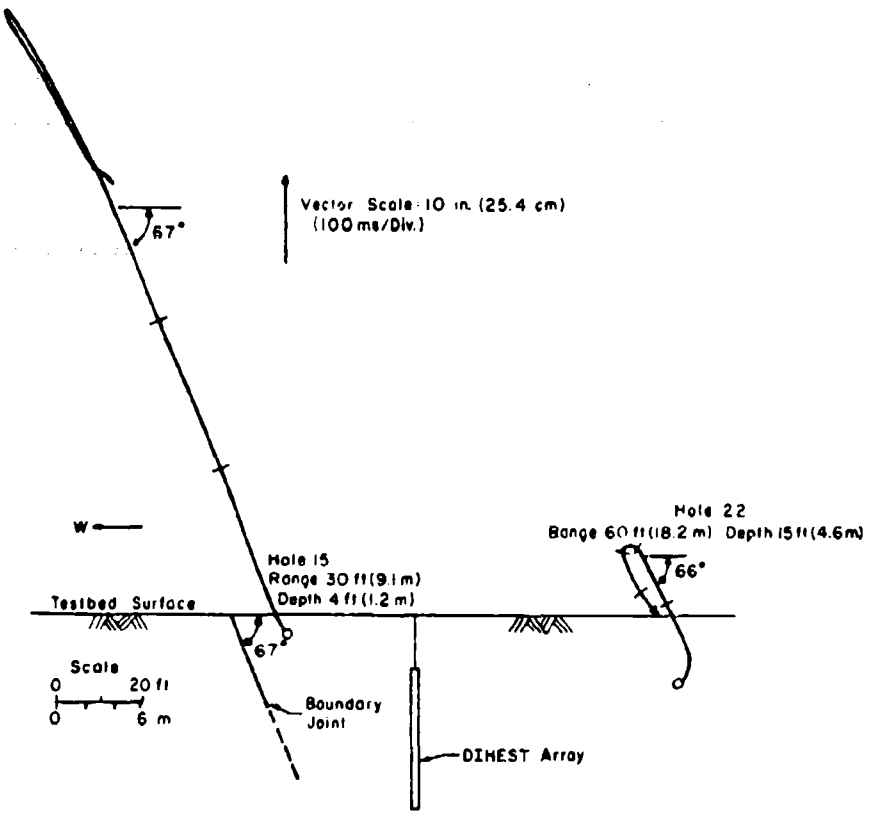

Figure 27. Displacement hodographs for opposite sides of STARMET array.

tical, which agree very well with those measured in the post-test survey at the testbed surface in this area.

The displacement hodograph from hole 22 on the opposite side of the array is surprisingly similar to that from hole 5. Initially, motion is upward and outward away from the explosive array, as would be expected from the initial arrival of compression waves from the detonation. However, within the first 40 ms, the displacement trajectory turns dramatically back toward the explosive array and then follows a path parallel to the boundary joint for nearly 200 ms, reaching a peak displacement of 15½ in. vertically upward and 6½ in. *toward* the array. Following the peak, there is a downward and outward return, similar to that in hole 5, again paralleling the boundary joint. The point comes to rest after about 500 ms, with a permanent displacement of 8 in. vertical and 2½ in. toward the array. This is in general agreement with the post-test surface displacements measured between the 40- and 50-ft ranges.

The relatively long, straight displacement trajectory parallel to that of the thrust block indicates that motion on the east side of the array may have been controlled by the northeast-southwest joint set of which the boundary joint on the west side of the thrust block is a part. Another possibility would be control by the north-south joint set having a dip similar in both angle and direction to the boundary joint. Occurrence of relative motion along either of these joint sets would be unexpected, since neither of them seems to offer a path of least resistance for relief of motion initially induced by the detonation. This can be seen in Figure 27, where the initial component of motion in hole 22 is nearly perpendicular to the subsequent path of relief. However, both the permanent displacement survey and the ejecta distribution pattern on the east side of the array strongly substantiate the hypothesis that motion was governed by a joint set dipping toward the east, away from the array.

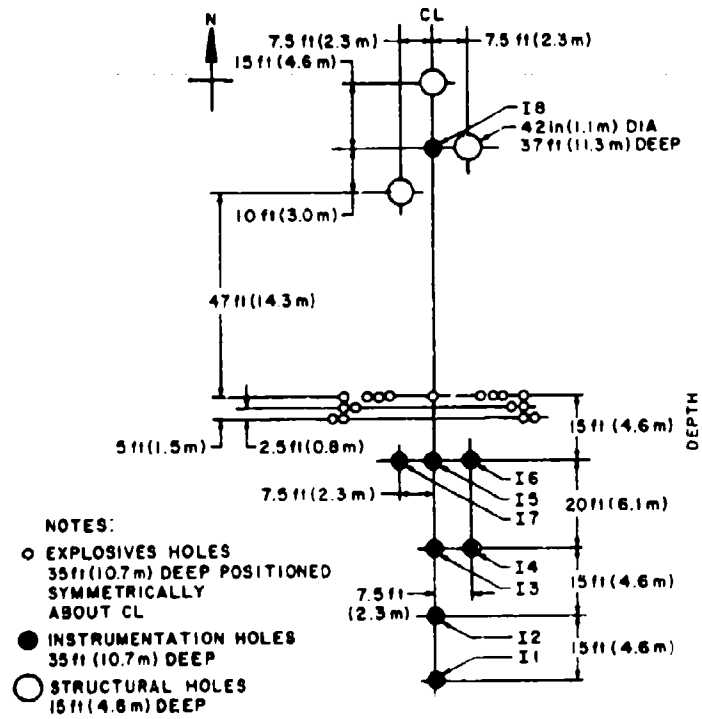

Figure 28. Plan view, explosive holes, PLANEWAVE II (from Blouin 1969).

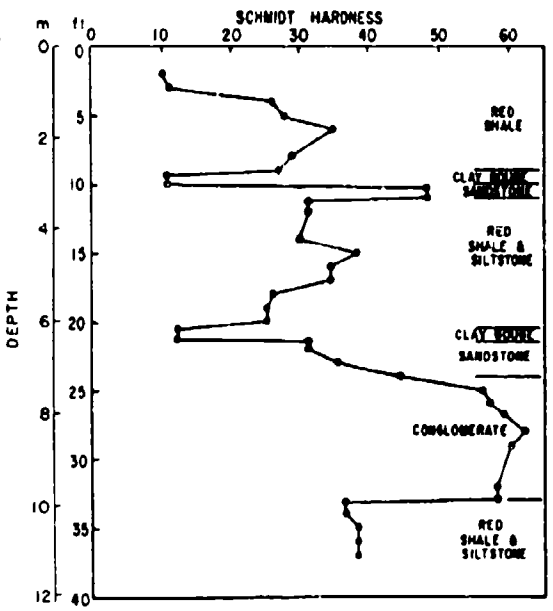

Figure 29. Schmidt hardness measured using a type N hammer on the walls of a 42-in. structural hole, range—57 ft (from Platt 1969).

PLANEWAVE II

Test description

PLANEWAVE II, fired on 16 March 1968, was the second DIHEST experiment in rock, and the only attempt at using a nonplanar explosive array designed to focus the energy into a prescribed volume of rock, thereby lessening the stress wave attenuation with range within this volume. While it is the only DIHEST experiment to conclusively exhibit relative displacements in layered sedimentary rock, such displacements have also resulted from high explosive cratering charge detonations (MIDDLE GUST, MIXED COMPANY) and from underground nuclear detonations (MIGHTY EPIC).

The explosive array, described by Blouin (1969), had a total yield of 2.1 tons and consisted of 105 standard 40 lb ammonium nitrate cratering charge canisters. These were grouted in 17 explosive holes, as shown in Figure 28, to form a "C" shaped array 45 ft in length with the center of charge at a depth of 22½ ft. This geometry was designed to minimize the peak particle velocity attenuation between the 15- and 35-ft ranges on the concave side of the explosive array.

As described by Pratt et al. (1969), the test site was located in the Estancia Valley, 45 miles east of Albuquerque, New Mexico, in a rather complicated sequence of interbedded sedimentary rock consisting of sandstones, siltstones, shales, quartz pebble conglomerates and limestones. Three 42-in.-diam. unlined structures were drilled, using a smooth wall boring technique, on the convex side of the "C" shaped explosive array as shown in Figure 28. The 37-ft deep structure, located at the 57-ft range provided an excellent view of the geologic section, a summary of which is shown in Figure 29. The top 3 ft consisted of a very soft clay shale. This was underlain by a harder red shale with occasional thin layers of soft clay shale, sandstone, and siltstone to a depth of 22 ft. A layer of sandstone extended from 22 to 25 ft where it graded into a conglomerate which extended to 33 ft. Red shale and siltstone underlay the conglomerate and extended to the bottom of the hole at 37 ft.

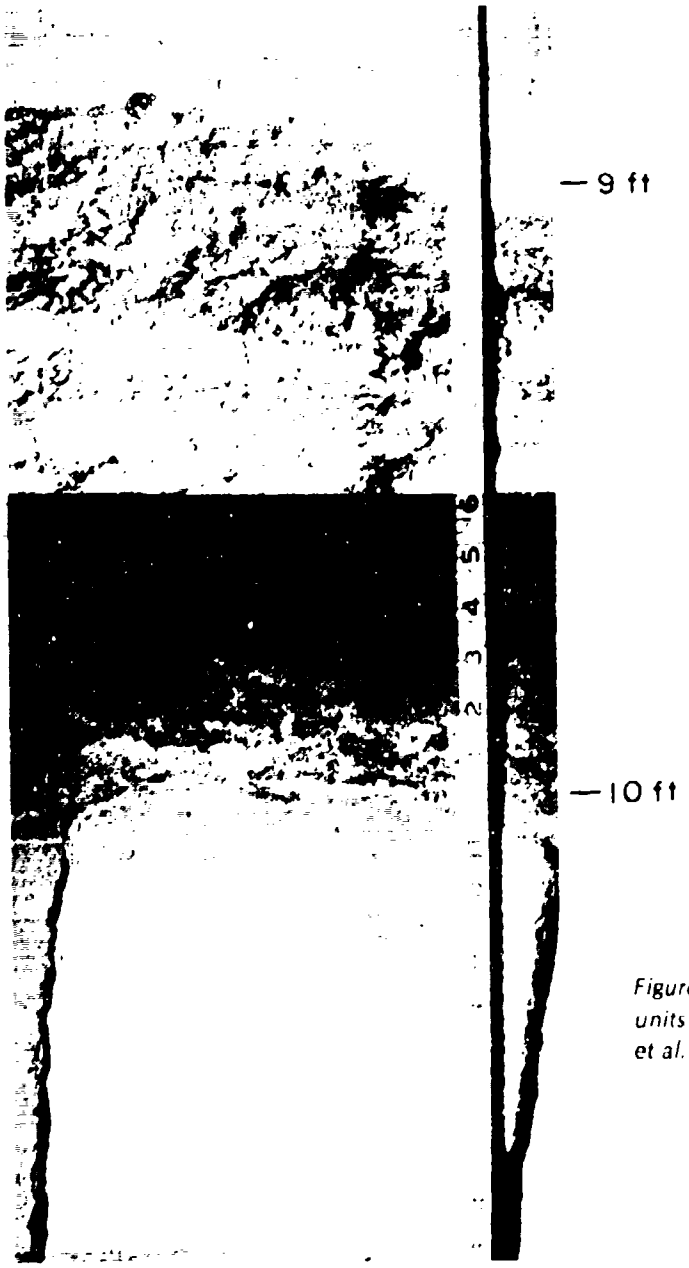

Figure 30. Contact between shale and sandstone units in 42-in. structural hole, depth — 10 ft (Flatt et al. 1969).

Included in Figure 29 are the results of a Schmidt hammer "hardness" survey taken at intervals throughout the depth of the hole. The Schmidt hammer is normally used to indicate unconfined compressive strengths of concrete. The rebound of a spring-loaded mass striking the concrete is indicated on the side of the hammer (the "hardness") and can be related to the compressive strength and Young's modulus of the concrete. The results of the survey are indicative of the tremendous variation in material properties between and within the individual layers. In general, the conglomerate was the "hardest" rock in the sequence followed in order by the sandstone, shale-siltstone, and soft clay shale.

Figures 30-36, from Pratt et al. (1969), illustrate the complexity and some of the more interesting details visible throughout the length of this hole. Figure 30 shows the shale sandstone interface at the 10-ft depth and the layer of soft

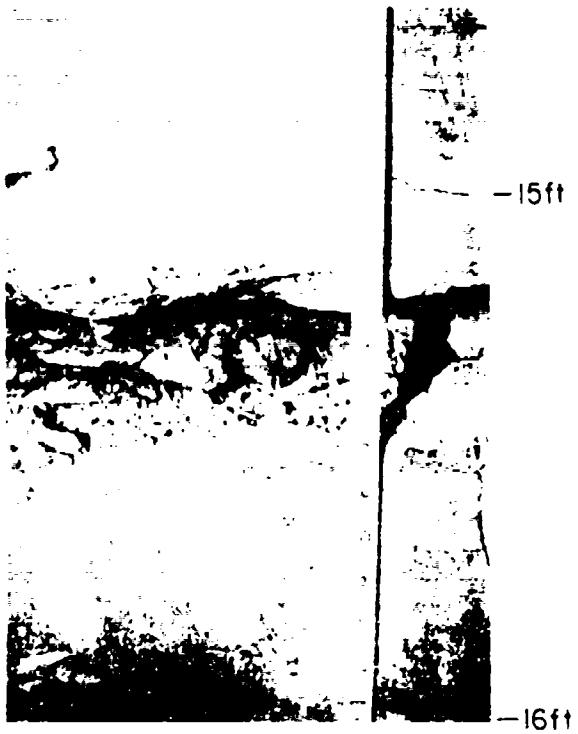

Figure 31. Gouge zone in red shale unit, depth—15 ft, 42-in. structural hole (from Platt and Zbur 1969).

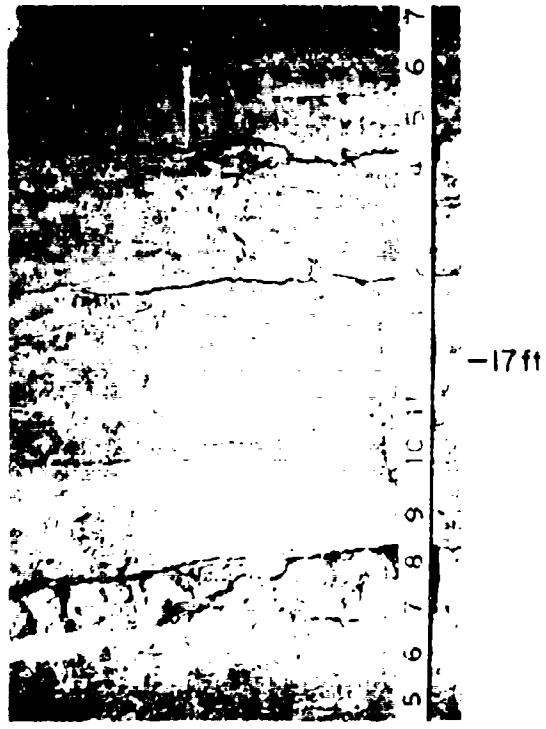

Figure 32. Horizontal partings in the red shale unit, depth—18 ft, 42-in. structural hole (from Platt et al. 1969).

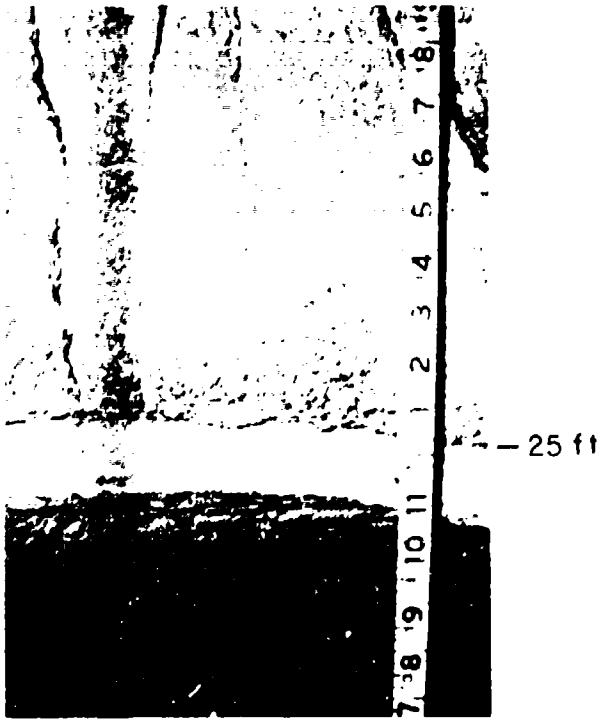

Figure 33. Siltstone lens in sandstone unit, depth—24 ft, 42-in. structural hole (from Platt et al. 1969).

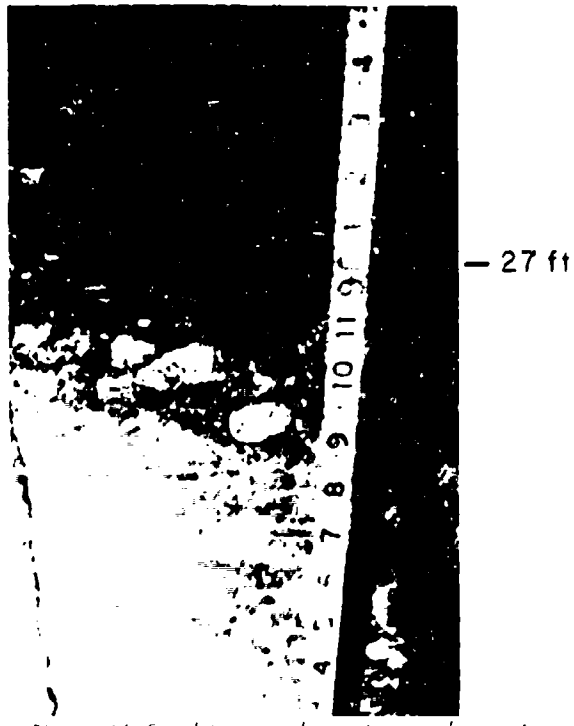

Figure 34. Sandstone and quartz conglomerate contact, depth—25 ft, 42-in. structural hole (from Platt et al. 1969).

Figure 35. Typical fracture in the quartz pebble conglomerate, 42-in. structural hole (from Platt et al. 1969).

clay shale between 9 and 10 ft. In general, the partings in the shale were horizontal, i.e. parallel to the bedding, while the jointing in the sandstone and conglomerate was vertical. Typical vertical joints in the sandstone layer are visible in the bottom half of the figure. Figures 31, 32 and 33 show some of the minor thin beds (1 to 4 in. thick) common throughout the sequence. The beds in Figures 31 and 32 occurred in the red shale at depths of 15½ and 17½ ft, respectively. These were composed of soft clay shale which partially washed out during the drilling. Note the predominant horizontal partings within the shale in Figure 32. A thin siltstone bed within the sandstone layer at a depth of 25 ft is shown in Figure 33. The sandstone-conglomerate interface at the 27 ft depth is shown in Figure 34. The intersection of the hole wall with the quartz inclusions in the conglomerate showed that the particle size of the quartz pebbles ranged up to approximately 2 in. in diameter. Figure 35 shows the intersection of a typical vertical joint in the conglomerate with the hole wall. The joint is open approximately ¼ in. at this point. A second open vertical joint in the conglomerate is shown in Figure

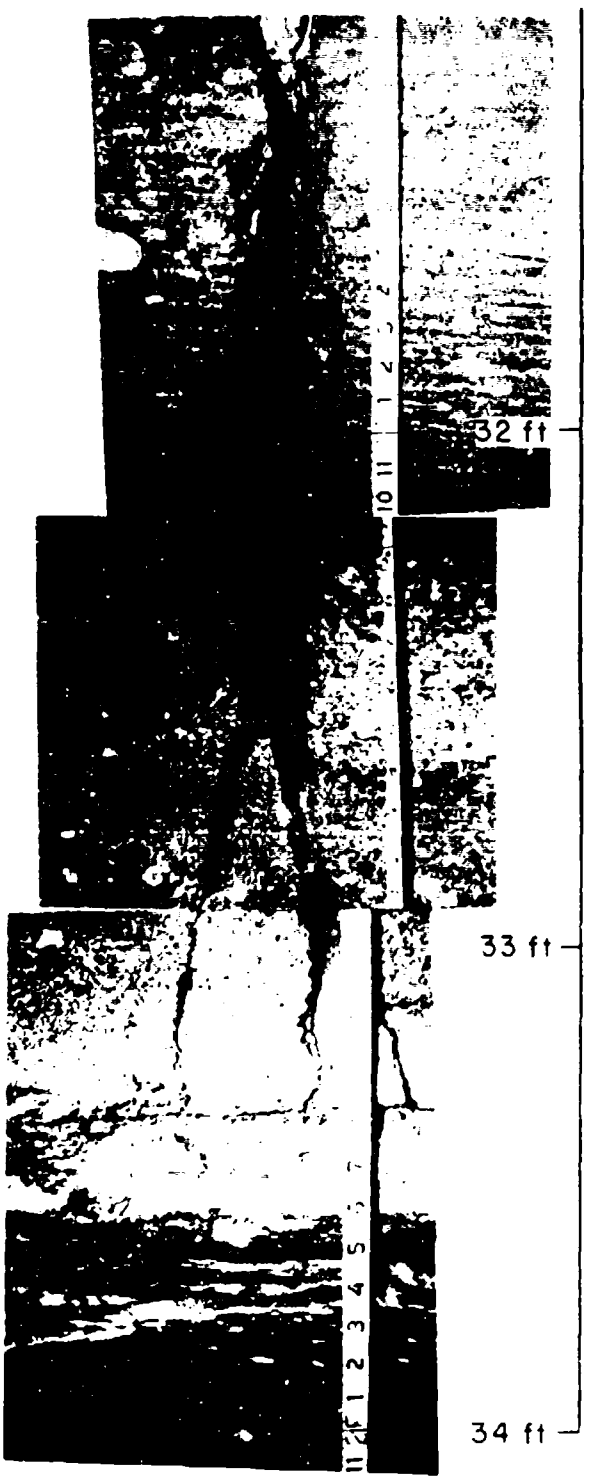

Figure 36. Very large vertical fracture in the quartz pebble conglomerate, depth — 32-34 ft, 42-in. structural hole (from Platt et al. 1969).

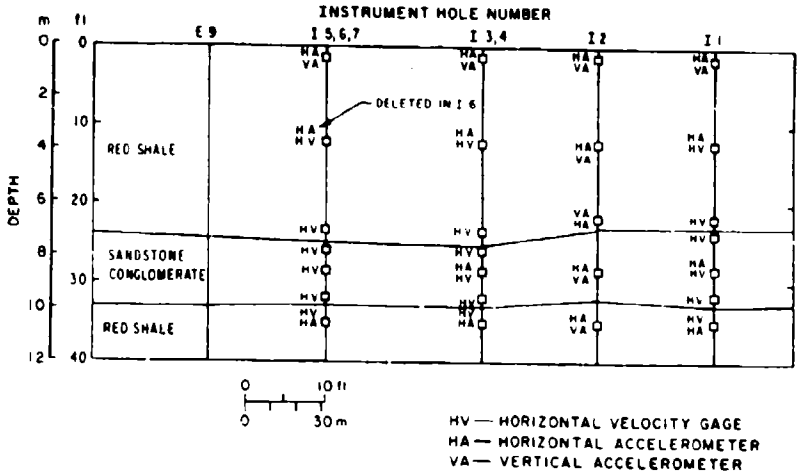

Figure 37. Section view, PLANEWAVE II instrumentation (from Blouin 1969).

36. This joint had an opening of nearly 1¼ in. at its widest point. Prior to drilling, the opening was filled with a soft clay material, as can be seen near the top of Figure 36, which washed out during the drilling. The interface between the bottom of the conglomerate and the underlying red shale is apparent near a depth of 33⅓ ft. Note the abrupt termination of the vertical joint in the interface.

For instrumentation purposes, the sequence was modeled as a three-layer system, with the sandstone-conglomerate taken as a single layer sandwiched between red shale on its top and bottom. Ground motions were monitored with velocity gages and accelerometers grouted in the eight free-field instrumentation holes shown in Figure 28. A section view of the instrumentation locations and idealized layers is given in Figure 37. Instrumentation was located near the top, middle and bottom of the top two layers and near the top of the bottom layer. Instrumentation hole 8, adjacent to the 37-ft structure, contained accelerometers only, between 20 and 35 ft deep.

Test results

The outstanding features noted post-test were a series of differential slips along horizontal beds or planes of separation in the structures at the 47- and 57-ft ranges (Vaughan 1969). These are shown in the downhole view of the 15-ft deep structure at the 47-ft range in Figure 38. At least six slip planes were visible. These allowed the base of the structure to move outward relative to the top in much the same manner as a deck of cards is displaced when pushed from the side. The sum of the individual displacements totaled approximately 5 in. The structure at the 57-ft range experienced similar motions with the top shale layer, though the displacements were only about half those of the 47-ft range structure. No significant differential motions occurred within the 72-ft range structure.

Figure 38. Differential displacements along bedding planes — PLANEWAVE II (from Blouin 1969).

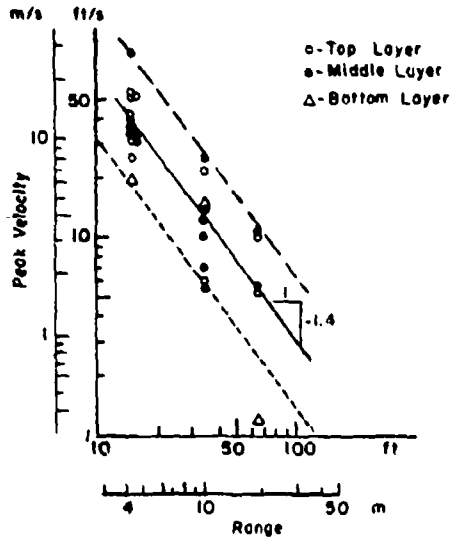

Figure 39. Peak velocity vs range—PLANEWAVE II.

With only minimal free field instrumentation on the structures' side of the array (only one accelerometer produced any data) the ground motion field in the vicinity of the structures must be estimated from the measurements on the opposite side of the array. Experience with the DIHEST geometry and data analysis has shown that at ranges beyond the half length of the array (in this case 22½ ft), the array geometry has little effect on the attenuation of ground motions; i.e. beyond this range the explosive array can be approximated as a point source equal in yield to the total DIHEST yield (Cooper and Blouin 1971). Thus, even though the PLANEWAVE II array was designed to reduce attenuation within 35 ft, it is estimated that at the ranges of the structures (more than two half-lengths) the peak particle velocities on one side differed little from those on the other. Figure 39 is a logarithmic plot of peak velocity as a function of range. The more

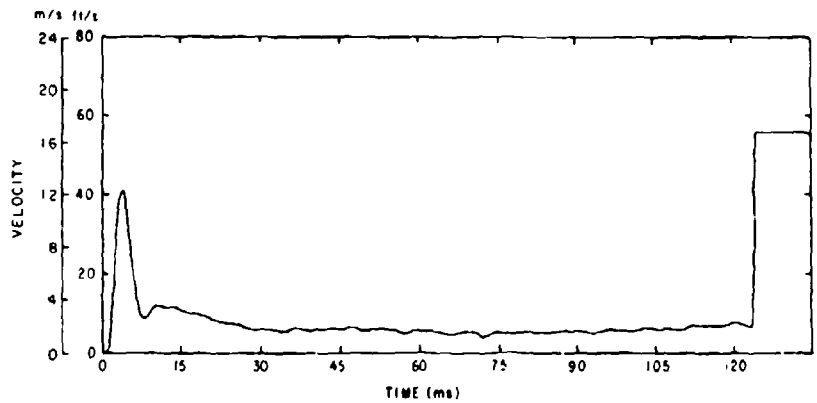

a. Range—15 ft, depth—12.5 ft.

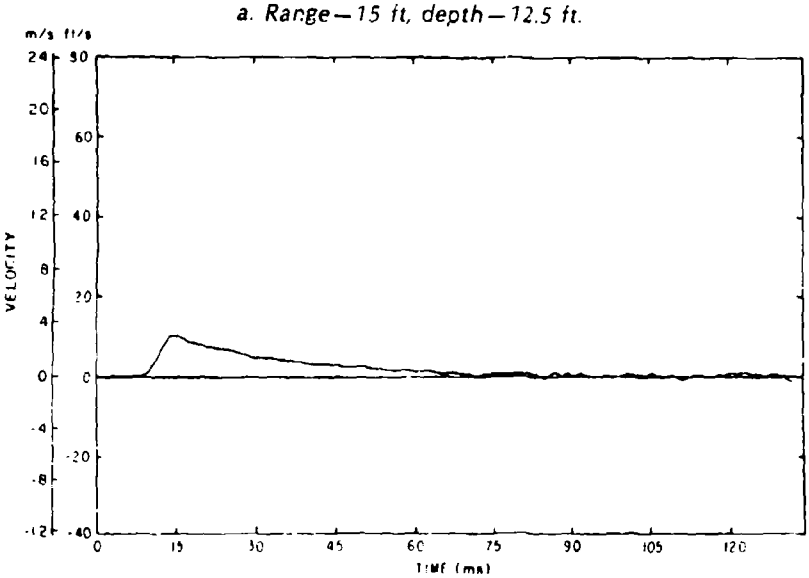

b. Range—65 ft, depth—12.5 ft.

Figure 40. Typical velocity vs time—PLANEWAVE II (from Blouin 1969).

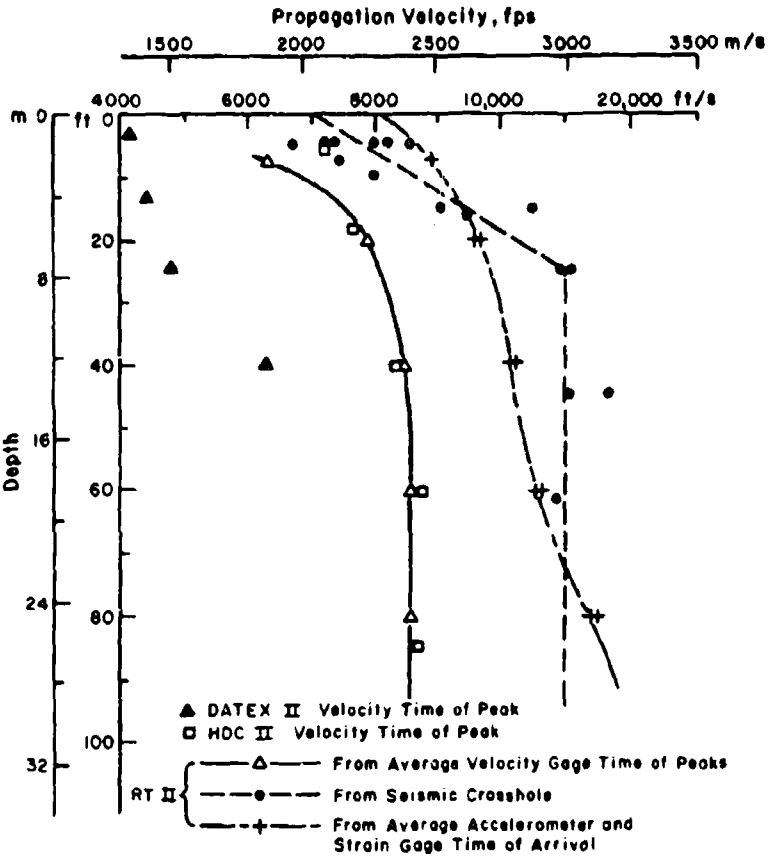

Figure 41. Seismic and peak horizontal stress propagation velocities for ROCKTEST II, HANDEC II, and DATEX II.

varied materials at the PLANEWAVE II site may account for the factor of five data scatter at any given range, which is somewhat higher than that experienced in other DIHEST shots. Taking the fit shown in Figure 39, the estimated average peak velocities at the 47-, 57-, and 72-ft ranges are 8½, 6½ and 5 ft/s, respectively. The single integrated accelerometer record at the 57-ft range agrees well with these estimates, having a peak velocity of 5 ft/s. The velocity positive phase duration between the 35- and 65-ft range averaged 41 ms. Typical velocity time-histories at the 15- and 65-ft ranges are shown in Figure 40. Because of poor instrument cable protection and baseline shifts, the data on peak and permanent displacements are inconclusive.

A concerted effort was made to define in situ material properties at the Cedar City site for use in computer calculations and predictions of ground motions. Results are summarized by Cooper and Blouin (1971) and by Blouin (1970d). Compression wave velocity as a function of depth at the ROCKTEST II site is shown in Figure 41. There is reasonable agreement between the seismic crosshole velocities and the velocities obtained from first arrival of the DIHEST pulse. These tend to show a substantial increase in velocity with depth in the top 30 ft of the testbed. Near surface velocities are on the order of 8,000 ft/s and range up to over 11,000 ft/s at depth. This corresponds to the transmission velocity of peak stress which is always slower than the seismic or first arrival velocities. The transmission velocity of peak stress ranges from approximately 6,000 ft/s near the testbed surface to 8,500 ft/s at depth. Cooper and Blouin (1970) note that the dynamic confined modulus of deformation, E_D given by

$$E_D = \varrho c_p^2 \qquad (1)$$

where ϱ is mass density and c_p the peak stress

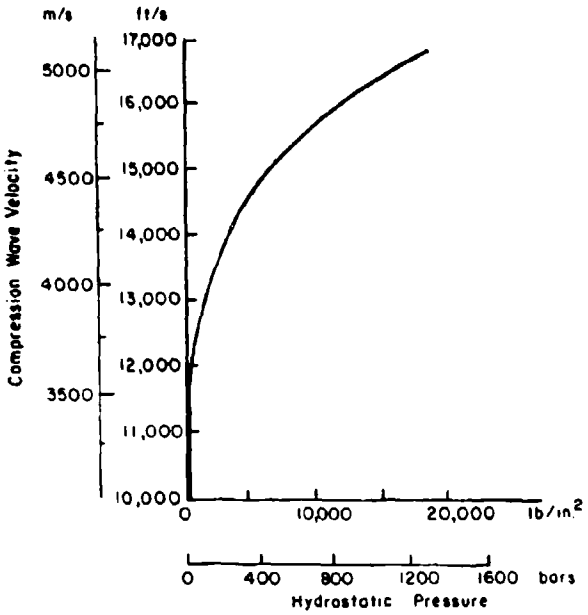

Figure 42. Laboratory compression wave velocity for HANDEC II site specimens vs hydrostatic pressure (from Calhoun and Stephenson 1969).

propagation velocity, controls deformations within a testbed. The peak stress propagation velocity, rather than the seismic velocity, is used to compute the deformation modulus.

An indication of the variation of material properties from site to site is also shown in Figure 41 where peak stress propagation velocities from DATEX II and HANDEC II are compared to those from ROCKTEST II. The HANDEC and ROCKTEST velocities are nearly identical, as would be expected from the close proximity of the two tests. The DATEX velocities are significantly lower than the others, possibly indicating a considerably softer in situ rock at that site. The DATEX site was somewhat removed from the others, being located approximately 600 ft east and downslope from the ROCKTEST site. Some of this velocity difference may be explained by the fact that both the ROCKTEST II and HANDEC II testbeds were under considerable confining pressure from the HEST event at the time the DIHEST was fired. For instance, the HANDEC II DIHEST was initiated 46.0 ms after detonation of the HEST explosives. Pressure in the HEST cavity is estimated to have been on the order of 1000 lbf/in.² during passage of the stress waves from the DIHEST detonation. Figure 42 shows the influence of confinement on sonic laboratory compression wave velocity in intact specimens from the HANDEC II testbed. If these data are extrapolated to the field situation, one would expect an increase of approximately 30% in stress wave transmission velocity to result from a 1000 lbf/in.² HEST loading. This would tend to negate some, but not all, of the difference between the DATEX II propagation velocities and those from HANDEC II and ROCKTEST II.

DATEX II

Test description

DATEX II was the first DIHEST array to utilize slurry explosives. To produce the ground motions needed for a viable test of the large ROCKTEST II structures, it was necessary to increase the explosive density used in past DIHEST arrays by nearly an order of magnitude. The use of explosive slurry pumped into unlined holes was chosen as the most expedient means of achieving this increase. DATEX II served as a proof test of the slurry explosive concept. A total of 41 tons of aluminized ammonium nitrate slurry* was loaded into 29 nominal 12-in.-diam explosive holes spaced 7.14 ft on center between a depth of 29 and 65 ft. The explosives were contained with keyed grout and concrete plugs as shown in the section view of Figure 43. The explosive array thus formed was 200 ft long and 36 ft high with the center of the explosive mass at a depth of 47 ft. Density was 11.4 lb/ft³ of array,

*DBA-X2M slurry explosive, manufactured by Inter-mountain Research and Engineering Co. Inc., West Jordan, Utah.

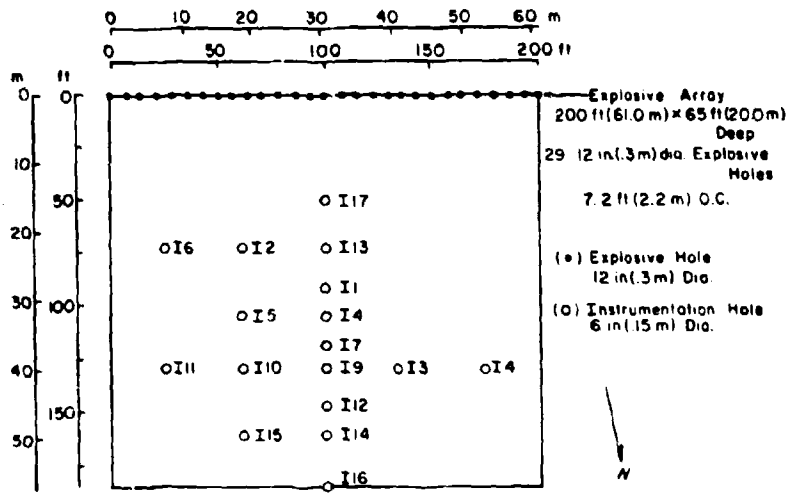

a. *Plan view.*

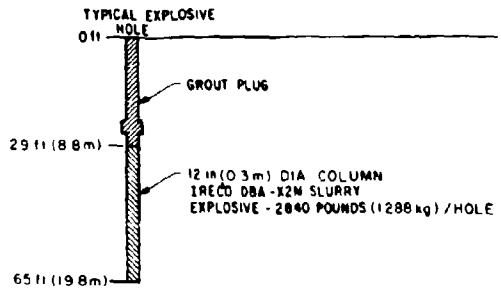

b. *Explosive hole section.*

Figure 43. Plan view of DATEX II (from Blouin 1970a).

which contrasts with a density of 1.1 lb/ft³ of array used on the DATEX I and HANDEC I arrays and 1.3 lb/ft³ used on STARMET.

With the increased density, it became necessary to cover the explosive array with a large trapezoidal earth berm in order to keep rock ejecta from endangering the instrumentation vans and personnel. The DATEX II berm, shown in section in Figures 44 and 45 averaged 45 ft high and contained approximately 115,000 cubic yards of soil.

As shown in Figure 43a, all active ground motion measurements were made on the north side of the explosive array at ranges from 50 to 185 ft. Instrumentation consisted of velocity gages, accelerometers, and strain gages which were located between 3 and 41 ft in depth. Four structures, described by Plamondon and Browder (1970), were located on the south side of the array. Structures 1, 2, and 4 were unlined, smooth-walled, 6 ft in diameter, 15 ft deep, and located at 95-, 110- and 125-ft ranges, respectively. Structure 3 was perimeter drilled, blasted and hand excavated. It had a liner consisting of a 6-ft-diam section of steel culvert backfilled to the rock walls with approximately 9 in. of nonreinforced concrete. There were no ground motion measurements on the structure's side of the array.

As with other early DIHEST experiments, no effort was made to determine post-test permanent displacements within the testbed. In fact, most of the DATEX II bed was covered with a thin layer of soil, which, combined with the huge amount of berm material lofted onto the testbed (see Fig. 44 and 45), would have made it impossible to detect any differential displacements within the testbed without an extensive post-test

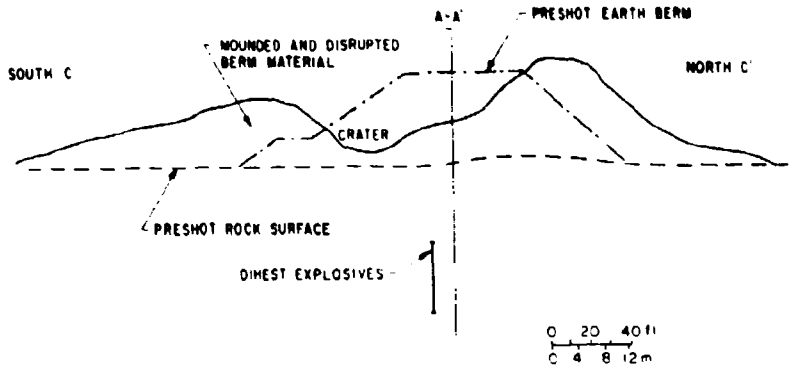

Figure 44. North-south section of DATEX II berm and apparent crater (from Blouin 1970a).

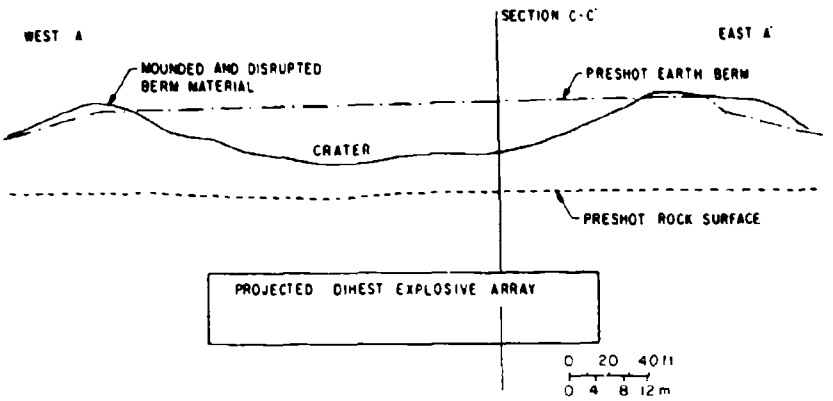

Figure 45. East-west section of DATEX II berm and apparent crater (from Blouin 1970a).

excavation program. Only the structures were surveyed pre-test and located and resurveyed post-test.

Test results

Dramatic evidence of relative displacements was observed in the DATEX II structures. This is summarized by Plamondon and Browder (1970) and by Blouin (1972). Structure 1 at the 95-ft range (Fig. 46) was so severely damaged that reentry was impossible. The pipe in the picture is what remains of one of the diameter change monitoring systems. Figure 47 is a view of structure 2 and the 110-ft range during reentry. Relative displacements (on the order of 2 ft) along nearly horizontal joints are visible in the photograph. The lined structure 3 at the 110-ft range suffered a severe relative displacement in which the top 5 ft of the structure was displaced 13 ft relative to the bottom section. The top section is shown in Figure 48 and the bottom section in Figure 49. Plamondon and Browder (1970) hypothesize that the structure was intersected by a joint dipping gently toward the explosive array, as shown schematically in Figure 50. Relative displacement along the joint is similar to that shown in the photograph of structure 2, but the magnitude is much greater. Though structure 4 was only about 20 ft from structures 2 and 3, it suffered relatively little damage from relative displacements along nearly horizontal joint planes. Rather, a block of rock bounded by two vertical joints was propelled nearly 6 in. into the structure on the blastward side as shown in Figure 51. The opposite effect was noticed at the back of the structure, where the same block moved several inches radially outward, indicating that the block, though only a little more than 1 ft thick, was quite extensive in area and extended a considerable distance below the structure.

Figure 46. Upper portion of DATEx II structure 1, range—95 ft.

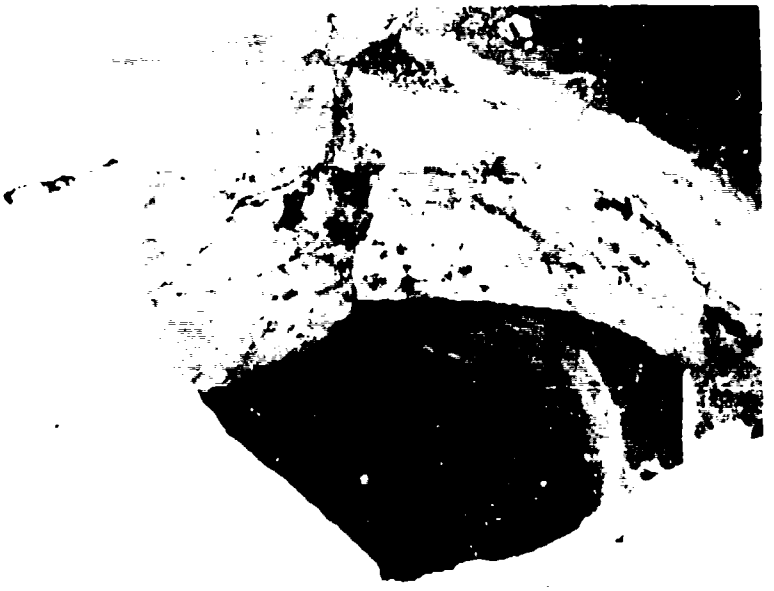

Figure 47. Upper portion of DATEX II structure 2, range—110 ft.

Figure 48. Top section of DATEX II structure 3, range — 110 ft.

Figure 49. Bottom section of DATEX II structure 3, range — 110 ft.

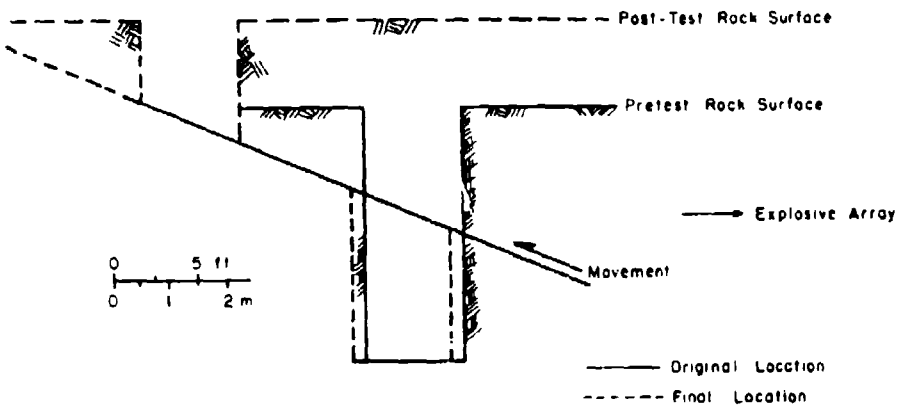

Figure 50. Hypothesized failure mechanism for DATEX II structure 3 (from Plamondon and Browder 1970).

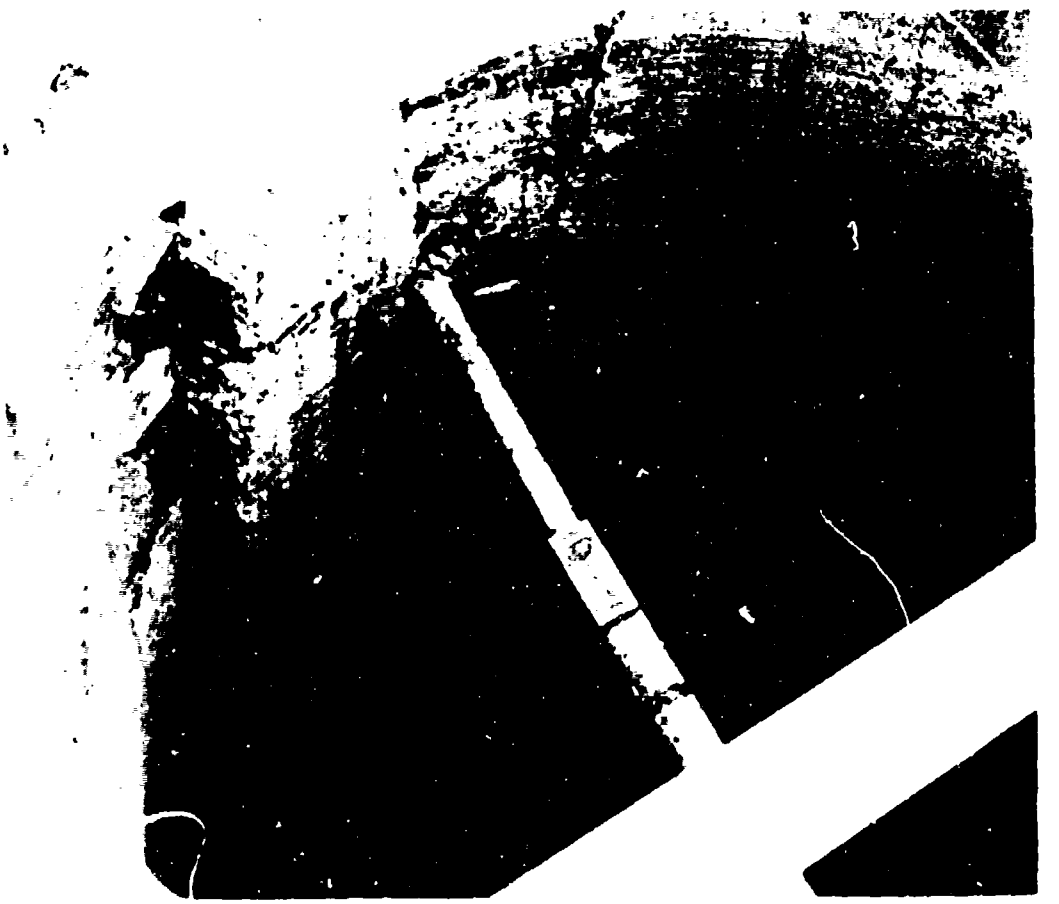

Figure 51. Top view of DATEX II structure 4, range = 125 ft (from Blouin 1970a).

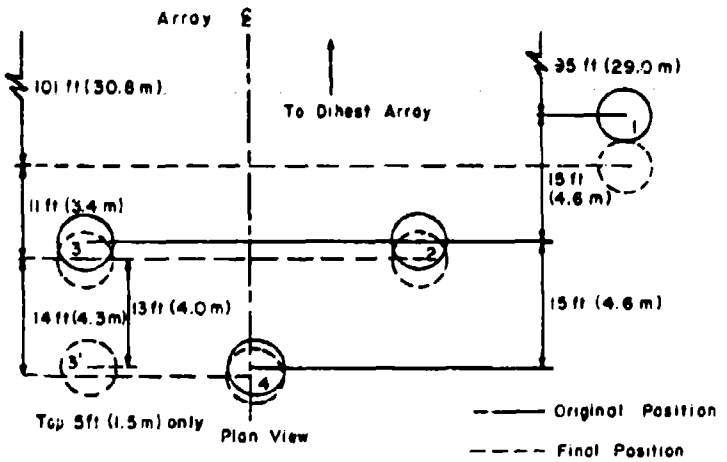

Figure 52. Permanent displacement of DATEX II structures (from Blouin 1970).

Figure 52 is a plan view of the nominal permanent displacements of the four DATEX II structures. Ignoring the 13-ft relative motion, these displacements vary from approximately 6 ft at the 95-ft structure to 1 ft at the 125-ft structure.

Since no active ground motion instrumentation was located on the structures' side of the array, the motion on the instrumentation side will be summarized, assuming that it is indicative of motion on the structures' side. Figure 53 is a displacement hodograph showing the displacement trajectories in the vertical plane of symmetry perpendicular to the explosive array. Though no post-test excavation was carried out to define the true crater boundaries, the ROCKTEST II crater (using a similar DIHEST explosive array) extended 80 ft from the array. If this dimension is assumed for the DATEX II crater, both the trajectories in hole 17 would be placed within the crater. Beyond the crater, displacement patterns are similar to those expected from calculations based on first principles of

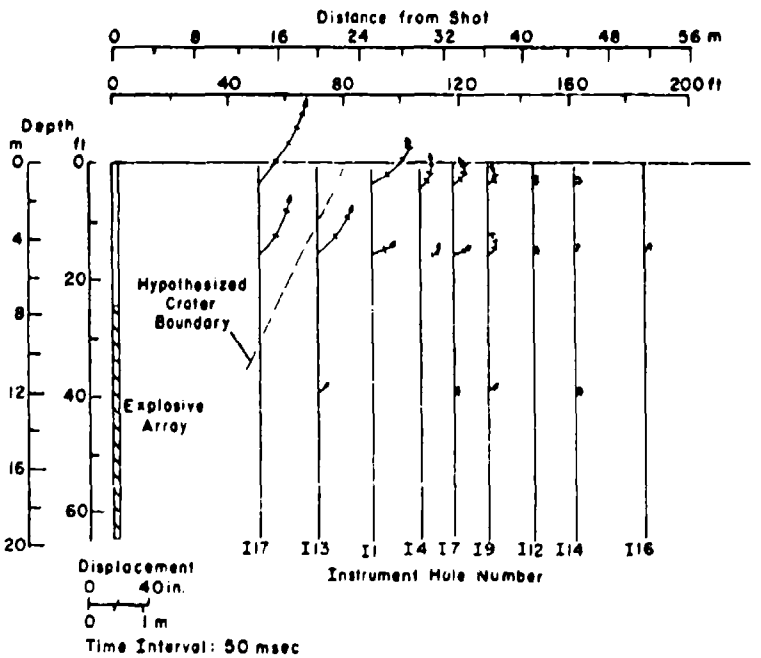

Figure 53. DATEX II displacement trajectories.

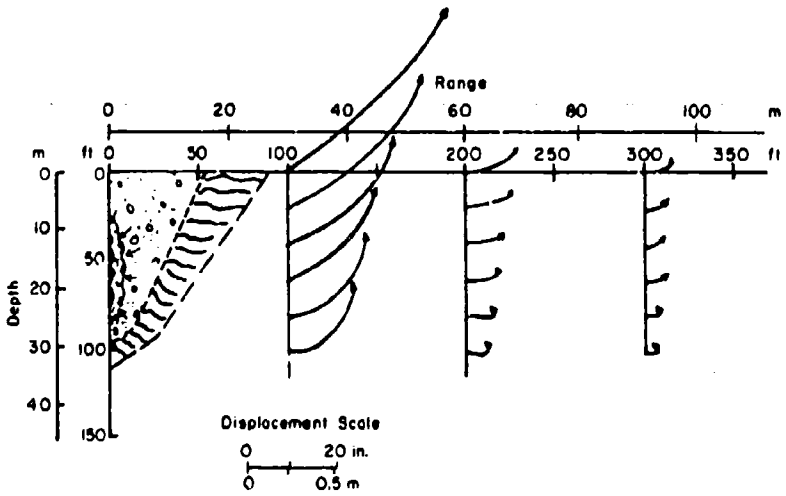

Figure 54. Typical computed DIHEST mean particle trajectories (from Cooper et al. 1971).

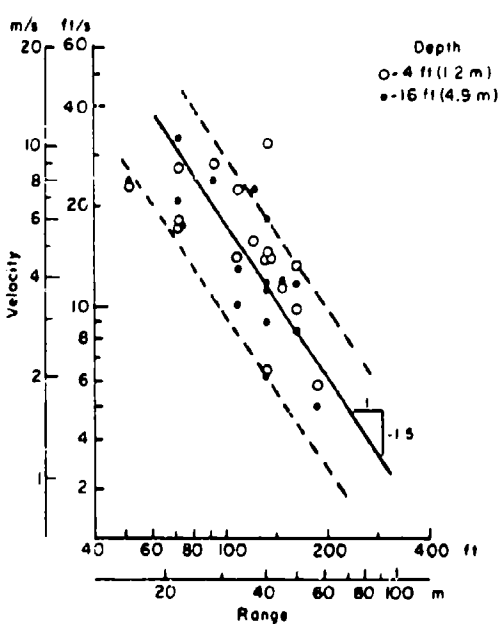

Figure 55. DATEX II near-surface peak horizontal velocities.

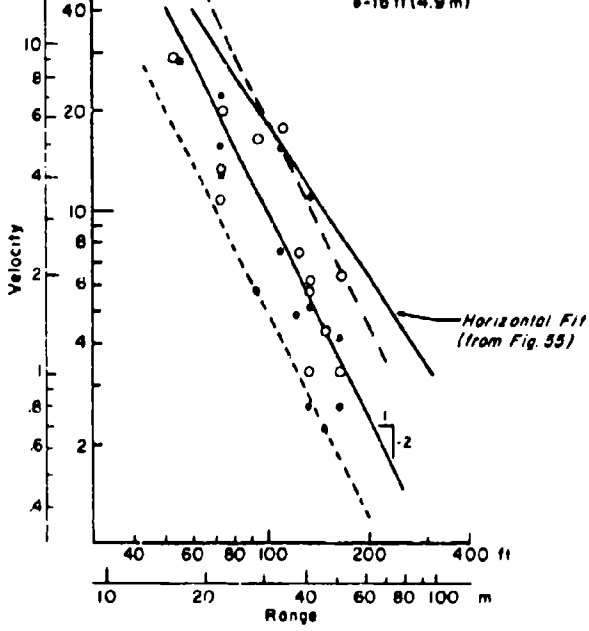

Figure 56. DATEX II peak vertical velocities.

mechanics (Cooper et al. 1971) shown in Figure 54. Initial motion results from arrival of the compression wave and is directed away from the array along a line originating at the center of mass of the charge. Soon thereafter, free surface effects tend to turn the displacements upward toward the surface. It is apparent from the DATEX II trajectories that significant near-surface displacements (1 ft or more) occurred out to a range beyond 130 ft. These tend to be in good agreement with the permanent structural displacements shown in Figure 52.

A plot of peak horizontal velocities from the near-surface gages is shown in Figure 55. Data scatter at any given range is nearly a factor of three. Using the fit shown, nominal projected

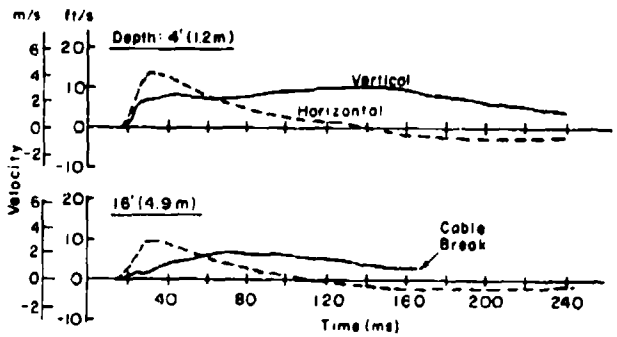

Figure 57. DATEX II velocity time histories for hole 4, range—110 ft.

horizontal velocity at the 95-ft structure was 18½ ft/s, dropping to 12½ ft/s at the 125-ft structure. A similar plot of peak vertical velocities is shown in Figure 56. A comparison to the horizontal fit shows peak vertical velocities to attenuate considerably faster than the peak horizontal velocities. Nominal projected vertical velocity at the closest structure is 10 ft/s and at the farthest structure 7½ ft/s. Typical vertical and horizontal time histories (from Blouin 1970a) are shown in Figure 57. These are from hole 4 at a range of 110 ft and depths of 4 and 16 ft. They are similar in form to the time histories from the east side of the STARMET array in that horizontal motion is restrained while vertical motion is not. Positive phase duration of the horizontal traces is approximately 100 ms, while the vertical duration extends well beyond 250 ms.

HANDEC II

Test description

HANDEC II was the second combined HEST-DIHEST shot at Cedar City. The first combined test, HANDEC I, used a duplicate of the DATEX I and STARMET DIHEST arrays but as noted previously, produced no significant relative displacements. A plan view of HANDEC II (as described by Blouin 1970b) is shown in Figure 58. The HEST was a nominal 60 ft long by 90 ft wide, and was designed to simulate the airblast and airblast-induced ground motions from a 1-megaton surface burst at the 3000-lbf/in.^{2} overpressure range. The DIHEST was detonated 46 ms after the HEST to produce the time delay between the airblast arrival and direct induced arrival appropriate for the design criteria. The DIHEST array was positioned 95 ft to the west of the HEST facility. The array had a total explosive yield of 46 tons. A 7.14-ft on-center hole spacing was used with the slurry contained at between a depth of 25 and 65 ft. The explosive slurry and other details of the array are identical to those described in the section on DATEX II.

A large earth berm was again employed to contain the ejecta from the DIHEST detonation. The height of the berm was reduced from 45 ft on DATEX II to about 40 ft. Pre- and post-shot sections through the berm and testbed are shown in Figures 59 and 60. Pre- and post-shot airphotos of the berm are shown in Figures 61 and 62. Note the close proximity of the ROCKTEST II testbed.

Active ground motion instrumentation was located in the 13 instrumentation holes shown in Figure 58 between ranges of 55 and 180 ft from the DIHEST array and at depths from the HEST testbed surface to 60 ft (see Blouin 1970c for a complete description of the instrumentation). As shown in Figure 58, the HEST bed was partitioned into two halves. The southern half contained the free field instrumentation, and the northern half contained two experimental structures, S_{11} and S_{12}, along with experimental closures, S_{13}-S_{19}, extending only a few feet into the testbed. Structure S_{11} had an inside diameter of 6 ft, a depth of 20 ft, and an 8-in. wall of reinforced concrete lined internally with a $^3/_{16}$-in. welded steel cylinder. Structure S_{12} was similar to S_{11} except that it was surrounded with a soft 6-in. layer of foamed concrete backpacking. Complete details of the structural experiments in HANDEC II can be found in Carellas and Browder (1969), Higgins (1970), and Carellas (1970).

The HEST bed was thoroughly cleaned prior to the test and a complete joint map, shown in Figure 63, was prepared. The predominant joint set strikes nearly north-south with a vertical dip.

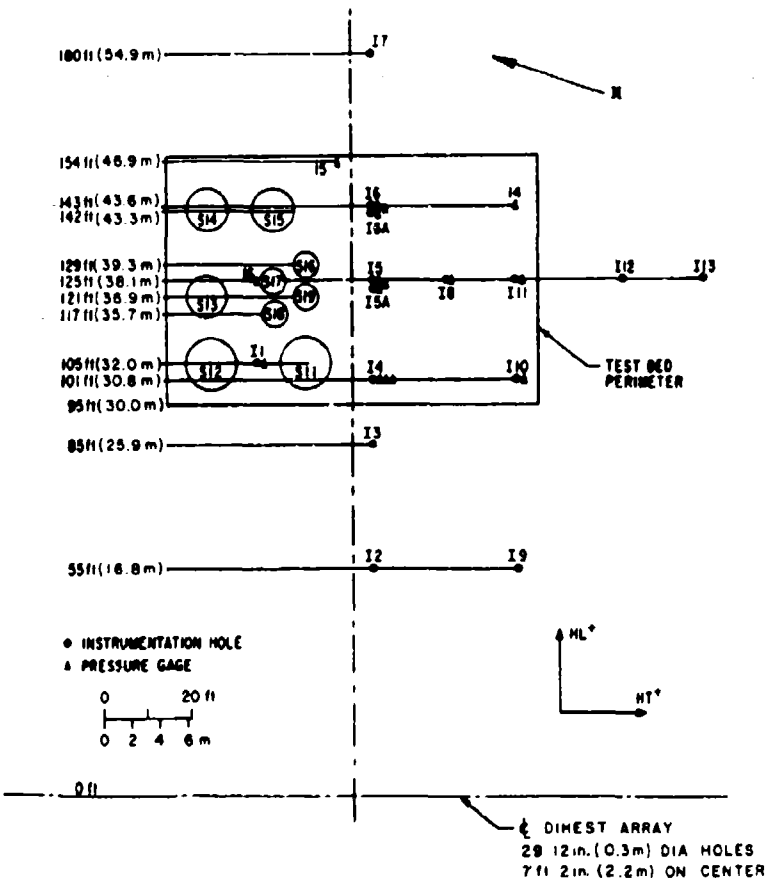

Figure 58. Plan view of HANDEC II (from Blouin 1970c).

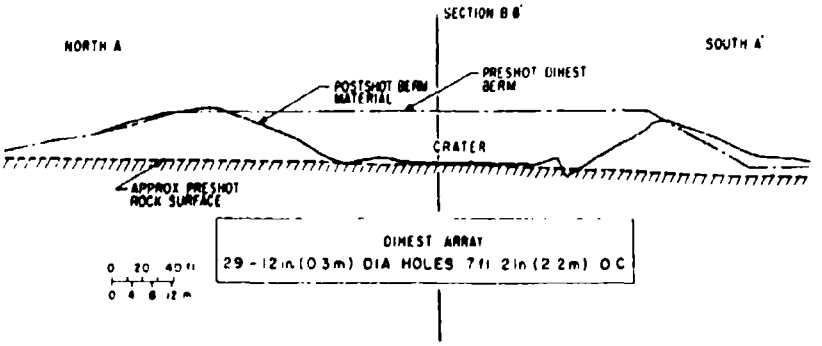

Figure 59. North-south section of HANDEC II berm and apparent crater (from Blouin 1970c).

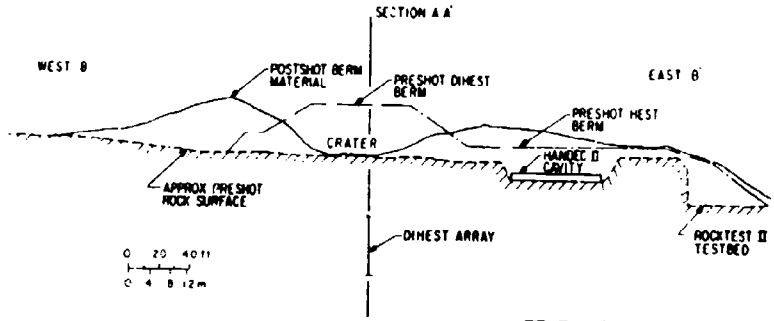

Figure 60. East-west section of HANDEC II berm and apparent crater (from Blouin 1970d).

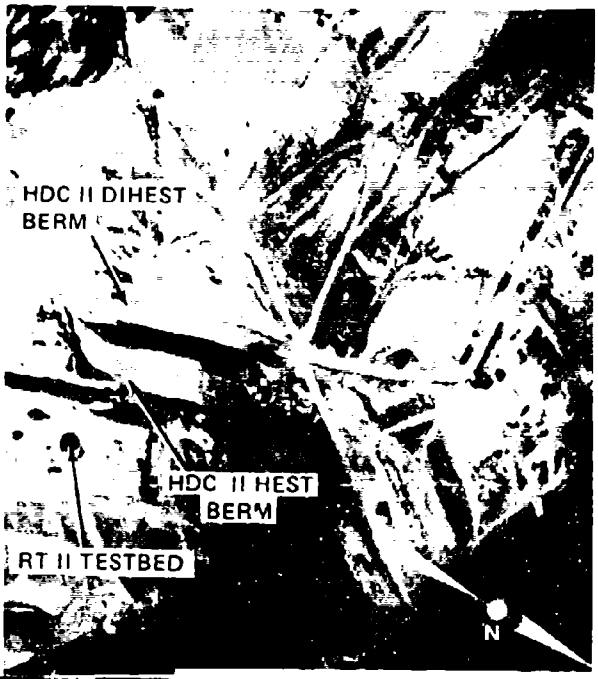

Figure 61. HANDEC II pre-shot airphoto.

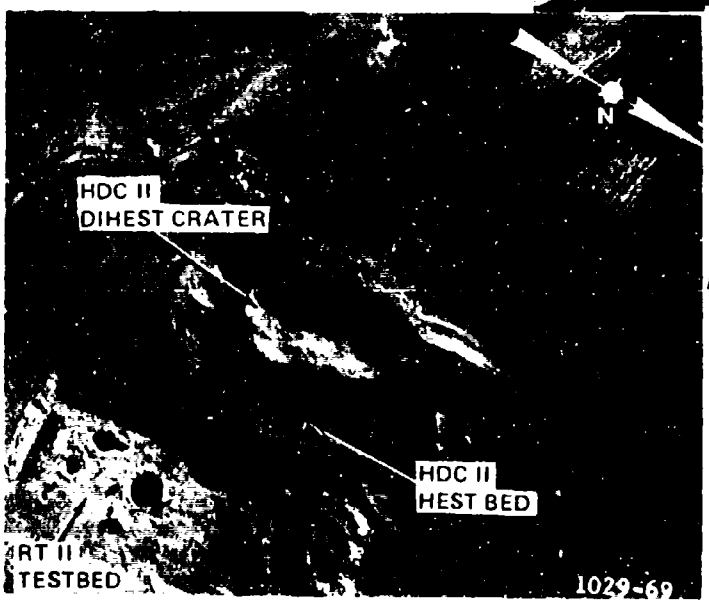

Figure 62. HANDEC II post-shot airphoto.

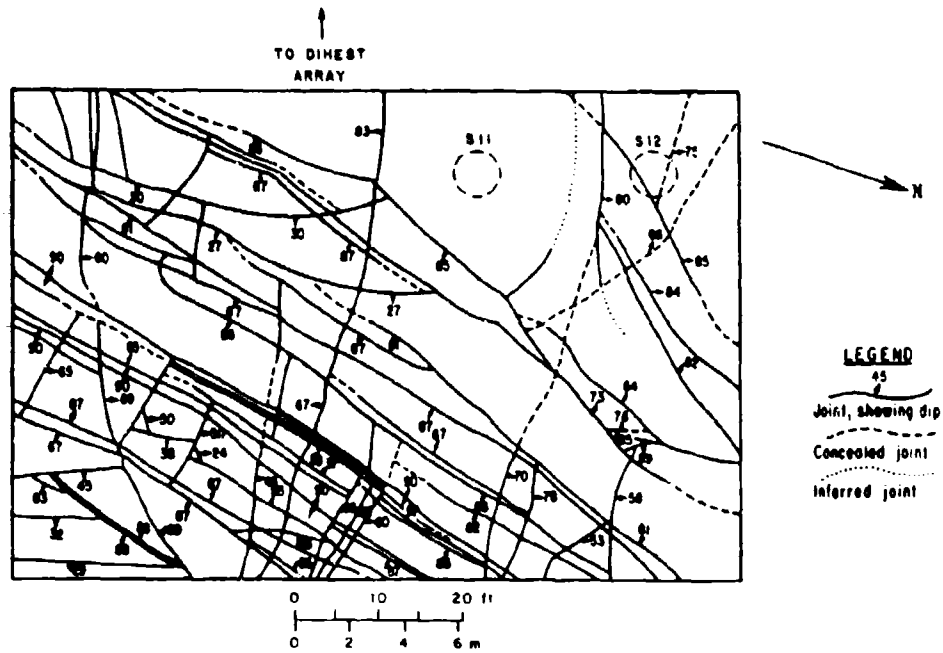

Figure 63. Joint map of HANDEC II test bed (from Blouin 1970c).

Spacing varied from several inches to more than 10 ft. In addition to the joint map, the base of each column used to support the roof and overburden of the HEST facility was located by survey. This resulted in a grid of surveyed points 4 ft on center in the east-west direction and 7½ ft on center in the north-south direction.

Test results

Significant relative displacements were measured post-test on the free field side of the HEST testbed and also within the HANDEC I testbed which lay obliquely off the south end of the HANDEC II DIHEST array. It is presumed that all displacements were due to the DIHEST detonation only. Figures 64 and 65 show the permanent horizontal and vertical displacements obtained from the pre- and post-test surveys of the column bases. Both horizontal and vertical displacements were significantly larger on the free field side of the testbed. This was a result of differential motion along the east-west joint dipping toward the south at 83° which nearly bisected the testbed between the structures and free-field instrumentation. The permanent horizontal displacements tended to follow the paths of least resistance offered by the vertical north-south joint set. Displacement was generally parallel to the strike of these joints and is believed to have been channeled by them, in the manner described previously by Johnson (1962).

Figures 66 and 67 are views of relative motion that occurred in the southwest corner of the testbed along one of the north-south joints which dipped gently toward the east (either at 30° or 27°, see Fig. 63). Figure 66 is a view looking toward the south along the joint. The rock on the right-hand side of the photograph (toward the explosive array) has been wedged downward and outward along the joint relative to the rock on the left. Figure 67 is a closeup of the same joint looking toward the north showing two column bases originally separated by a distance of 4 ft. The rock toward the explosive array (on the left in this photograph) has moved outward a distance of 22 in. and downward a distance of approximately 18 in. relative to the rock on the right. The displacement vectors in Figure 65 indicate that all surveyed points within the testbed had upward permanent displacements, despite the considerable relative vertical motions indicated in Figure 67. A schematic section view of this relative displacement is shown in Figure 68, which shows a general uplift and tilting of the testbed from front to back. Figure 68 also includes the relative motion along the joint, where the block near the explosive array moved downward and outward relative to the block farthest from the array, but at the same time displayed absolute displacement upward and outward.

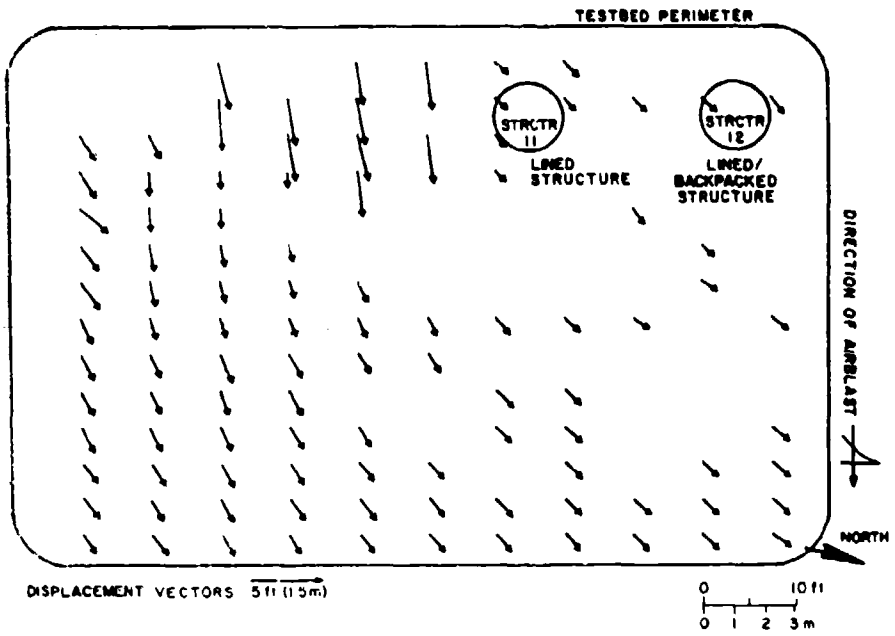

Figure 64. HANDEC II permanent horizontal displacements (from Higgins 1970).

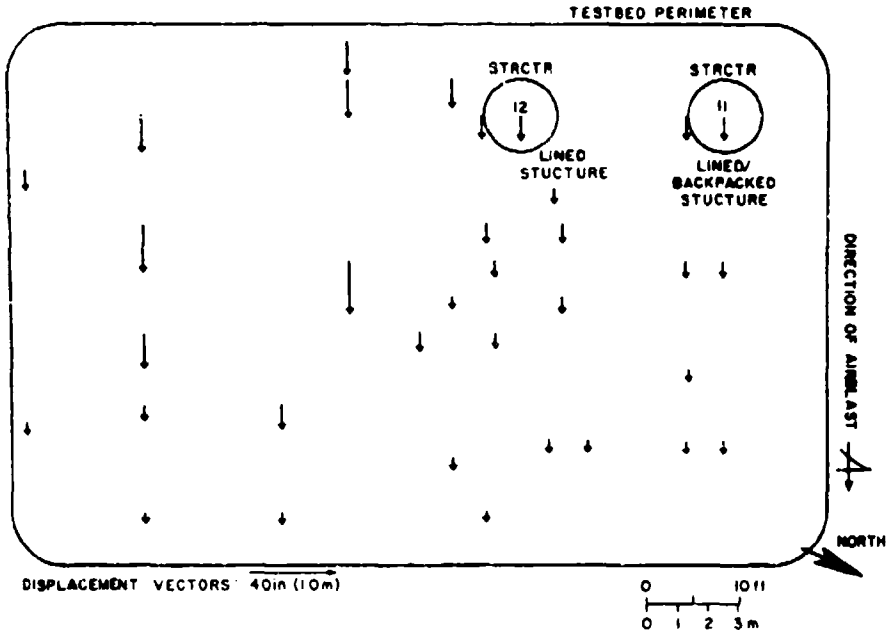

Figure 65. HANDEC II permanent vertical displacements (from Higgins 1970).

This relative motion is unique to those experienced in the DIHEST series in that it did not appear to follow a path of least resistance. Rather, the block close to the explosive array seemed to act as a wedge being driven beneath the adjacent block but with a net upward displacement.

A detailed account of the HANDEC II structural performance is given by Higgins (1970). He indicates that the lined silo (S_{11}) suffered major structural damage below a depth of 10 ft due to a relatively minor relative displacement of 0.3 ft along a joint intersecting the structure at that

Figure 66. HANDEC II relative displacement, looking south (from Blouin 1970).

Figure 67. HANDEC II relative displacement in the southwest corner of test bed (from Blouin 1970c).

depth. Figure 69 shows that the bottom of the structure moved toward the northeast relative to the top. Motion occurred along a joint striking N27°W dipping 26° toward the northeast, which was projected to intersect the upper north corner of the explosive array as shown in Figure 70. It is noted that the intersection of this joint with the testbed surface is not evident on the pre-test joint map, nor does this joint show up on the pre-test joint map of the structure walls produced from photographs and field observations.

The backpacked silo S_{12} suffered no damage

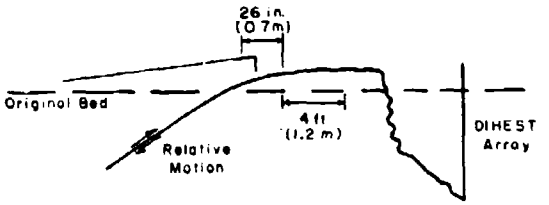

Figure 68. HANDEC II relative displacement, schematic view.

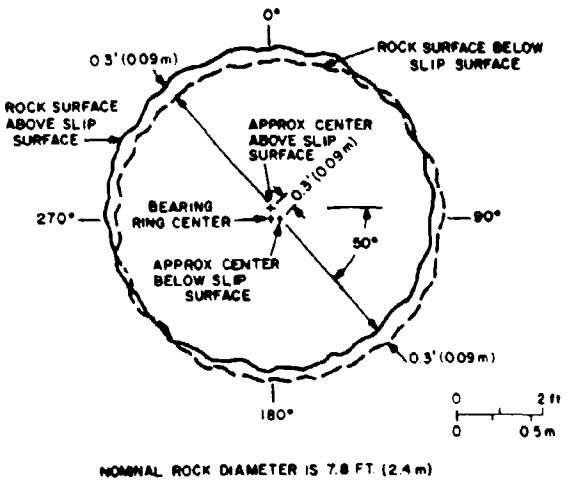

Figure 69. Cross-sectional comparison of the rock surfaces above and below the transverse slip surface in HANDEC II lined silo S_{11} (from Higgins 1970).

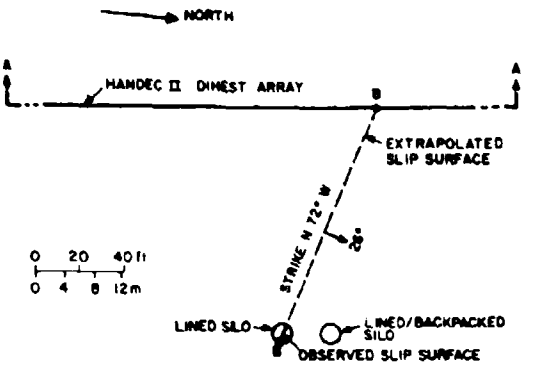

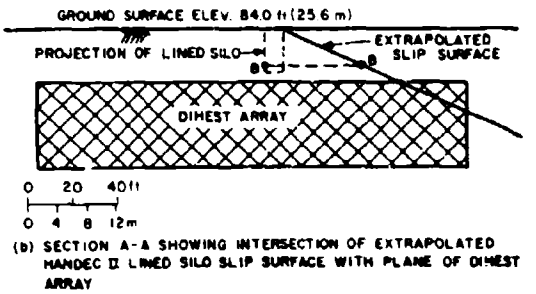

Figure 70. Projection of the transverse slip surface in lined silo S_{11} to HANDEC II DIHEST array (from Higgins 1970).

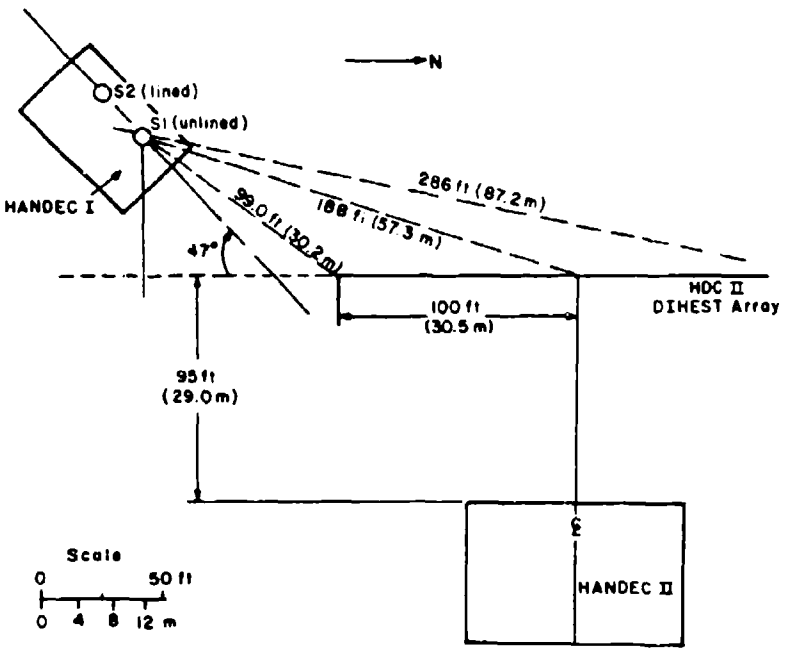

Figure 71. Plan view of HANDEC I and II test bed.

to the inner steel liner and only very minor cracking of the concrete liner, although Higgins (1970) reported that there were small relative motions or a "tendency toward motion" along many of the pre-existing joints in the surrounding rock. He noted that the foam concrete backpacking was compressed at least 1 to 2 in. and possibly as much as 4 in. in some areas, indicating that relative motions were minor and that the backpacking was able to absorb the motions without damage to the structure.

The most dramatic relative displacements resulting from the HANDEC II DIHEST occurred in the adjacent HANDEC I testbed, shown in the plan view of Figure 71. The HANDEC I testbed was located to the southwest of the HANDEC II DIHEST array with the nearest structure some 99 ft from the south end of the array and 188 ft from the center of the array. HANDEC I was a combined HEST-DIHEST event utilizing a 40-×60-ft HEST cavity, and a 2.2-ton DIHEST array which was a duplicate of that employed on the DATEX I and STARMET DIHEST only shots. A description of HANDEC I is given by Blouin (1970b) and Carellas et al. (1969). There were no significant relative displacements observed on the test. The lined structure S_1, with a 6-ft inside diameter, a 20-ft depth, and a nominal 8-in. reinforced concrete lining surrounding a ½-in. steel inner lining, exhibited only minor bulging in the steel liner. The unlined structure S_2, also 6 × 20 ft, showed very small relative displacements along preexisting joints.

The HANDEC I structures were severely damaged by the HANDEC II DIHEST array as shown in Figures 72 and 73. Figure 72 shows the complete collapse of the steel liner in the reinforced structure S_3 which resulted from a large relative displacement along a transverse joint dipping toward the DIHEST array. A view of the lined structure S_1 with the steel lining removed is shown in Figure 74.

The joint surface dipping toward the DIHEST array at the top of the photograph is clearly visible. According to Higgins (1970) the top of the structure has displaced approximately 2½ ft horizontally and 1½ ft vertically relative to the bottom. The transverse boundary joint strike is approximately N45°W and its dip is between 25° and 30° toward the northeast. The relative motion is very similar to that hypothesized to have sheared the top of structure 3 in the DATEX II experiment.

The lateral boundary on the east side of the slip block was a vertical joint which intersected the unlined structure S_2 approximately ⅓ of the way between the front and the back. This joint is clearly visible in Figure 73. According to Higgins (1970), the portion of the structure in the right-hand portion of the photograph is contained within the thrust block and has moved relative to the stationary rock in the left half of the photograph. The vertical joint which strikes toward the south end of the HANDEC II DIHEST array forms the SE boundary of the thrust block. This is shown in the schematic plan view of Figure 75, which extrapolates the vertical joint (striking N11°E) to an intersection with the DIHEST array very near the south end of the array. Figure 76 is a schematic section view of the transverse joint forming the base of the thrust block. It intersects the DIHEST array near the center of mass of the explosives. The extrapolated locations of the boundary joints indicate that the block which moved relative to the surrounding rock was similar to the thrust blocks hypothesized on DATEX II and documented on STARMET. It moved along paths of least resistance which intersected or came close to the explosive array.

A section view of the displacement hodographs from the instrumentation adjacent to the testbed centerline is shown in Figure 77. Displacement trajectories are similar to those from other DIHEST experiments, moving initially outward away from the center of mass of the explosives, followed by an upward turn as the effects of the free surface come into play. Magnitudes and direction of the near surface displacements are in general agreement with the permanent displacements indicated in Figures 64 and 65. The horizontal displacement hodographs from depths of 4 and 18 ft (shown in Figures 78 and 79, respectively) vary significantly from the permanent horizontal surface motions indicated by the displacement vectors in Figure 64. While the magnitudes are in general agreement, the transverse component is in the opposite direction, i.e. the instrumentation indicates that displacement was outward from the array and toward the south, while the post-test survey indicates that motion was outward from the array and towards the north. The probable cause of this discrepancy is that somewhere in the instrumentation hookup, or in the data reduction, the polarity of the instrumentation measuring horizontal transverse motion was reversed. Unfortunately, this is a fairly common occurrence, even to this day. It would be considerably more difficult to argue that the results of the post-test

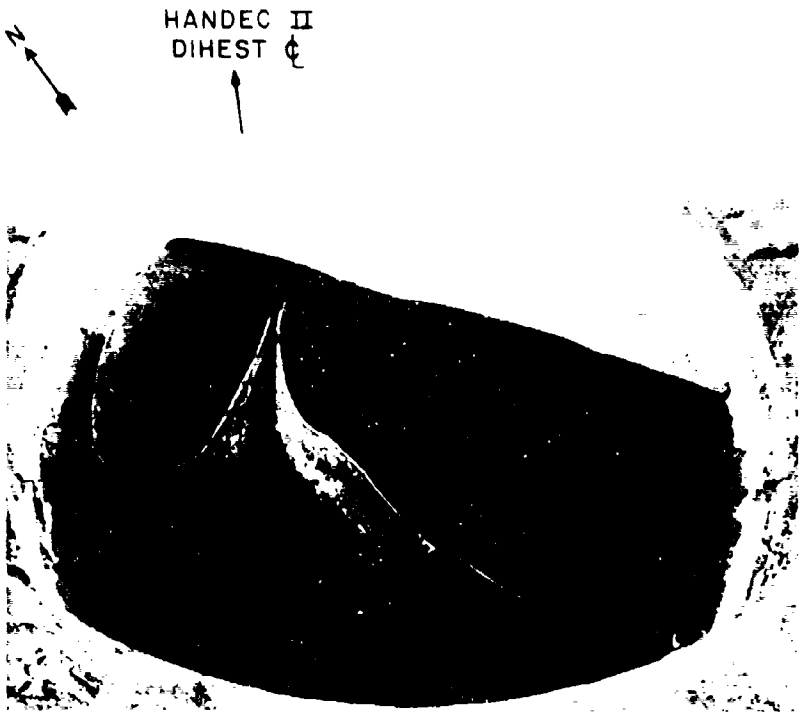

Figure 72. View of HANDEC I lined structure S_1 (from Higgins 1970).

Figure 73. View of HANDEC I unlined structure S_2 (from Higgins 1970).

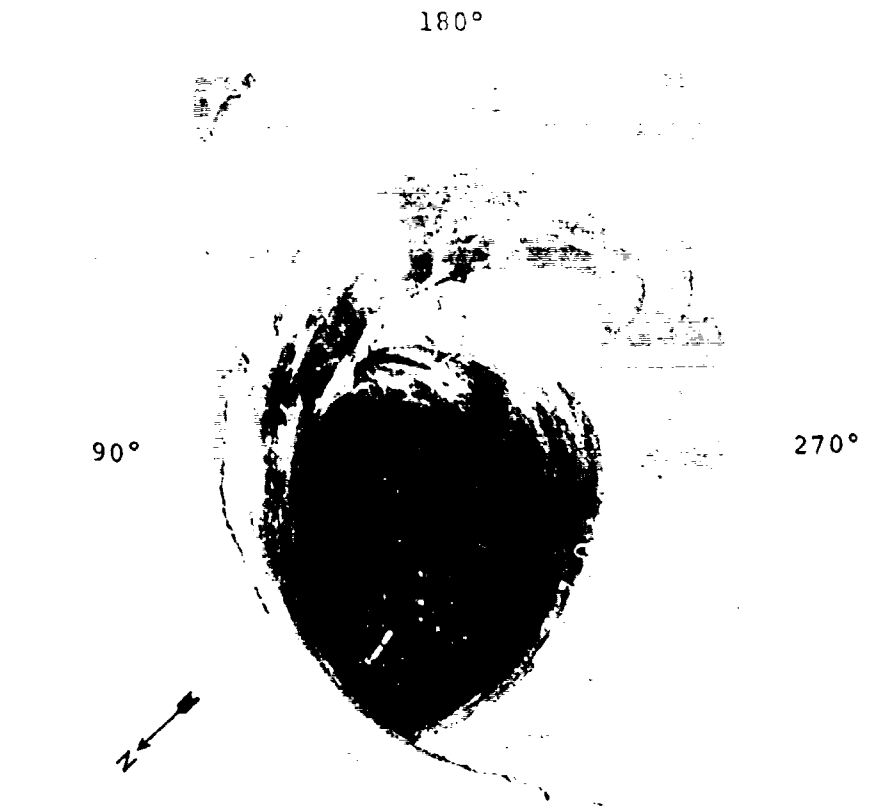

a. Viewed from 0° to 180°.

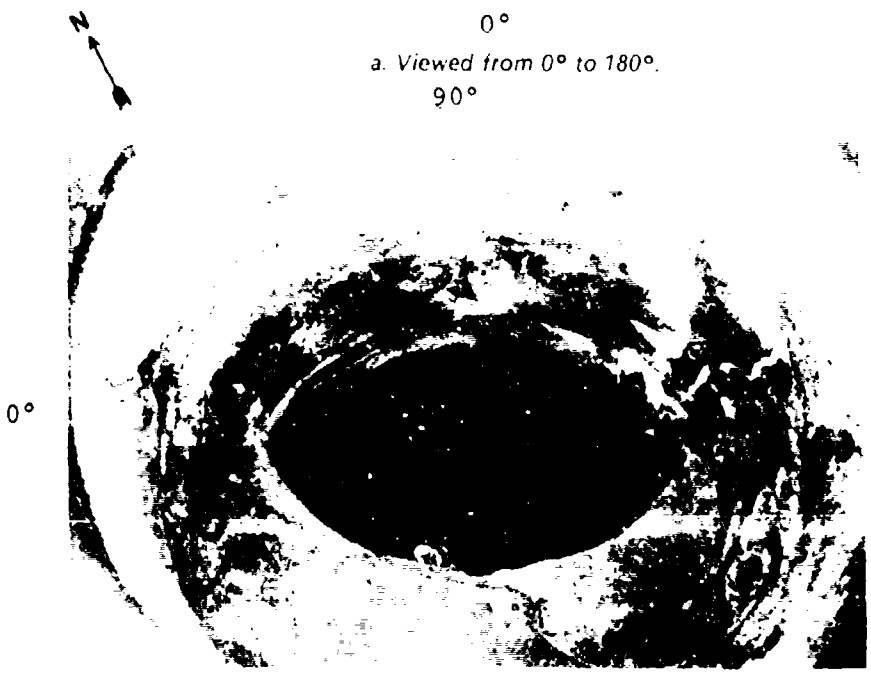

b. Viewed from 270° to 90°

Figure 74. Two views of HANDEC I lined structure S, with the steel lining removed (from Higgins 1970).

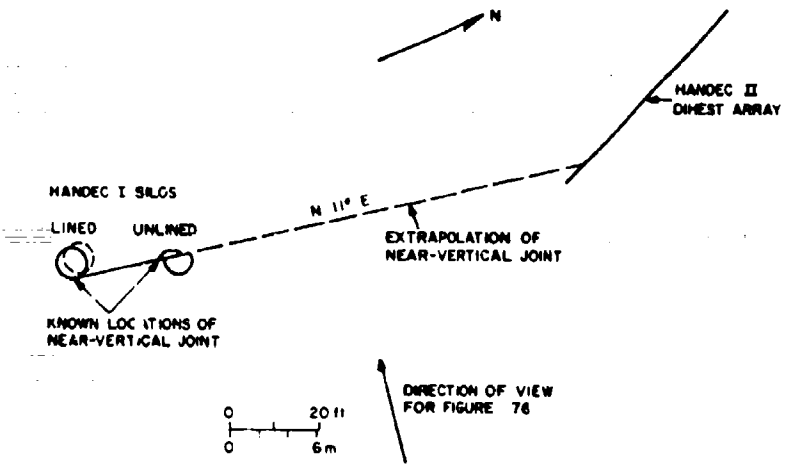

Figure 75. Extrapolation of the near-vertical joint at the HANDEC I structures to the HANDEC II DIHEST array (from Higgins 1970).

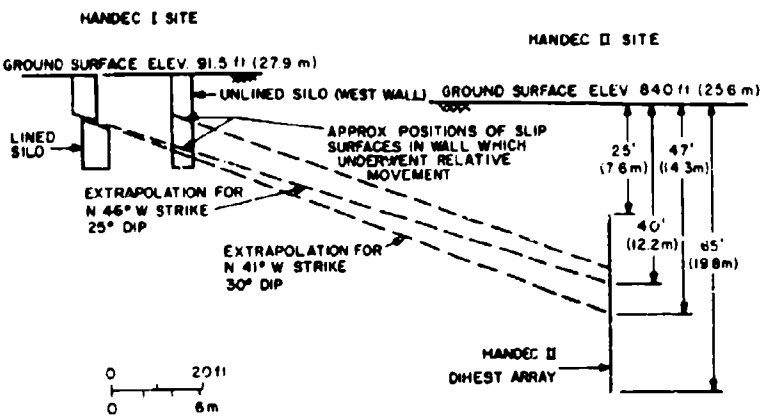

Figure 76. Extrapolation of the transverse slip surface at the HANDEC I DIHEST array (from Higgins 1970).

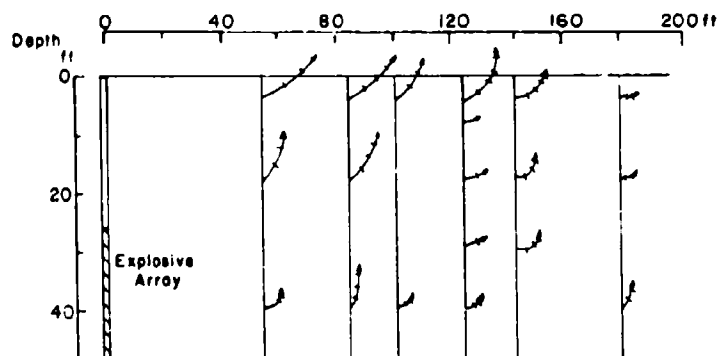

Figure 77. HANDEC II displacement trajectories.

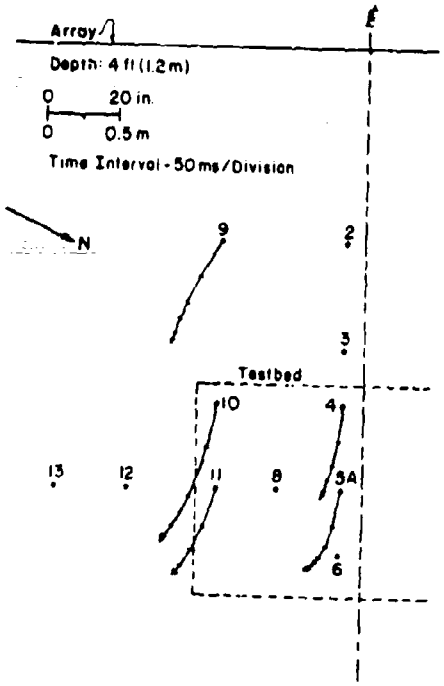

Figure 78. HANDEC II horizontal displacement trajectories, depth – 4 ft.

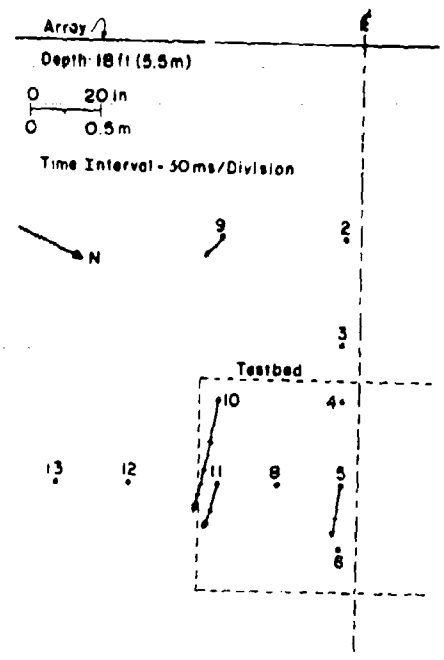

Figure 79. HANDEC II horizontal displacement trajectories, depth – 18 ft.

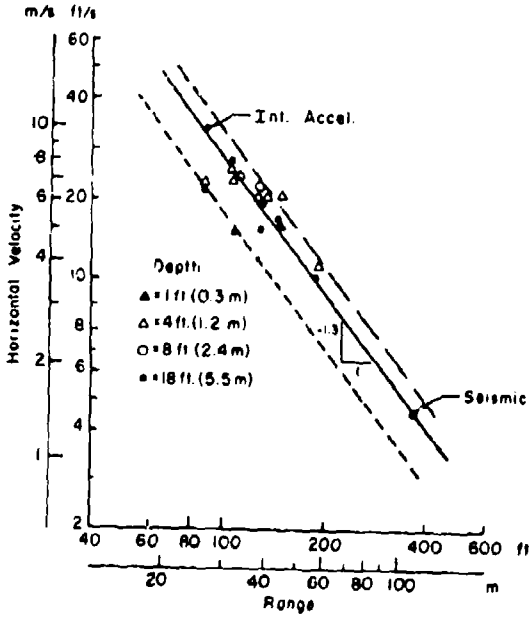

Figure 80. HANDEC II near-surface peak horizontal velocity.

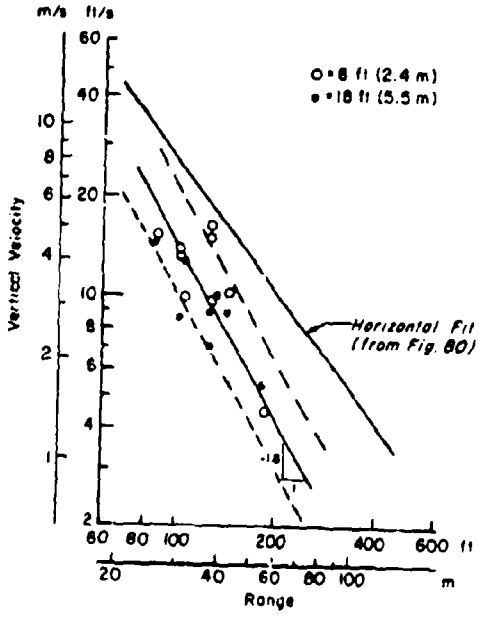

Figure 81. HANDEC II near-surface peak vertical velocity.

survey are in error. If the horizontal transverse polarities are reversed, the displacement trajectories are in good agreement with the surveyed permanent displacements

Peak horizontal and vertical near-surface ocities from the HANDEC II DIHEST are shown in Figures 80 and 81. They tend to fall on the upper side of the DATEX II peak velocities, partially as a result of the increased yield and partially because the HANDEC II testbed was somewhat "harder" than the DATEX II bed (Blouin 1971). Attenuation also appeared to be

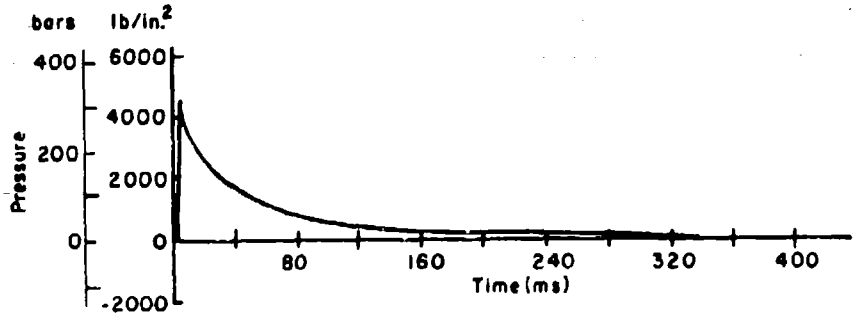

Figure 82. HANDEC II smoothed and corrected air pressure time-history.

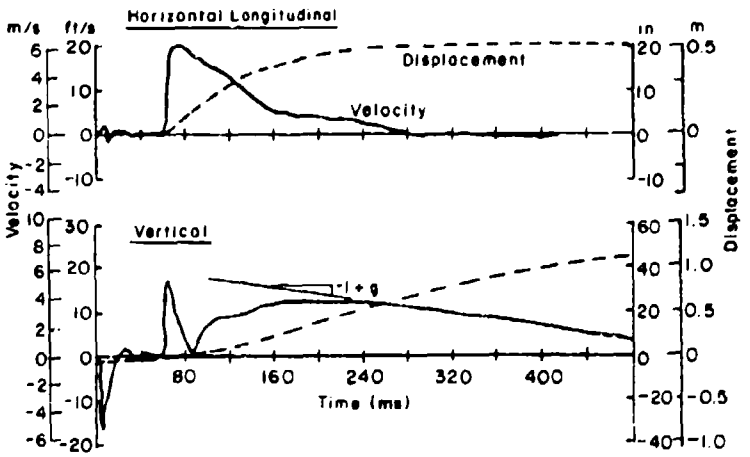

Figure 83. Typical HANDEC II time-history from hole 5, depth—4 ft.

slightly lower in the HANDEC II bed. As was the case with DATEX II, the horizontal velocities are slightly higher than the vertical velocities close to the array, becoming significantly higher farther from it. Peak velocities at the range of the large differential displacements within the HANDEC II bed (approximately 110 ft) averaged 22½ ft/s horizontally outward and 12 ft/s vertically upward. The peak velocities in the vicinity of the HANDEC I structures can only be estimated because no data are available from that location and, as shown in Figure 71, the HANDEC I structures lie off the south end of the DIHEST array. Assuming that only the south half of the DIHEST array contributes to the motions at the HANDEC I structures and that peak velocity scales with the cube root of the yield, peak horizontal velocity at the unlined structure S_2 (a distance of 142 ft from the explosive center of mass) would average about 12½ ft/s and peak vertical velocity slightly over 6 ft/s. Averages at the lined structure S_1 (approximately 165 ft distant) are estimated at 10½ ft/s horizontally and 4½ ft/s vertically.

It should be noted that, because the HEST was initiated prior to the DIHEST, there was a substantial amount of air pressure on the HEST bed at the time of arrival of the DIHEST pulse. Intuitively, one would expect this pressure to minimize relative motions within the testbed along transverse joints because of the added friction component tending to resist motion resulting from the added normal stresses. Figure 82 is a smoothed and corrected air pressure time history taken near the center of the HEST bed. The DIHEST arrival time at this point was approximately 60 ms at which time there was roughly a 1000 lbf/in.² air overpressure on the testbed. Since typical positive phases of the near surface horizontal velocity time histories averaged 150–200 ms, the air overpressure on the bed should have dropped to about 200 lbf/in.² by the time peak horizontal displacements were reached.

Typical HANDEC II near-surface velocity and displacement time-histories from hole 5 near the center of the testbed are shown in Figure 83. The passage of the air shock is obvious on the ver-

tical time history where it results in a substantial negative velocity peak near time zero. The arrival of the DIHEST signal at approximately 60 ms is evident on both the horizontal and vertical traces. The shapes of the DIHEST portion of the pulses are similar to those from DATEX II. Horizontal motion is of relatively short duration compared to the vertical motion. The linear slope of the vertical velocity trace, being slightly higher than 1 g, indicates that the surface of the testbed was in spall. However, since the direct induced pulse was sufficient to spall the surface normal stresses on transverse joints would be expected to approach zero, thereby negating any restraining effects of increased air overpressure on relative displacement.

ROCKTEST II

Test description

ROCKTEST II, fired in March of 1970, was the largest HEST-DIHEST shot to date. The primary goals were to test a full-scale, half depth conceptual missile silo in rock and to demonstrate the ability to simulate a combined nuclear airblast overpressure and direct induced pulse on a large scale (AFWL 1970). As shown in Figure 61, the 250-ft-long × 400-ft-wide testbed is located just to the southeast of the HANDEC II bed. The DIHEST array, shown in the plan view of Figure 84, was located 75 ft east of the HEST bed. The time delay between the HEST detonation and the DIHEST detonation was exactly 45.0 ms. The array was 501 ft, 8 in. long with the explosives contained between the 35- and 75-ft depths. The cross section of the explosive holes is similar to that for HANDEC II, i.e. a 40-ft explosive column but with a 10-ft deeper bural so that the center of mass of the explosive charge was at a depth of 55 ft. The explosive hole spacing (approx. 7 ft, 2 in.) and explosive density per unit area of array (11.7 lb/ft^2) were approximately equal to those used on DATEX II and HANDEC II. The total weight of explosives in the ROCKTEST II array was 117 tons. The DIHEST array was covered with an earth berm similar to those used on DATEX II and HANDEC II. The height of the berm was increased from 40 ft used on HANDEC II, to approximately 45 ft. Pre- and post-test sections through the berm are shown in Figure 84.*

Active ground motion instrumentation was located in the 18 instrumentation holes shown in the plan view in Figure 85 at ranges from the DIHEST array of between 40 and 425 ft. Depth of measurements ranged from the testbed surface to 100 ft. Details of the instrumentation layout and operation are given in AFWL-TR 70-111, 1970.

Of the many structural experiments located in the ROCKTEST II testbed, the ones relevant to the post-test permanent displacements are identified in the plan view of Figure 85. Structure 01 was a full size side-by-side silo with a rise and rotate closure. It was heavily reinforced and extended to a depth of 75 ft. Structure 02 was a half scale side-by-side silo with rise and rotate closure which extended to a depth of 35 ft. Structure 03A was a 12-ft-diam unlined silo with closure extending to a depth of 10 ft. Structures 05, 06 and 07 were 6-ft-diam x 40 ft deep silos with closures. Structure 05 was lined with a reinforced concrete liner, 07 was lined with a reinforced concrete liner surrounded by a foamed concrete back packing, and 06 was unlined (AFWL 1971).

The HEST bed was cleaned prior to construction of the HEST overburden support structure and thoroughly mapped. The joint map is shown in Figure 86. Two important joint sets are delineated on the separate maps shown in Figures 87 and 88. The first is the nearly vertical north-south set which controlled motions in the HANDEC II bed. The second is a set or sets of low angle joints which tend to strike parallel to the DIHEST array and which dip towards it (easterly) at between 25° and 45°. Joints from these two sets combined to control relative displacements within the ROCKTEST II bed. Unfortunately, subsequent to the preparation of the joint map, the testbed was drilled, blasted and excavated to an elevation 6 ft lower than that shown. Since there was insufficient time for preparation of another map, exact locations of joints on the final testbed can only be approximated from these maps.

Test results

Figure 89 shows the major relative permanent displacements in the ROCKTEST II bed resulting from the DIHEST detonation. The largest displacements occurred in the north half of the testbed in the form of the large block shown in Figure 89 bounded by preexisting joint surfaces. The block extended approximately 140 ft west from the edge of the DIHEST crater (which in

*J. V. Kaiser, personal communication, 1970

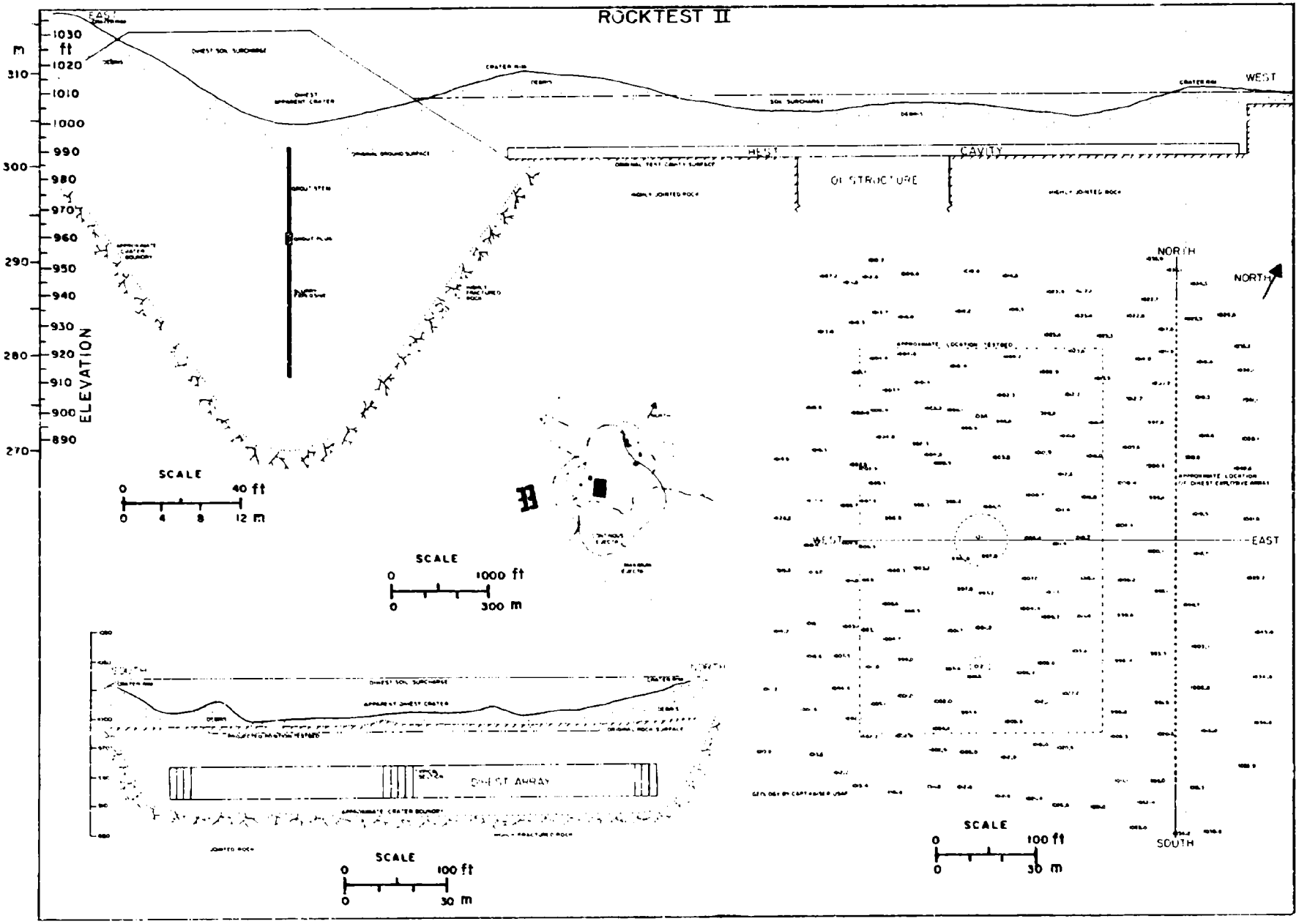

Figure 84. Plan and section views of ROCKTEST II DIHEST.

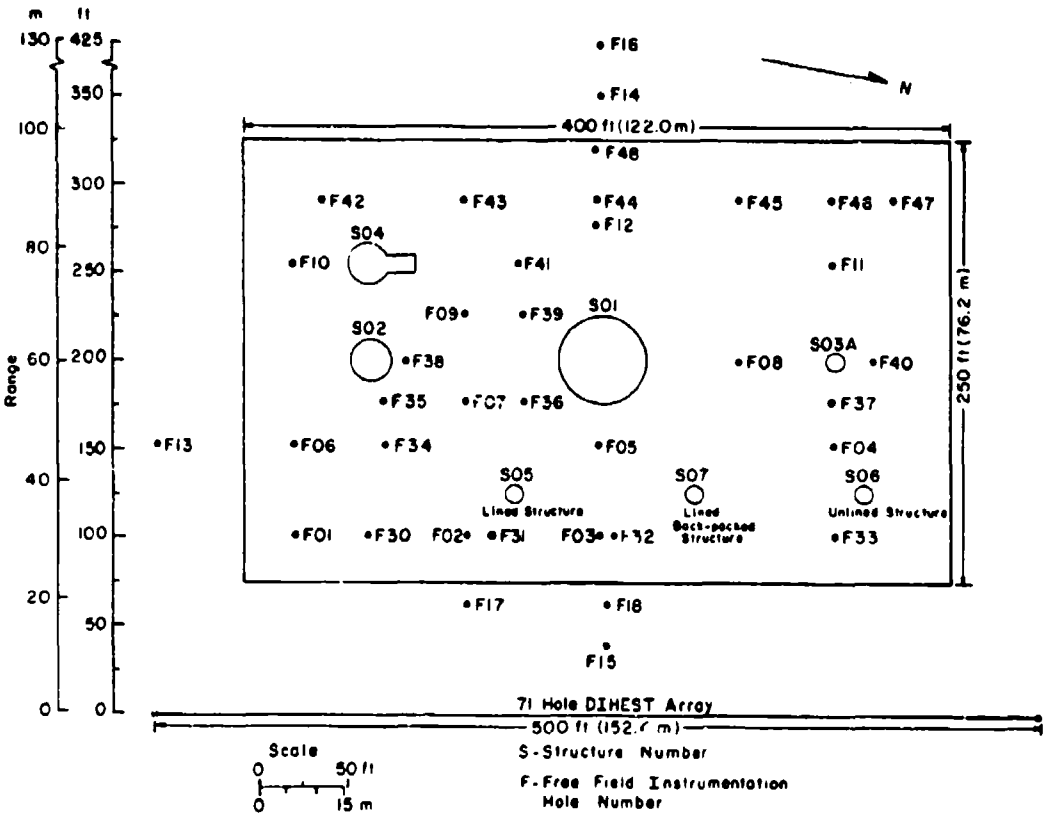

Figure 85. Plan view, ROCKTEST II.

turn extended approximately 80 ft from the DIHEST array). The block averaged about 150 ft in width. It was thrust toward the west along a joint of the low angle set shown in Figure 88 which dipped toward the explosive array at an angle of approximately 20°. The block encompassed the top portions of structures 03A, 07 and 06 (see Fig. 89). Permanent horizontal displacements were approximately 10-12 in. in the vicinity of structure 03A. Melzer (1970) noted that this magnitude was reduced somewhat toward the intersection of the joint with structure 01. Near this intersection, the displacements appeared to branch along two joints, one running to the side of the S01 structure and the other bending toward the east. The southern boundary of the thrust block was formed by a near-vertical joint which bisected a line between structures 05 and 07. The northern boundary of the block was formed by a combination of vertical joints running just to the north of structure S03A almost perpendicular to the DIHEST array. Approximately 15 ft west of structure 06, the displacement branches along another vertical joint striking northeast toward the north end of the DIHEST array.

An airphoto of the thrust block is shown in Figure 90, looking east toward the DIHEST array. Closures for structures are 01, 03A, 06, and 07 are identified. The low angle boundary joint dipping toward the DIHEST array is clearly visible as well as the system of vertical joints forming the northern boundary of the thrust block. The eastern edge of the block at the crater boundary is identifiable in the cleared east-west swath. The 03A closure had been upturned by the action of the thrust block wedging the base of the closure against the stationary rock beneath the boundary joint. Figure 91 is a view of the low-angle boundary joint looking north along the joint. The stationary side of the joint is to the left of the photograph while the thrust block lies to the right. The upturned 03A closure can be seen in the background. A projection of the joint in the vicinity of structure 03A back to the DIHEST array is shown in Figure 92. The joint intersects instrumentation hole F04 at a depth of 20 ft, at the location of a cable break which occurred at

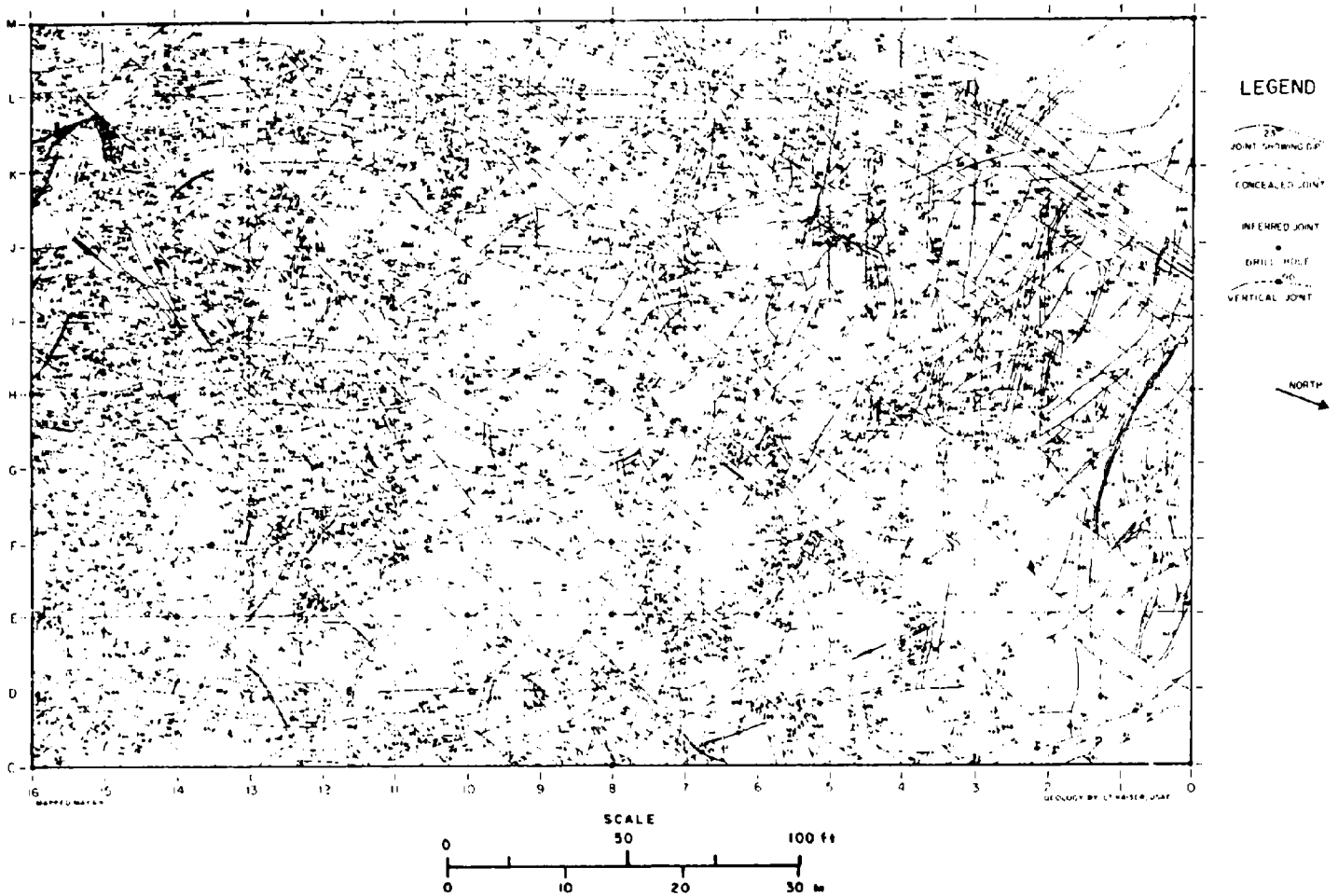

Figure 86. Joint map of ROCKTEST II test bed.

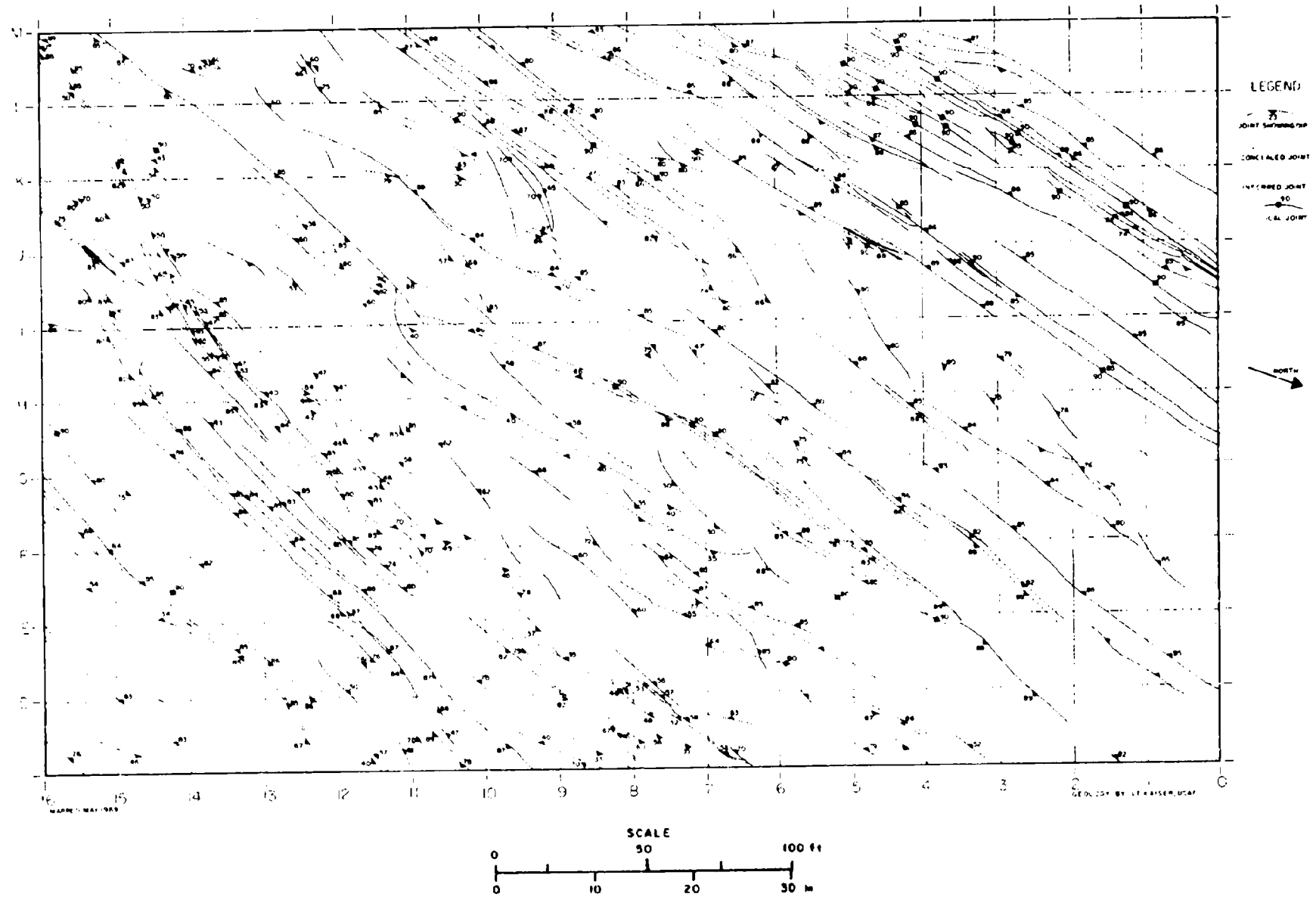

Figure B7. High angle joints in the ROCKTEST II test bed.

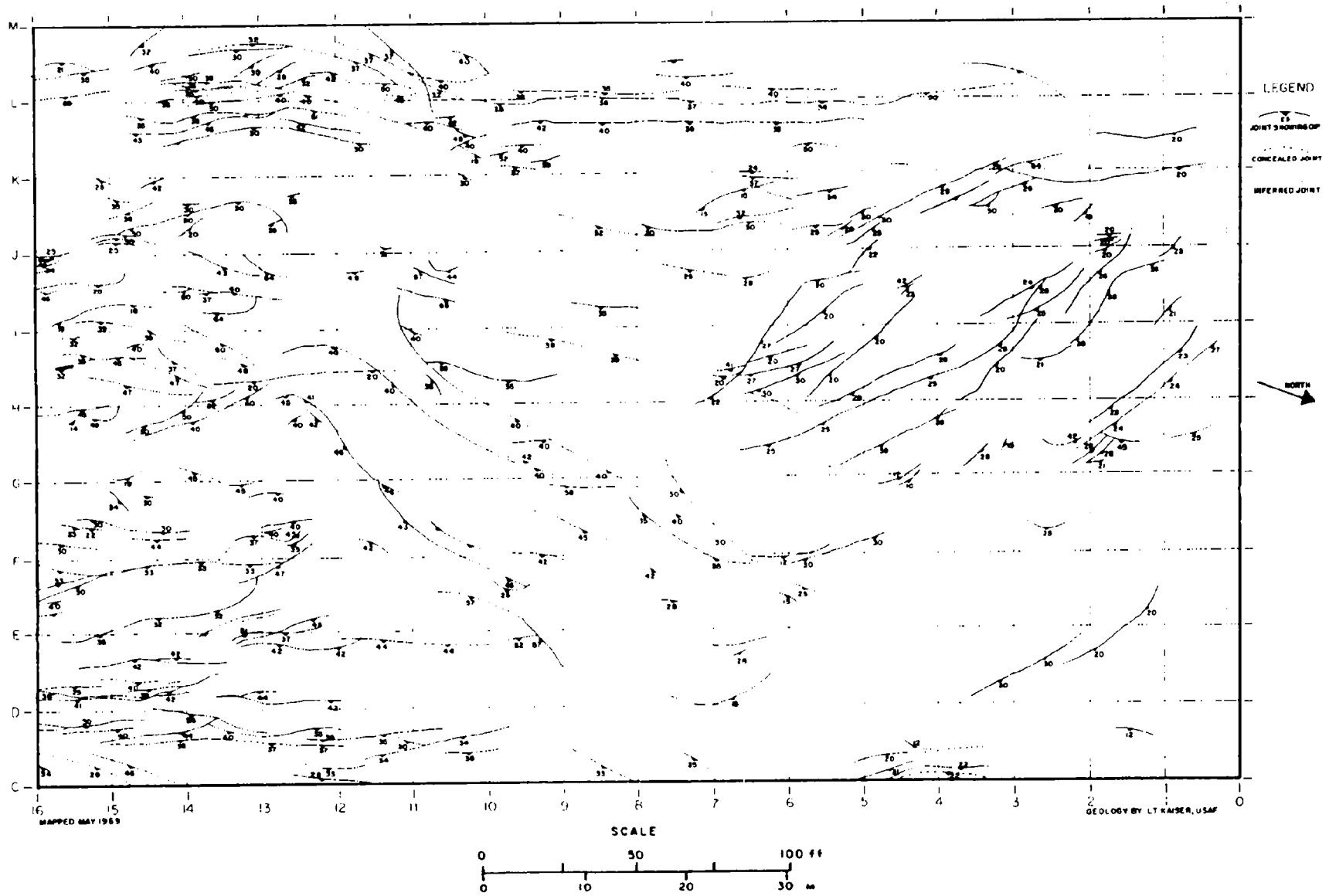

Figure 88. Low angle joints in the ROCKTEST II test bed.

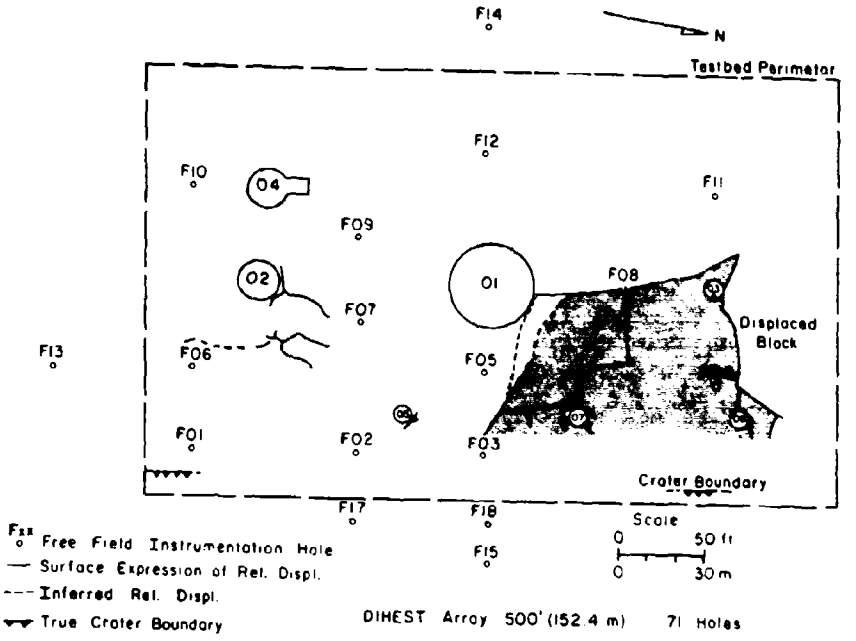

Figure 89. Plan view of surface relative displacements in the ROCKTEST II test bed.

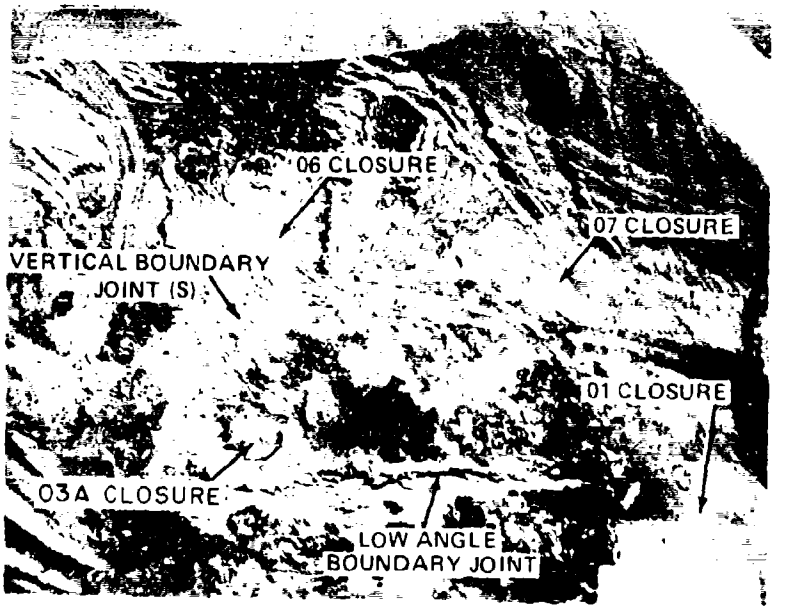

Figure 90. Aerial view of the ROCKTEST II thrust block.

Figure 91. View north along the ROCKTEST II low angle boundary joint.

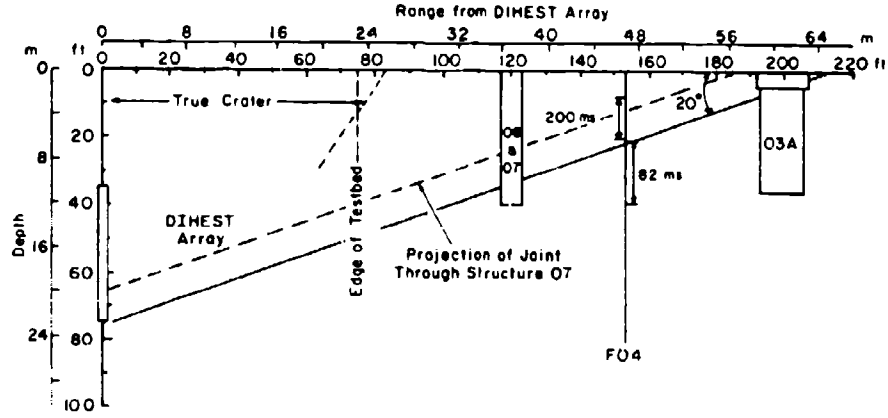

Figure 92. East-west cross section through structures 03A, 06, 07 and hole F04. Times at F04 are those at which all gage or cable systems below that zone produced no data.

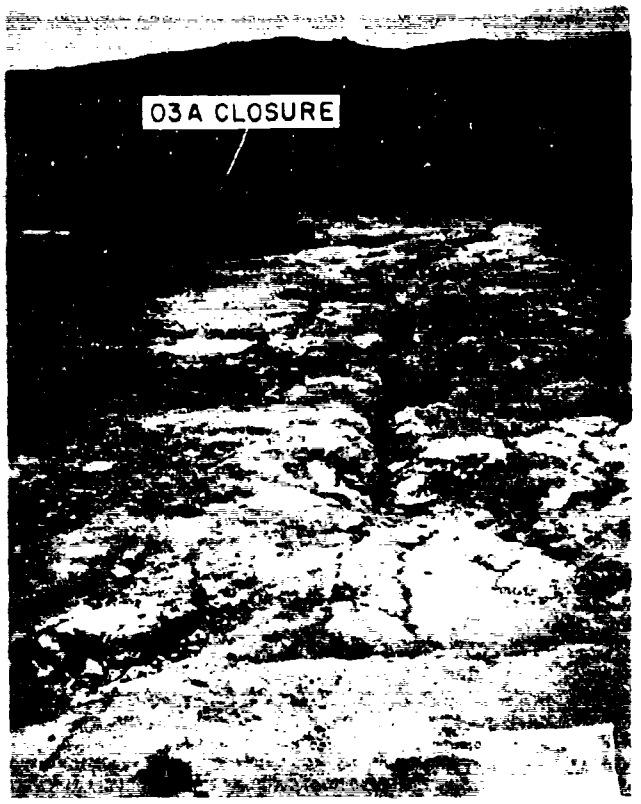

Figure 93. View west of vertical joints at the north edge of the ROCKTEST II thrust block.

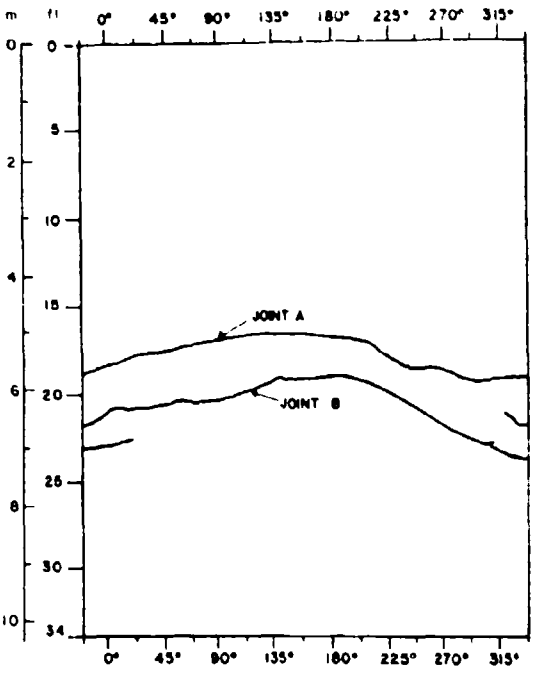

Figure 94. Joints in structure 07 in which major relative motion occurred (from Higgins 1971).

82 ms (i.e. 37 ms after the DIHEST array was fired). The joint intersects the unlined structure 06 between the 30 and 35 ft depth and the DIHEST array very near its base. Figure 93 is a view of a portion of the vertical joint(s) forming the northern boundary of the thrust block looking west toward the 03A closure.

The thrust block observations on the testbed surface are in excellent agreement with post-test observations made in sructures 05 and 07 by Higgins (1971). Damage to the lined structure 05 resulted from crushing and buckling near the 90 and 270° azimuths (the 0° azimuth extends toward the DIHEST array), with little or no damage due to relative displacements along preexisting joint surfaces. However, the lined backpacked structure 07, which was within the thrust block as shown in Figure 89, was heavily damaged by relative displacements along the 20° boundary joint. The intersection of this joint with the structure 07 (superimposed on Fig 92) is projected to occur between the 20- and 25-ft depths. Higgins (1971) notes that the major structural damage occurred between the 15- and 23-ft depths. The top of structure 07 moved 6½ in. horizontally outward from the DIHEST array relative to the bottom as well as 2 in. vertically upward. Motion occurred along two nearly parallel joints which intersected the structure between 15 and 23 ft as shown in Figure 94. The upper joint (Joint A) had a strike of S 75° E and dipped toward the array at an angle of 19°, while the lower joint had a strike of S 44° E and dipped toward the array at an angle of 28°. The orientation and projected intersection of those two joints with the explosive array is shown in Figure 95. As was often the case, neither of these joints was identified before the test. From Higgins's (1971) observations, it would appear that there was some branching of the displacements along at least two low-angle joints near the southern boundary of the thrust block. This is probably also evidenced on the testbed surface by the branching noted in the vicinity of structure 01.

There was very little evidence of relative displacements in the south half of the ROCKTEST II

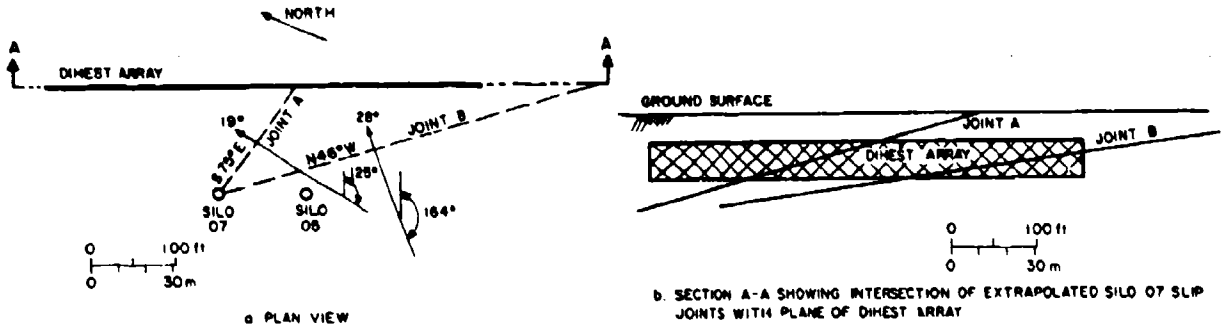

Figure 95. Extrapolation of transverse slip joints from structure 07 to ROCKTEST II array (from Higgins 1971).

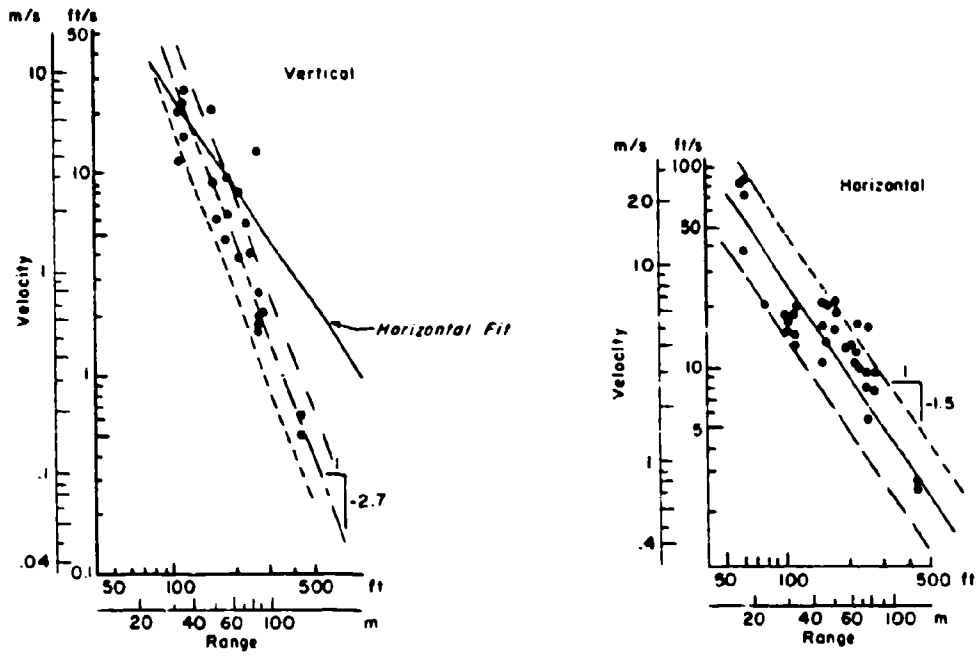

a. Horizontal. *b. Vertical.*

Figure 96. ROCKTEST II near-surface peak horizontal and vertical velocities.

bed. Melzer (1970) recorded only small, scattered fractured zones on the testbed surface. There was a zone of very small relative displacements which intersected the north side of structure 02, as shown in Figure 89. The cracking around structure 02 differed from that around structure 01 in that it pierced the concrete collar and caused buckling of the steel liner at the 270° azimuth within the equipment room. The only other significant cracking in the south half of the testbed was the small zone approximately 25 ft east of structure 02, also shown in the plan view of Figure 89. The relative motions in this area were also very small and difficult to trace along the surface. Melzer (1970) estimated that the maximum relative displacement in these areas occurred near the south edge of the testbed and had a magnitude of approximately 2 in.

A plot of near-surface peak horizontal and vertical velocities from the ROCKTEST II DIHEST is shown in Figure 96. These both tend to attenuate somewhat faster than the HANDEC II velocities. Peak velocities at the 125-ft range of the close structures averaged about 20 ft/s, both horizontally outward and vertically upward. Horizontal velocity averaged slightly lower than that at the HANDEC II structures while vertical velocity was significantly higher owing to the deeper

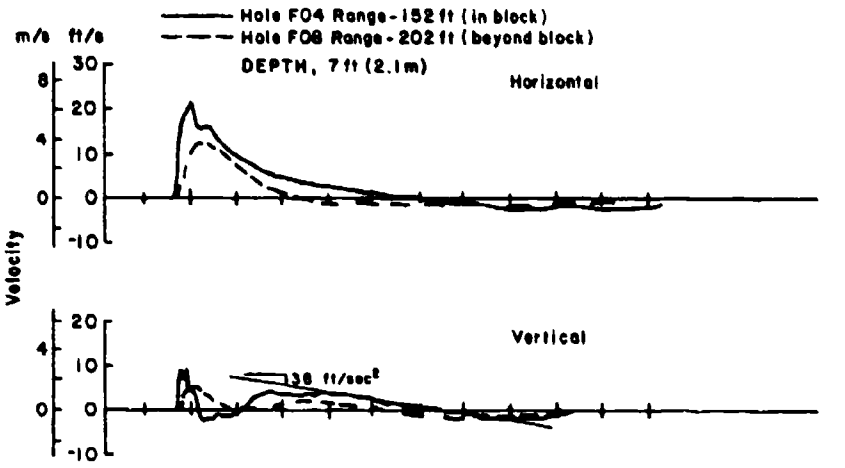

a. Velocity vs time.

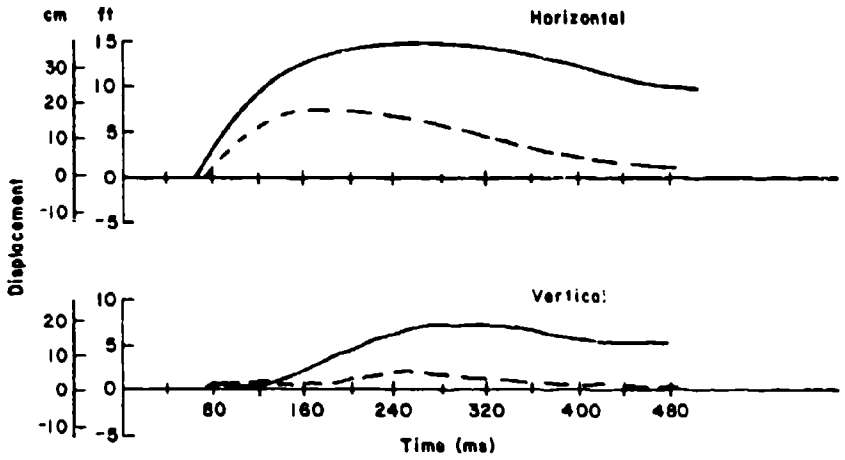

b. Displacement vs time.

Figure 97. ROCKTEST II motion in and beyond the thrust block.

burial of the DIHEST explosives. At the structure 03A near the outer edge of the block (at a range of 200 ft), horizontal velocities averaged 9½ ft/s and vertical velocities had dropped to about 5 ft/s. As in the other DIHEST experiments, vertical velocities tended to attenuate more rapidly than horizontal velocities.

Typical DIHEST induced wave forms are shown in Figure 97. Because the HEST overpressure and resulting vertical velocities are classified, only the portion of the time-histories associated with the DIHEST detonation at 45.0 ms are shown. Velocity and displacement time-histories at the 7-ft depth are shown from instrumentation hole F04 within the thrust block and hole F08 just beyond the intersection of the boundary joint with the testbed. The positive phase duration of the horizontal velocities was significantly higher within the thrust block, 220 vs 120 ms, a difference which is manifest in the displacement time histories. It is similar to the differences noted in the comparisons of data from within and without the STARMET thrust block, though not nearly as pronounced, since the total displacement of the ROCKTEST II block was less than 1/5 that of the STARMET block. The vertical velocity traces are quite similar, but the longer positive phase duration on the second peak from the gage within the block accounts for the net permanent displacement of that gage. Indicated permanent displacements beyond the block are negligible, while those within the block are in substantial agreement with the permanent displacements reported by Melzer (1970).

As was the case with the HANDEC II test,

Table 2. Block motion summary — DIHEST experience.

Test (Rock type)	Description	Displacement magnitude (ft)	Maximum distance of displacement from DIHEST array (ft)	Crater radii (ft)	Peak velocities at maximum distance (ft/sec) Horizontal (Outward)	Vertical (Upward)	Estimated block size (tons)
PLANEWAVE II (Layered sedimentary)	Multiple displacements along horizontal bedding planes	0.15	56.8		6½	—	—
DATEX II (Soft Tonalite)	Thrust block displacement along low angle joint dipping toward array	13.0	113.0	1.6*	15*	7½	—
	Thin block bounded by parallel vertical joints intersecting array	0.5	128.0	1.8*	12	5½	—
HANDEC II (Soft Tonalite)	Wedge-like displacements along joint dipping away from array in HANDEC I bed	2.4	120.0	1.7	20	9½	—
	Thrust block displacement along intersection of low angle joint dipping toward array and vertical joint forming boundary of thrust block Joints intersected structures in HANDEC I testbed	2.9	188.0 (see qualifying description in text)	2.5*	10½*	4	—
ROCKTEST II (Soft Tonalite)	Thrust block displacement along low angle joint dipping toward array	1.1	22.5	2.8	9½	5	33,500
STARMET (Hard granite)	Thrust block displacement along joint dipping toward array	5.6	42.0	2.3	15	15	7,500
	Inferred displacement upward and back toward explosive array along joints dipping away from array opposite side from thrust block	1.5	50.0	2.8	13	11½	—

*Estimated values

there was a significant HEST air overpressure on the testbed during passage of the DIHEST pulse. Quantitative information on the overpressure pulse can be found in AFWL (1970). The extent of the influence of the overpressure on the block motion is difficult to ascertain, because the data indicate that the testbed surface was in a state of spall despite the additional load. The straight line fit to the vertical velocity trace (Fig. 97) indicates a net downward acceleration of 1.2 g, similar to that experienced on the bed surface during HANDEC II. A figure in excess of 1 g would be expected to result subsequent to spall, because the downward acceleration due to the overpressure on the bed would be added to the gravitational acceleration.

SUMMARY AND DISCUSSION

A summary of the DIHEST related block motions is given in Table 2. There are several obvious conclusions which can be drawn from this table and the supporting data presented in the text.

Most of the relative displacements occurred along paths of least resistance provided by the joints and joint systems surrounding the explosive arrays. Typical examples are the thrust blocks on the STARMET and ROCKTEST II experiments. These were bounded on their base by extensive joints striking roughly parallel to the explosive array and dipping towards them, offering a convenient slip plane to transport the block upward and outward away from the array in about the same direction as the initial velocity imparted to the blocks from the arriving compression waves. These thrust blocks are typically bounded on their ends by near vertical joints or joint sets striking perpendicular to the explosive arrays.

The thrust blocks can extend considerable distances from the explosive arrays. In the case of ROCKTEST II, the thrust block extended horizontally nearly three crater radii from the array. The vertical extent of relative motions was never determined. Extrapolation of the joint surfaces toward the DIHEST array is inconclusive, because in some instances the joints apparently intersect the array (such as in ROCKTEST II), and in others, they apparently dip well beneath it (as in STARMET).

In at least two instances relative motions did not seem to follow paths of least resistance. The first instance was motion of the east side of the STARMET array, which appeared to be substantially reversed. Late time motion turned upward and back *towards* the array, in a manner evidently governed by the joint set which controlled the thrust block motion on the opposite side of the array. Net permanent displacement was upward and toward the array. The second instance was in HANDEC II where relative displacement occurred along a joint running nearly parallel to the array but dipping away from it. Here, the block nearest the array moved downward and outward relative to the block farthest from the array. It should be noted, however, that while relative motion was downward, absolute displacement of both blocks was upward and outward as is typically observed.

An inescapable conclusion from several of the more dramatic block motion measurements is that the exact location of these motions may be impossible to predict. In the case of STARMET, the joint, or joints, forming the base of the thrust block did not appear on the pre-test joint map. While it was obvious post-test that these joints extended laterally more than 100 ft, only about a 5 ft section was observed and mapped prior to the test. Similar instances are described where the major displacements within the structures on HANDEC II and ROCKTEST II occurred along joints which were not identified pre-test.

The lack of ability to predict exact block motion locations in advance of an experiment where the location and properties of the dynamic loading are known poses difficult design and analysis problems. It is vital that these uncertainties be incorporated into any design philosophy for hardened structures in rock.

Based on the very limited amount of data generated by the DIHEST series, it would appear that a "sure safe" zone from a cratering burst in rock might begin beyond three crater radii from the burst point. The vertical extent of relative displacements would probably be less than the horizontal because of the increased confinement and in situ stresses at depth. It is hoped that quantitative expressions of these differences can be obtained from analysis of underground nuclear shots. The accuracies of today's weapons delivery systems, however, make the utilization of such a "sure safe" zone impractical, so that the system designer is left with several options, all of which will require extensive additional analysis and proof testing. These options are the following:

1. Make near-surface components non-critical to system performance. In other words, the de-

signer would "write off" near-surface portions of the system in event of attack. (This, of course, leaves the definition of near-surface to future research.)

2. Use redundant and dispersed critical near-surface components; i.e. make the attacker use an unacceptable number of weapons to assure a hit on the system.

3. Design critical system components to absorb anticipated relative displacements. This might be accomplished by inclusion of soft back packing, rattle space, etc. This option depends on the development of a prediction technique for both near-surface and deeply buried displacement magnitudes.

4. Mitigate both the occurrence and magnitude of relative displacements by using rock reinforcement, such as rock bolts and grouting. Other schemes, e.g. dewatering or aeration might be effective in saturated rock where dynamic pore pressure buildups would lower effective stresses, and;

5. Employ combinations of options 1-4.

LITERATURE CITED

Air Force Weapons Laboratory (1970) ROCKTEST II instrumentation and free field data report AFWL-TR-70-111, vol. I, (Secret)

Air Force Weapons Laboratory (1971) Design and construction of test facilities to simulate the effects of a nuclear detonation—ROCKTEST II. Bob Rutherford Construction Company. AFWL-TR-70-137.

Bache, T.C. and Lambert, D.G. (1976) The seismological evidence for the triggering of block motion by large explosions. Systems, Science and Software, La Jolla, California, SSS R-77-3118, DNA 4323T

Blouin, S.E. (1969) DIHEST development tests MINIDIHEST I and II and PLANEWAVE I and II. AFWL-TR-69-12.

Blouin, S.E. (1970a) Data report DATEX II. AFWL-TR-69-149

Blouin, S.E. (1970b) HANDEC I free field data report. AFWL-TR-70-11.

Blouin, S.E. (1970c) HANDEC II free field data report. AFWL-TR-70-13.

Blouin, S.E. (1970d) In-situ material properties of the air Force's Cedar City, Utah test site. AFWL-WLC-TM-70-012

Blouin, S.E. (1972) Lessons from ROCKTEST and SIMDEP CRREL Memo (unpublished).

Blouin, S.E. and Kaiser, J.V., Jr. (1972) Project STARMET ground motion data. vol I, AFWL-TR-72-68.

Bratton, J.L. (1967) Simulation of airblast-induced ground motions using HEST. *Proceedings of the Conference on Military Applications of Blast Simulators*, Suffield Experiment Station, Canada.

Bratton, J.L. and Mitchell N.R., (1970) A summary of parameters for designing and predicting the airblast environment of HEST experiments. *Proceedings of Eric H. Wang Symposium on Protective Structure Technology, vol II, AFWL.*

Calhoun, D.E. and Stephenson D.E., (1969) Material model for HANDEC II. Letter Report, Eric H. Wang Civil Engineering Research Facility.

Carellas, J.G. (1970) Structural photographic documentary—HANDEC test series. AFWL-TR-70-5.

Carellas, J.G. and Browder L.E. (1969) HANDEC II structural data report. AFWL-TR-69-164.

Carellas, J.G., Browder and Linger D.A. (1969) HANDEC I structural data report. AFWL-TR-69-102.

Cooper, H.F. Jr (1970) On the simulation of ground motions produced by nuclear explosion. AFWL-WLC-TM-70-001.

Cooper, H.F. Jr. and Blouin, S.E. (1971) Dynamic in-situ properties from buried high explosive arrays. *Dynamic Rock Mechanics, Twelfth Symposium on Rock Mechanics*, American Institute of Mining, Metallurgical, and Petroleum Engineers, Inc., New York.

Cooper, H.F. Jr., Blouin, S.E. and Thompson, J.C. (1971) Recent ground motion studies at the Air Force Weapons Laboratory. AFWL TN-72-001.

Higgins, C.J. (1970) Post-test investigation of HANDEC silos. AFWL-TR-70-39

Higgins, C.J. (1971) Post-test investigation of ROCKTEST II silos. AFWL-TR-70-177.

Johnson, R.B. (1972) Effect of geologic factors on cratering experiments in basalt, Buckboard Mesa, Nevada Test Site. U.S. Geological Survey Technical Letter Area 18-1.

Melzer, L.S. (1970a) The Sugarshot test series. Free Time Consultants, Inc. TR-1

Melzer, L.S. (1970b) ROCKTEST II relative displacements. AFWL Memorandum (unpublished).

Plamondon, M.A. (1969) Rock-structures interaction studies. *Strategic Structures Vulnerability Hardening Long Range Planning Meeting*, DASA 2288-1, DASIAC.

Plamondon, M.A. and Browder, L.E. (1970) Response of lined and unlined vertical cylinders in rock. *Proceedings, Strategic Structures Vulnerability/Hardening Long Range Planning Meeting*, DASIAC Special Report 107.

Pratt, H., Bratton, J.L. and Zbur, R. (1969) Geology and material properties of the Estancia Valley test site, New Mexico. AFWL-TR-69-24

Stephenson, D.E. and Engel, H. (1971) Intact rock properties of granite from Project STARMET. AFWL-TR-71-16

Terlecky, F.M. Jr., Spalvins, K. and Repichowski, J. (1971) BRICKPILE. A feasibility study on the influence of jointed rock materials on small explosion-produced craters AFWL-DE-TN-71-004.

Vaughan, R. (1969) Project PLANE WAVE II, Technical Report to Air Force Weapons Laboratory by E.H. Wang Civil Engineering Research Facility, Albuquerque, New Mexico.

Walsh, J.B., Brace, W.F. and Wawersik, W.R. (1970) Attenuation of stress waves in Cedar City quartz diorite. AFWL-TR-70-8

A facsimile catalog card in Library of Congress MARC format is reproduced below.

Blouin, Scott
Block motion from detonations of buried near-surface explosive arrays / by Scott Blouin. Hanover, N.H.: U.S. Cold Regions Research and Engineering Laboratory; Springfield, Va.: available from National Technical Information Service, 1980.
vi, 71 p., illus.; 28 cm. (CRREL Report 80-26.)
Prepared for U.S. Air Force Weapons Laboratory, Kirtland Air Force Base by U.S. Army Cold Regions Research and Engineering Laboratory.
Bibliography: p. 62.
1. Block motion. 2. Explosion effects. 3. Explosives. 4. Hardened structures. 5. Rock dynamics. I. United States. Army. Corps of Engineers. II. Army Cold Regions Research and Engineering Laboratory, Hanover, N.H. III. Series: CRREL Report 80-26.

*U.S. GOVERNMENT PRINTING OFFICE: 1981—700-643/302